Dedicated to My Family

Declaration

I hereby declare that the matter embodied in the thesis entitled "***Electronic, Optical and Charge Transfer Properties of A Few Quantum Dots and MoS_2 Layer: A Density Functional Theory Study***" is the result of investigations carried out by me at the New Chemistry Unit, Jawaharlal Nehru Centre for Advanced Scientific Research, Bangalore, India under the supervision of Prof. Swapan K. Pati and that it has not been submitted elsewhere for the award of any degree or diploma.

Arkamita Bandyopadhyay

Certificate

I hereby certify that the matter embodied in this thesis entitled "***Electronic, Optical and Charge Transfer Properties of A Few Quantum Dots and MoS_2 Layer: A Density Functional Theory Study***" has been carried out by Ms. Arkamita Bandyopadhyay at the New Chemistry Unit, Jawaharlal Nehru Centre for Advanced Scientific Research, Bangalore, India under my supervision and that it has not been submitted elsewhere for the award of any degree or diploma.

Prof. Swapan K. Pati

Acknowledgments

G. K. Chesterton, famous for his pithy saying, once said: ‘I would maintain that thanks are the highest form of thought...’. I want to thank all those people who were there beside me always throughout all these years and I take the M.S. thesis as an opportunity to acknowledge their support.

There is no gainsaying of the fact that a seed needs nurturing from the very beginning to develop into a full-grown tree. Many a promising career has been lost in the whirligig of life. I am eternally grateful to my parents, ‘Maa’ and ‘Baba’, grandparents, my ‘alaku’, aunts, uncles and cousins, Dodo and Chotku, to help me find my bearings – to help me think what I want to do with my life. Thus, in a word, gratitude makes sense of my past, brings peace for today and creates a vision for tomorrow.

The thesis required a lot of guidance and assistance from many people and I consider myself extremely fortunate to have got this all along, especially from my revered guide Prof. Swapan K. Pati, without whom everything would have fallen to pieces. Not only he is a great guide, but he has also been a constant source of support, encouragement and enthusiasm whenever I needed. His towards different scientific problem has influenced me a lot. He has spent his precious time to go through the projects and make necessary corrections as and when it was required. I also thank Anusooya ma'am for being so affectionate and friendly. She has created a homely atmosphere for me. With sir and ma'am, I never felt away from home.

I owe my profound gratitude to all my course instructors in JNCASR who honed and fine-tuned me by providing all the necessary techniques and information to complete such an uphill task. I am very grateful to Prof. C. N. R. Rao for encouraging and helping me to choose my area of research. Also, all the faculty members of New Chemistry Unit, especially Dr. T Govindaraju, Dr. Subi George and Dr. Jayanta Halder, have helped me to be what I am today. I am indebted to all of them.

I want to acknowledge my high school and undergraduate teachers for teaching me to be disciplined, the basics of science and for setting up a goal for me. Thank you Ruma di, Ambarish da, Pranab da, Bidhan da and Matin da.

How could I ever forget the contributions of my past and present lab-mates, Dr. Ganga, Dr. Siam, Dr. Meera, Dr. Prakash, Arun, Pralok, Sharma, Alex, Dibya, Ershaad, Somananda, Swastika, Pallavi, Wasim, Bradraj, Nabanita, Divya and Cristina for their timely support and encouragement, without which this work would not have been completed. I owe my special thanks to Sharma from whom I learnt how to tackle scientific problems, how to read and write scientific literature and move forward in this field.

I would like to thank my Integrated Ph.D chemical science and material science batch mates Rajsekhar, Anirban, Sisir, Koushik, Ram, Chandan Kumar, Chandan De and Ankush for their constant support and encouragement.

I take this opportunity with all humility to remember my friends Prakash, Sudip, Partha, Arup, Sananda, Debu, Suman, Sutapa, Arpan, Ritesh, Rana, Sudeshna, Jia, Subhajit, Saikat, Sougata, Moumita, Sunita, Tarak, Vijay, Rajdeep, Syamantak, Chandradhish, Pallabi, Anindita , Debopriti, Nivedita, Bhawani, Mohini, Abhijit and Rajib, who help me to tide over all the initial troubles and homesick blues. My special thanks for those two persons who have never let me feel alone anywhere, Kalyan and Madhura. The SUCCESS is all YOURS - the FAULT is MINE.

I would also like to extend my sincere regards to JNCASR for providing a world class environment to peruse research. I am thankful to all the academic, administrative, technical, security, Complab, health center and CCMS staffs for making our campus life so smooth and easy going.

Synopsis

From the last decade, the low dimensional materials, namely, 2-D, 1-D and 0-D materials have become an intense interest for the scientists. Because of their interesting properties, they can be potent candidates for novel nano-devices. These materials have restricted motion or quantum confinement of the electrons in the three-dimensions. This gives rise to the unique properties of the low dimensional systems which are not found in higher dimensions. The ability to tune various properties of these materials has attracted attention as this opens up the road towards novel nano-devices.

In this thesis, electronic, magnetic, optical and charge transfer properties of some of the low dimensional materials, namely, 2-D MoS_2 single layer, 0-D graphene and BN quantum dots have been studied. This thesis is mainly focused on the effect of the adsorption of dopants, or substitution of atoms in these low dimensional materials. These types of modifications in the systems can fine tune the properties.

The first chapter of this thesis begins with a brief discussion about low dimensional materials. First, some general information is given about the different systems under consideration, namely, graphene, graphene nanoribbon, graphene quantum dots and inorganic analogues of graphene. Next, the methodology, namely, Density Functional Theory (DFT), which is used to calculate the properties of the low dimensional materials, have been explored. This chapter is concluded with the outline of the whole thesis.

In the second chapter, we have listed studies on the electronic, optical and charge transfer properties of single layer MoS_2 and MoS_2- organic molecule (i.e. Tetracyanoquinodimethane (TCNQ), Tetracyanoethylene (TCNE) and Tetrathiafulvalene (TTF)) systems. We have found that all the molecules are physisorbed on MoS_2 due to the π-stacking interaction. Our calculations show that, there is no significant charge transfer present in case of TCNQ and TCNE and a small but finite amount of charge transfer present in case of TTF-MoS_2 system. We have also found a change in the electronic properties of single layer MoS_2 by observing the presence of discrete molecular level near

Fermi level. Moreover, we have calculated the low frequency optical conductivity to prove that charge transfer interaction can change the optical conductivity of the systems.

In the third chapter, spin-polarized DFT calculations have been performed to tune the electronic and optical properties of graphene (G) and boron-nitride (BN) quantum dots (QDs) through molecular charge-transfer using TCNQ and TTF as dopants. From the calculations, we have found that the nature of interaction between the dopants and QDs is similar to the interaction between the dopants and their two-dimensional counter parts of the QDs–namely, graphene and hexagonal boron-nitride sheets. We find that both the dopants are physisorbed on the QDs. Also, we find that GQDs interact strongly with the dopants compared to the BNQDS. The interactions between the dopants and the QDs lead to a decrement in the HOMO-LUMO gap of QDs by more than half of their original value. Mülliken population analysis, Density of States (DOS), projected DOS (pDOS) plots and optical conductivity calculations have been performed to support and understand the reasons behind the above mentioned findings.

In the fourth chapter, we have examined the structural stability, electronic and magnetic properties of rectangular graphene and Boron Nitride (BN) quantum dots. We have considered the size variations and found that the band-gap decreases with an increase in the width or length of the GQDs. We have substituted BN in graphene quantum dots (GQDs) and C in BN quantum dots (BNQDs) along the edges in different ways to explore the changes in the properties of the quantum dots. We have applied an external electric field on the systems along the diagonal of the rectangular QD and found that it turns the systems into semi-half-metallic from semiconducting and there is oscillatory behaviour in band-gap with field strength. Also we have studied the optical absorption properties of the quantum dots and found the systems can absorb in a broad energy range, from IR to UV.

In the last chapter, we have calculated the electronic and magnetic properties of X-shaped GQD, BNQD and the effect of BN/carbon atom substitution on GQDs/BNQDs. We have found that the GQDs are stable in AFM and the BNQDs are stable in FM ground state. A semiconducting (insulating) → metallic → semiconducting transition is found in both graphene and h-BN QDs as the systems are substituted from pristine-QDs → V-edge-sub-QDs → completely-sub-QDs. Also, the systems change to un-spin polarized → spin polarized → un-spin polarized ground states under these conditions. V-edge-sub-QDs are found to show a unique property, the half-metallicity.

Table of Content

Declaration .... **iii**

Certificate .... **v**

Acknowledgments .... **vii**

Synopsis .... **ix**

Table of Content .... **xii**

List of Figures .... **xiv**

List of Tables .... **xix**

CHAPTER 1 .... **21**

Introduction **21**

1.1 Graphene 22

1.2 Graphene Nanoribbons (GNRs) 26

1.3 Graphene Quantum Dots (GQDs) 30

1.4 Inorganic Analogues of Graphene 33

1.5 Methods 37

1.6 Outline of Thesis 44

CHAPTER 2 .... **47**

Effect of Organic Molecule Adsorption on Single Layer MoS_2: A Detailed Theoretical Study **47**

2.1 Introduction 47

2.2 Computational Details 49

2.3 Results and Discussion 49

2.4 Conclusion 57

CHAPTER 3 59

Molecular Charge Transfer Interactions to Tune the HOMO-LUMO Gaps of Graphene and BN Quantum Dots 59

3.1 Introduction 59

3.2 Computational Details 60

3.3 Results and Discussion 61

3.4 Conclusion 73

CHAPTER 4 75

Structural Stabilities, Electronic, Magnetic and Optical Properties of Rectangular Graphene and Boron-nitride Quantum Dots: Effect of Size, Substitution and External Electric Field 75

4.1 Introduction 75

4.2 Computational Details 77

4.3 Results and Discussion 77

4.4 Conclusion 90

CHAPTER 5 93

Electronic and Magnetic Properties of X-shaped Graphene, BN and hybrid CBN Quantum Dots 93

6.1 Introduction 93

6.2 Computational Details 96

5.3 Results and Discussion 97

6.4 Conclusion 109

References 111

List of Figures

FIGURE 1.1: SCANNING ELECTRON MICROGRAPH OF A RELATIVELY LARGE GRAPHENE CRYSTAL, WHICH SHOWS THAT MOST OF THE CRYSTAL'S FACES ARE ZIGZAG AND ARMCHAIR EDGES AS INDICATED BY BLUE AND RED LINES AND ILLUSTRATED IN THE INSET (A. K. GEIM *ET AL.*[47]). 23

FIGURE 1.2: FINITE QUASI-1D TERMINATION OF GRAPHENE TO GET ZIGZAG AND ARMCHAIR EDGES IN GRAPHENE. 27

FIGURE 1.3: SCHEMATIC REPRESENTATION OF (A) SEMICONDUCTOR OR INSULATOR (DEPENDING UPON ΔE), (B) METAL AND (C) HALF-METAL. THE FERMI ENERGY (E_F) LIES BETWEEN THE VALENCE BAND (VB) AND THE CONDUCTION BAND (CB). ΔE REPRESENTS THE BAND GAP. 30

FIGURE 1.4: GQDS OF DIFFERENT SHAPES AND SIZES: (A) DIAMOND-SHAPED (B) TRIANGULAR (C) RECTANGULAR AND (D) HEXAGONAL GQDS..31

FIGURE 1.5: SINGLE LAYER BN SHEET, WHERE THE PINK BALLS ARE B ATOMS AND THE BLUE BALLS ARE N ATOMS..35

FIGURE 1.6: SINGLE LAYER MOS_2 SHEET, (A) TOP VIEW AND (B) SIDE VIEW. 36

FIGURE 2.1: MOLECULAR STRUCTURE OF (A) TETRACYANOQUINODIMETHANE (TCNQ) (B) TETRACYANOETHYLENE (TCNE) AND (C) TETRATHIAFULVALENE (TTF) MOLECULES. .50

FIGURE 2.2: OPTIMIZED GEOMETRIES OF (A) TCNQ (B) TCNE (C) TTF ON MOS_2 SINGLE LAYER (SKY BLUE BALLS, YELLOW BALLS, GREY BALLS, DARK BLUE BALLS AND WHITE BALLS ARE MO, S, C, N AND H ATOMS RESPECTIVELY). 51

FIGURE 2.3: SIDE-VIEW OF (A) TCNQ (B) TCNE (C) TTF MOLECULES ON MOS_2 SINGLE LAYER. 51

FIGURE 2.4: WAVE FUNCTION PLOTS OF (A) TCNQ, (B) TCNE AND (C) TTF ON MOS_2 LAYER (ISOVALUE IS 0.02 E/Å^3 FOR ALL THE CASES)...53

FIGURE 2.5: SIDE-VIEW OF THE WAVE FUNCTION PLOTS OF (A) TCNQ, (B) TCNE AND (C) TTF ON MOS_2 LAYER (ISOVALUE IS 0.02 E/Å^3 FOR ALL THE CASES)................................53

FIGURE 2.6: BAND STRUCTURE PLOTS OF (A) SINGLE LAYER MOS_2, (B) MOS_2-TCNQ, (C) MOS_2-TCNE AND (D) MOS_2-TTF. THE RED LINE CORRESPONDS TO THE MID-GAP MOLECULAR LEVEL. THE FERMI LEVEL IS SET TO ZERO THE K, M AND Γ POINT HAVE THE COORDINATES (0.667, 0.333, 0.000), (0.5, 0.5, 0.5) AND (0.0, 0.0, 0.0) RESPECTIVELY....54

FIGURE 2.7: PDOS PLOTS OF (A) SINGLE LAYER MOS_2, (B) MOS_2-TCNQ, (C) MOS_2-TCNE AND (D) MOS_2-TTF. THE FERMI LEVEL IS SET TO ZERO. THE GAUSSIAN BROADENING PARAMETER USED IS 0.025 EV...55

FIGURE 2.8: LOW FREQUENCY REGION OF OPTICAL CONDUCTIVITY PLOTS FOR PURE MOS_2 SINGLE LAYER AND MOS_2-MOLECULE COMPOSITES. THE GAUSSIAN BROADENING PARAMETER USED IS 0.05 EV..56

FIGURE 3.1: (A) TETRACYANOQUINODIMETHANE (TCNQ) AND (B) TETRATHIAFULVALENE (TTF) MOLECULES...61

FIGURE 3.2: (A) TCNQ ADSORBED ON (21, 8) GQD, (B) TTF ADSORBED ON (21, 8) GQD, (C) TCNQ ADSORBED ON (21, 6) GQD AND (D) TTF ADSORBED ON (21, 6) GQD. 63

FIGURE 3.3: (A) TCNQ-(21, 8) BNQD, (B) TTF-(21, 8) BNQD, AND SIDE-VIEW OF (C) TCNQ-(21, 8) BNQD, (D) TTF-(21, 8) BNQD 63

FIGURE 3.4: (A) TCNQ ADSORBED ON (21, 8) GQD, (B) TTF ADSORBED ON (21, 8) GQD, (C) TCNQ ADSORBED ON (21, 8) GQD AND (D) TTF ADSORBED ON (21, 8) GQD. IN THIS

FIGURE, THE POSITIONS OF THE TCNQ AND TTF ON GQD ARE SWAPPED WITH THEIR POSITIONS ON BNQD IN THE FIGURE 3.2, AND VICE-A-VERSA FOR BNQD. 64

FIGURE 3.5: PROJECTED DENSITY OF STATES (PDOS) PLOTS FOR (A) (21, 8) BNQD, (B) TCNQ-BNQD AND (C) TTF-BNQD SYSTEMS. THE FERMI LEVEL IS SET TO ZERO. THE PDOS LINES ARE BROADENED WITH GAUSSIAN FUNCTIONS OF WIDTH 0.025 EV. 69

FIGURE 3.6: DOS PLOTS OF (A) (21, 8) GQD, (B) TCNQ AND (C) TTF. THE DOS LINES ARE BROADENED WITH GAUSSIAN FUNCTIONS OF WIDTH 0.025 EV. 70

FIGURE 3.7: LOW-FREQUENCY REGION OF OPTICAL CONDUCTIVITY FOR (A) (21, 8) BNQD, (B) TCNQ-(21, 8) BNQD, AND (C) TTF-(21, 8) BNQD. THE LINES ARE BROADENED WITH GAUSSIAN FUNCTIONS OF WIDTH 0.05 EV. 71

FIGURE 4.1: OPTIMIZED GEOMETRIES OF ALL THE (21, 8) NANO-FLAKES UNDER OUR STUDY. (A) GQD, (B) GQD WITH THE EDGE ATOMS PARTIALLY SUBSTITUTED WITH BN ATOMS, (C) GQD WITH ALL THE EDGE ATOMS SUBSTITUTED WITH BN ATOMS, (D) BNQD (E) BNQD WITH ALL THE EDGE ATOMS SUBSTITUTED WITH C ATOMS (F) BNQD WITH THE EDGE ATOMS PARTIALLY SUBSTITUTED WITH C ATOMS. 79

FIGURE 4.2: DENSITY OF STATES PLOTS OF (A) GQD, (B) GQD WITH THE EDGE ATOMS PARTIALLY SUBSTITUTED WITH BN ATOMS, (C) GQD WITH ALL THE EDGE ATOMS SUBSTITUTED WITH BN ATOMS, (D) BNQD (E) BNQD WITH ALL THE EDGE ATOMS SUBSTITUTED WITH C ATOMS (F) BNQD WITH THE EDGE ATOMS PARTIALLY SUBSTITUTED WITH C ATOMS. FERMI LEVEL IS SET TO ZERO. GAUSSIAN BROADENING PARAMETER IS 0.025 EV. 82

FIGURE 4.3: HOMO AND LUMO PLOTS FOR THE (21, 8) GQDS. ISOVALUE IS 0.02 E/$Å^3$ FOR ALL THE CASES. 82

FIGURE 4.4: HOMO AND LUMO DIAGRAMS FOR α SPIN AND β SPIN OF (21, 8) SYSTEM. ISOVALUE IS 0.02 E/$Å^3$ FOR ALL THE CASES. 84

FIGURE 4.5: HOMO AND LUMO DIAGRAM FOR α SPIN AND β SPIN (21, 8) SYSTEM. ISOVALUE IS 0.02 E/Å^3 FOR ALL THE CASES. 85

FIGURE 4.6: HOMO AND LUMO DIAGRAM FOR α SPIN AND β SPIN (21, 8) BNQD. ISOVALUE IS 0.02 E/Å^3 FOR ALL THE CASES. 86

FIGURE 4.7: HOMO AND LUMO ENERGIES FOR α SPIN AND β SPIN (21, 8) OF BNQD WITH ALL THE EDGE BN ATOMS SUBSTITUTED WITH CARBON WITH THE CHANGE IN WIDTH. 87

FIGURE 4.8: HOMO AND LUMO DIAGRAM FOR α SPIN AND β SPIN (21, 8) SYSTEM. ISOVALUE IS 0.02 E/Å^3 FOR ALL THE CASES. 87

FIGURE 4.9: HOMO AND LUMO DIAGRAM FOR α SPIN AND β SPIN (21, 8) SYSTEM. ISOVALUE IS 0.02 E/Å^3 FOR ALL THE CASES. 88

FIGURE 4.10: HOMO-LUMO GAPS OF THE (21, 4) GQD DEPENDING UPON THE EXTERNAL ELECTRIC FIELD STRENGTH. 89

FIGURE 4.11: ABSORPTION PROFILE PLOTS FOR (A) GQD, (B) GQD WITH ALL THE EDGE ATOMS SUBSTITUTED WITH BN ATOMS, (C) GQD WITH THE ZIGZAG EDGES PARTIALLY SUBSTITUTED WITH BN ATOMS AND (D) BNQD, (E) BNQD WITH ALL THE EDGE ATOMS SUBSTITUTED WITH C ATOMS AND (F) BNQD WITH ZIGZAG EDGES PARTIALLY SUBSTITUTED WITH BN ATOMS. 90

FIGURE 5.1: X-SHAPED QUANTUM DOTS (A) PRISTINE-X-SHAPED-GQD, (B) COM-ED-SUB-GQD, (C) V-ED-SUB-GQD, (D) PRISTINE-X-SHAPED-BNQD (E) COM-ED-SUB-BNQD (F) V-ED-SUB-BNQD. 100

FIGURE 5.2: VARIATION OF E_{FORM} WITH NUMBER OF CARBON ATOMS. 101

FIGURE 5.3: VARIATIONS OF HOMO-LUMO GAPS WITH SUBSTITUTION AND SIZE OF THE SYSTEMS CONSIDERED. 102

FIGURE 5.4: (SPIN-UP) – (SPIN-DOWN) DENSITY OF THE SPIN-POLARIZED SYSTEMS WITH 308 ATOMS. (A) PRISTINE-X-SHAPED-GQD (B) V-ED-SUB-GQD AND (C) V-ED-SUB-BNQD. 103

FIGURE 5.5: (SPIN-UP) – (SPIN-DOWN) DENSITY OF THE SPIN-POLARIZED SYSTEMS WITH 176 ATOMS. 104

FIGURE 5.6: DENSITY OF STATES (DOS) PLOTS FOR (A) PRISTINE-X-SHAPED-GQD, (B) COM-ED-SUB-GQD, (C) V-ED-SUB-GQD, (A') PRISTINE-X-SHAPED-BNQD (B') COM-ED-SUB-BNQD (C') V-ED-SUB-BNQD WITH 308 AND 176 ATOMS. 105

FIGURE 5.7: PROJECTED DENSITY OF STATES (P-DOS) PLOTS FOR (A) PRISTINE-X-SHAPED-GQD, (B) COM-ED-SUB-GQD, (C) V-ED-SUB-GQD, (A') PRISTINE-X-SHAPED-BNQD (B') COM-ED-SUB-BNQD (C') V-ED-SUB-BNQD WITH 308 AND 176 ATOMS. 106

FIGURE 5.8: TOP PANEL CORRESPONDS TO: HOMO AND LUMOS OF (A) PRISTINE-X-SHAPED-GQD, (B) COM-ED-SUB-GQD, (C) V-ED-SUB-GQD; BOTTOM PANEL CORRESPONDS TO: HOMO AND LUMOS OF (A) PRISTINE-X-SHAPED-BNQD (B) COM-ED-SUB-BNQD (C) V-ED-SUB-BNQD WITH 308 ATOMS..107

FIGURE 5.9: (SPIN-UP) – (SPIN-DOWN) DENSITY OF THE SPIN-POLARIZED SYSTEMS WITH 308 ATOMS. (A) PRISTINE-X-SHAPED-GQD (B) V-ED-SUB-GQD AND (C) V-ED-SUB-BNQD. 109

List of Tables

Table 2.1: Adsorption energies, distances and charge transfers between the molecules and single layer MoS2. In case of TTF, the data correspond to 96/192/288 atoms containing supercells (we have not given data for other systems as there are no significant changes). ……………………………………………………………………………………52

Table 3.1: Energies of the GQD-dopant complexes with a variation in the position of the dopant on QD. Energies are scaled to the most stable conformation. ……………………………………………………………………………………62

Table 3.2: Energies of the complexes in different spin states (with respect to their ground-state) are given……………………………………………………………………...64

Table 3.3: Formation energy of the complexes, optimum-distance of dopants above QDs and the amount of charge-transfer between dopants and QDs for (21, 8) QDs are given. ……………………………………………………………………………………65

Table 3.4: Spin-polarized H-L gaps of TCNQ and TTF adsorbed (21, 8)-QDs. …………..………………………………………………………………………...68

Table 3.5: Spin-polarized H-L gaps of TCNQ and TTF adsorbed (21, 6)-QDs……………………………………………………………………..……72

Table 4.1: Formation energies (eV) of the systems (21, 4), (21, 6) and (21, 8). Numbers inside the brackets (in bold-italics) are the (N_B + N_N) : (N_C) ratios ……………….……79

Table 4.2: HOMO-LUMO gap (eV) for the systems (21, 4), (21, 6) and (21, 8) in both α- and β-spins. ………………………………………………………………..….80

Table 4.3: HOMO-LUMO gap (eV) for the systems (33, 4), (33, 6) and (33, 8) in both α- and β-spins. ………………………………………………………………..….81

Table 5.1: Formation energy, Fermi-energy, magnetic moment, band-gap of the systems in both ferro and anti-ferro magnetic spin configurations for (2.44, 2.48) nm ribbon. ……………………………………………………………...………………….…....98

Table 6.2: Formation energy, Fermi-energy, magnetic moment, band-gap of the systems in both ferro and anti-ferro magnetic spin configurations for (4.16, 3.97) nm ribbon. ……………………………………………………………...…………………......99

Chapter 1

Introduction

Low-dimensional systems, namely, zero dimensional (0D), one dimensional (1D) and two dimensional (2D) systems, recently have been the most interesting materials in nanosciences and nanotechnology because of their unique electronic, optical and mechanical properties and they have attracted huge attention of scientists in the last decade.[1, 2] The appearance of interesting and novel properties in these materials, many of which are not seen in bulk systems, has made them really interesting to investigate. The main reason behind all the interesting properties seen in these systems is because of quantum confinement effects which prevail in low dimensions.[3-9] The motions of microscopic degrees of freedom such as electrons, phonons etc. get constrained due to the reduction of length scale in these materials. In such a situation, electronic correlations and restricted boundary conditions introduce various exotic properties in these materials.[10-14] To explain these special features of low dimensional systems, one needs to use new approaches of theoretical sciences which are different from the approaches used in three dimensions. In general, low dimensional systems are treated in fully quantum mechanical way to explain various effects such as Aharonov-Bohm effect[15], persistent currents[16], phase-coherent transport[17] etc. Very recently, metal-insulator transitions,[18] high temperature superconductivity[19, 20] and Kondo effect[21-24] in low dimensions also have created a huge curiosity among the scientists.

Because of the recent advancement in the experimental techniques, researchers are able to get a detailed insight into the various low-dimensional materials. Improvement in different experimental tools, such as, molecular beam epitaxy (MBE), scanning tunneling microscopy (STM)[25-27], mechanically controlled break junction[28, 29], atomic force microscopy (AFM)[30-34], transmission electron microscopy (TEM)[35, 36] and angle resolved photoemission spectroscopy (ARPES)[37, 38] have introduced highly exceptional ways to fabricate and characterize the low-dimensional materials. In this thesis, we have focused on various types of low-dimensional systems and explored a number of interesting and novel properties which arise due to various kinds of interactions in low-dimensions, which are not present in bulk systems.

In this introductory chapter, we briefly discuss about various low-dimensional materials, mainly 2D and 0D materials, characteristic properties of which are studied in this thesis. Also, we include a brief overview of the theoretical and computational methods which we have used to study the different properties of these materials. In this thesis, we mostly focus on the electronic, optical and charge transfer properties of different types of low-dimensional systems, namely, graphene quantum dots and single layer MoS_2. In the following section, we provide a brief description of the low dimensional carbon based systems such as graphene (2D), graphene nanoribbon (quasi 1D), graphene quantum dots (0D) whose properties have been explored in the thesis. Next, we provide an introduction to inorganic analogues of graphene, that is, transition metal based dichalcogenites, among which we mainly focus on the 2D single layer MoS_2 system. Finally, we will describe the methodology which we have used in our studies, briefly. We conclude this chapter by giving a general introduction about various methods used to calculate the desired properties.

1.1 Graphene

Graphene is a planar monolayer structure of carbon atoms tightly packed into a two-dimensional (2D) honeycomb lattice, and it can be considered as a basic building block for graphitic materials of all other dimensionalities. The carbon-carbon bond length in graphene is about 1.42 Å. Graphene sheets can stack to form graphite with an interplanar spacing of 3.35 Å. It can also be made into 0D fullerenes, 1D nanotubes by rolling the sheet. Graphene can also be considered as an indefinitely large aromatic molecule, so the limiting case of the family of flat polycyclic aromatic hydrocarbons. We can consider benzene as the basic unit of graphene. Theoretically, graphene has been studied for a long time,[39-41] and from a long time itself it was used to describe the properties of various carbon-based materials. It was proposed by Landau and Peierls long back in 1935 that a pure 2D crystal can never be thermodynamically stable,[42, 43] so, a 2D crystal cannot be obtained experimentally. Their theory proposes that contribution of thermal fluctuations in low-dimensional crystal lattices should lead to a large amount of displacement of atoms that they become comparable to interatomic distances at any finite temperature. This theory was later extended by Mermin[44] and was supported by many experimental findings. 2D materials, for this reason tend to aggregate together to form multilayer material, also these material tend to decompose easily. So, without a 3D base, a 2D crystal was nearly impossible to obtain[45, 46] until in 2004 graphene was experimentally synthesized by A. K. Geim *et al.* [46] In case of graphene, 2D crystals are stable because it is not always flat, there are ripples in graphene which make the structure stable, so the earlier predictions remain true. These ripples occur because of quantum and thermal fluctuations. However large crystals of graphene with high crystal quality can be obtained (figure 1.1).[47]

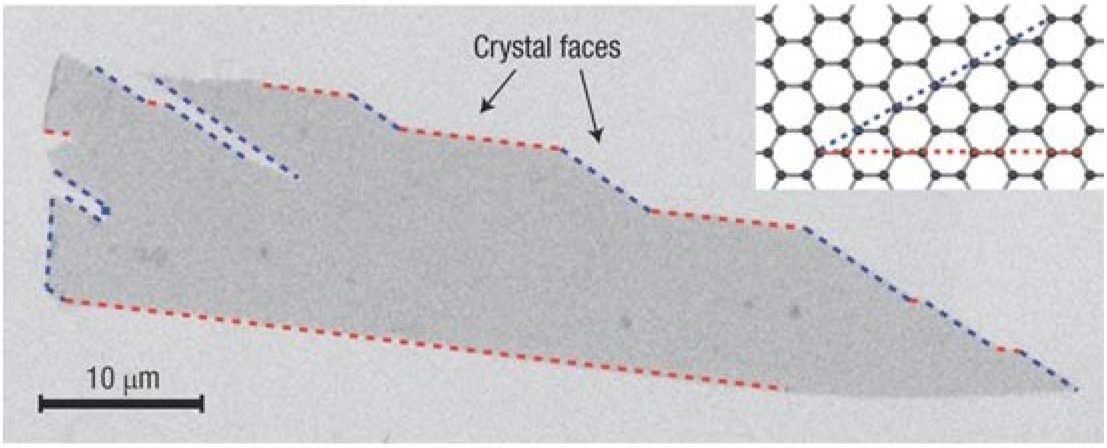

Figure 1.1: Scanning electron micrograph of a relatively large graphene crystal, which shows that most of the crystal's faces are zigzag and armchair edges as indicated by blue and red lines and illustrated in the inset (A. K. Geim *et al.*[47]).

In the next section, we will explain some of the experimental methods to prepare graphene.

1.1.1 Experimental Synthesis

Basically, there are two different approaches for preparing graphene. In the first approach graphene will be obtained through peeling off of an already existing graphite crystal, the so-called exfoliation methods,[48],[49] and in the second approach the graphene layer will be grown directly on a substrate surface.[50]-[51] The first reported preparation of graphene was by Novoselov and Geim in 2004 by exfoliation using a simple adhesive tape.[48] Here some of the synthetic procedures to obtain graphene are discussed below:

Mechanical exfoliation of graphene or The “Scotch Tape Method”

This is a micromechanical exfoliation method, where graphene is extracted from a graphite crystal using adhesive tape.[48] After peeling multilayer graphene (>10 layers) off from the graphite, it remains to stick on the tape. After repeated peeling of the multi-layer graphene by adhesive tape the obtained graphene is cleaved into various flakes of few-layer graphene (1-10 layers). Afterwards the tape is attached to a substrate and the glue is solvated by any organic solvent, e.g., acetone, in order to detach the tape. In this process the obtained graphene is transferred to the substrate. In the obtained flakes, the sizes range from a few nanometers to several tens of micrometers for a single-layer graphene. But it is very difficult to prepare large amount of graphene by this method. Also high quality graphene samples cannot be prepared by this method.

Liquid phase synthesis of graphene by dispersion of graphite

Graphene can be prepared in liquid-phase from a dispersion of graphite in solvent. This method can be used in order to obtain larger amounts of graphene. The easiest method implemented is to disperse the graphite in an organic solvent with nearly the same surface energy as graphite.[52] Thereby, the energy barrier is reduced, which has to be overcome in order to detach a graphene layer from the crystal. Next, either the solution is sonicated in an ultrasound bath for multiple hours or a voltage is applied to the solution.[49] After the dispersion, the solution is centrifuged in order to dispose of the thicker and so heavier flakes. The obtained graphene flakes through this method are of very high quality when compared to the graphene flakes obtained through the scotch tape technique. But the size of the graphene obtained is small and also no controllability is there.

Epitaxial growth by chemical vapor deposition on metal substrate

This method uses the atomic structure of a metal substrate to initiate the growth of the graphene (epitaxial growth). In this method graphene is grown on a metal substrate generally by chemical vapor deposition (CVD) of very small substrates, like methane. Graphene grown on a metal substrate may not always yield a sample with a uniform thickness of graphene layers. Bonding between the bottom graphene layer and the substrate may also affect the properties of the carbon layers, for example graphene grown on ruthenium substrate interacts strongly with the substrate.[53] On the other hand, graphene grown on iridium substrate interacts weakly with the metal, it is uniform in thickness, and can be made highly ordered.[54] High-quality sheets of few-layer graphene having a relatively high surface area have been synthesized via chemical vapor deposition (CVD) on thin nickel films with methane as a carbon source.[55] These sheets can be successfully transferred to various substrates, and can be used for numerous electronic applications.[56],[55] This CVD technique has been can also be used to employed copper foil as substrate to prepare very high quality graphene sample. At very high temperature and very low pressure methane and hydrogen reacts to produce graphene. The growth of graphene stops automatically after a single graphene layer forms, and, using this method, one can generate relatively large graphene films.[57]

1.1.2 Properties of Graphene

Graphene, being a two dimensional material, possesses many unique properties.

Electronic properties

2D graphene is a zero band-gap semiconductor or a semi-metal. However, it has zero density of states at the Fermi level. The band structure of graphene can be understood from the band structure of graphite itself. It was proposed by P. R. Wallace[39] that the energy vs. K (E-K) relation is linear for low energies near the six corners of the two-dimensional hexagonal Brillouin zone, which leads to zero effective mass for electrons and holes. Due to this linear (or conical) dispersion relation at low energies, electrons and holes near these six points behave like relativistic particles described by the Dirac equation for spin 1/2 particles. So in graphene, the electrons and holes are called Dirac fermions and the six corners of the Brillouin zone are called the Dirac points.

Transport Properties

Measurement of transport of electrons or holes in various experiments show that graphene has a remarkably high electron mobility at room temperature, with values as high as 15,000 $cm^2\ V^{-1}\ s^{-1}$.[47] The symmetry of the experimentally measured conductance indicates that the mobilities of holes and electrons are nearly the same. The mobilities of hole or electron are nearly independent of temperature between 10 K and 100 K, which means the main scattering mechanism in graphene is the defect scattering, not the thermal scattering.[58]

1.2 Graphene Nanoribbons (GNRs)

Graphene nanoribbons can be viewed as quasi one dimensional systems of 2D graphene sheet.[59] Generally, a graphene fragment which has a width which is 10 times smaller than the length can be considered as a graphene nanoribbon. As discussed in previous section, graphene is zero band gap semiconductor or semi-metal. In GNRs, apart from the presence of some of the unique properties of graphene, a quantum confinement effect in 1D leads to the opening of a band gap in the system. This band gap can be fine-tuned by tuning the edge nature of a GNR. Depending upon the termination, GNRs have two main probable edge types. They are termed as zigzag graphene nanoribbons (ZGNRs) and armchair graphene nanoribbons (AGNRs), respectively (figure 1.2) and show very different electronic properties arising from their contrasting boundary conditions. The atoms along a zigzag edge will come from the same sublattice, whereas the atoms from two different sublattices make bonds along the armchair edges. The widths of these GNRs are determined along the cross ribbon direction.[59] As it is evident from Fig. 1.2, the edge atoms in the cross ribbon direction of ZGNRs form armchair structure and hence, the width is determined by counting the number of armchair edge atoms (N_Z) in the cross ribbon width and hence, the ZGNRs are named as N_Z-ZGNRs, where N_Z is also the number of zigzag chains in cross ribbon width direction. In case of AGNRs, the width is determined by the number of atoms along the terminating zigzag edge in the cross ribbon direction and named as N_A-AGNRs, where N_A is the number of atoms along the terminating zigzag edge in the cross ribbon direction. Recent experimental techniques have made possible the formation of such systems of varying widths with almost smoothly defined edges. The finite termination of GNRs result in valency unsatisfied edge states which are named as dangling bonds.[60] These edge states are reactive, and generally, undergo various edge reconstructions. To stabilize the edge states, the hydrogen passivation is considered to be practical from the energetics viewpoints. In fact, there are large numbers of studies, which have considered the H-passivation in exploring the electronic structure of GNRs.[61, 62] The H-passivated ZGNRs show spin-symmetric semiconducting properties for the low-energy antiferromagnetic (AFM) ground state[62] structure while H-passivated AGNRs are also semiconducting and have AFM ground state.

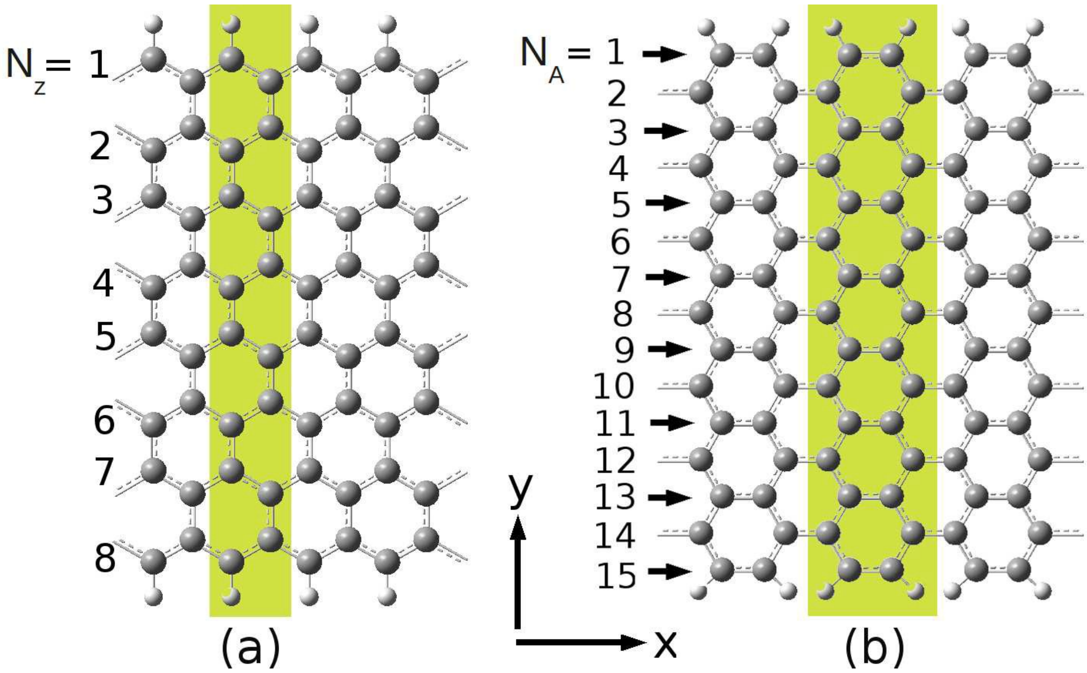

Figure 1.2: Finite quasi-1D termination of graphene to get zigzag and armchair edges in graphene.

1.2.1 Experimental Synthesis

Experimentally, synthesis techniques of GNRs can be classified into two categories: bottom up and top down approaches. The bottom up approach follows the strategy of attaching small molecular building blocks to grow giant graphene structures using very precise synthetic chemistry routes. This approach can provide desired graphene nanostructures like nanoribbons, nanoflakes *etc.* with full control over their edge geometries.[63] Most importantly, these structures with smooth edges can be found in exactly single layers and can be used in device fabrication.

Generally GNRs can be achieved by a top down approach by cutting them out of a graphene sheet. GNRs can be obtained by etching the graphene surface with a STM (scanning tunnelling microscope) tip applying higher (than required for imaging) constant bias potential with atomic level precision and exact edge control.[64, 65] The epitaxially grown few layer graphene has also been patterned by conventional lithographic techniques to fabricate GNR based devices. Plasma etching or gas phase chemical etching can be used in such purposes.[66] Thermally activated metallic nanoparticles have also been used for atomically-precise-etching along the crystallographic axes of a graphene sample to obtain graphene nanoribbons.[67] Also it had been observed that the solution dispersion and sonication of exfoliated graphite can give nanoribbons with ultra-smooth edges, even for sub 10 nm width GNRs. The arc-discharge technique can also be employed to obtain graphene flakes[68] with which it is easy to dope with boron and nitrogen atoms. But generally the top down approaches result in irregular edge geometry with a little control over the number of obtained layers. But, with a technique which employs unzipping and flattening of the carbon nanotubes it is possible to obtain smooth edge GNRs with exact edge control.[69] Large quantities of width controlled GNRs have been produced via graphite nanotomy process as reported by Mohanty *et al.*,[70] where sharp diamond knife application on graphite produces graphite nanoblocks, which are exfoliated to produce GNRs.

1.2.2 Properties of GNRs

The properties of graphene nanoribbons highly depend on the edge nature of the ribbon, for example, zigzag and armchair graphene nanoribbons can show very different types of properties.

Armchair Graphene Nanoribbon (AGNR)

Depending on the value of N_A, where N_A is the number of atoms along the terminating zigzag edge in the cross ribbon direction, the AGNRs can be classified into three categories,[71] namely, N_A= 3p, 3p + 1 and 3p + 2 (p is a positive integer) with widely varying electronic properties. All the three types of AGNRs show semiconducting behavior with a direct band-gap at k = 0 and the gap (Δ_a) decreases with an increase in width (w_a), following the relation $\Delta_a \infty w_a^{-1}$. It is noticeable that the AGNRs with N_A= 3p + 2 show the smallest gap in all approximations compared to the other two families.[71]

The band gap of semiconducting AGNRs can be modulated by applying an external electric field across the ribbon width.[72] The band gap starts decreasing beyond a certain critical field strength depending on the width. The AGNRs with N_A= 3p + 1 show larger band gap variation with electric field, which suggests an enhanced response towards the external perturbation.

Zigzag Graphene Nanoribbon (ZGNR)

The periodic ZGNRs show localized electronic states at the edges, known as edge states.[60] These edge states are extended along the zigzag edges and they decay exponentially towards the ribbon center. Because of the presence of such edge states, ZGNRs can show a wide range of interesting electronic properties and also their electronic structure and band gap can be fine-tuned by structural or chemical modifications as well as with doping and external perturbations.[73-75]

The ground state of ZGNRs has parallel spin alignment along each zigzag edge, whereas the spin alignments across two edges are antiparallel to each other. The spins prefer to be antiferromagnetically coupled within the nearest neighbor sites throughout the lattice with decay of spin moments towards the center of the ribbon.[76] This kind of antiparallel spin ordering has been predicted by Lieb's theorem[77] for a bipartite lattice and this makes the ground state antiferromagnetic (AFM). Also the α and the β-spins prefer to localize on two different sublattice points of the bipartite lattice. The AFM ZGNRs exhibit a direct band gap (Δ_Z) at $k = 2\pi/3$, which varies inversely with the ribbon width (w_Z).[71]

The periodic ZGNRs with AFM ground state have been predicted to show half-metallicity, when exposed to a certain critical external electric field along the cross ribbon width direction.[78] Half-metallic materials, unlike conventional metals or semiconductors, show zero band gap for electrons with one spin channel, whereas the other spin channel remains semiconducting or insulating, as shown in figure 1.3. Owing to this unique property, this class of materials gives us complete control over the spin polarization of current with higher efficiency for magnetic memory storage.

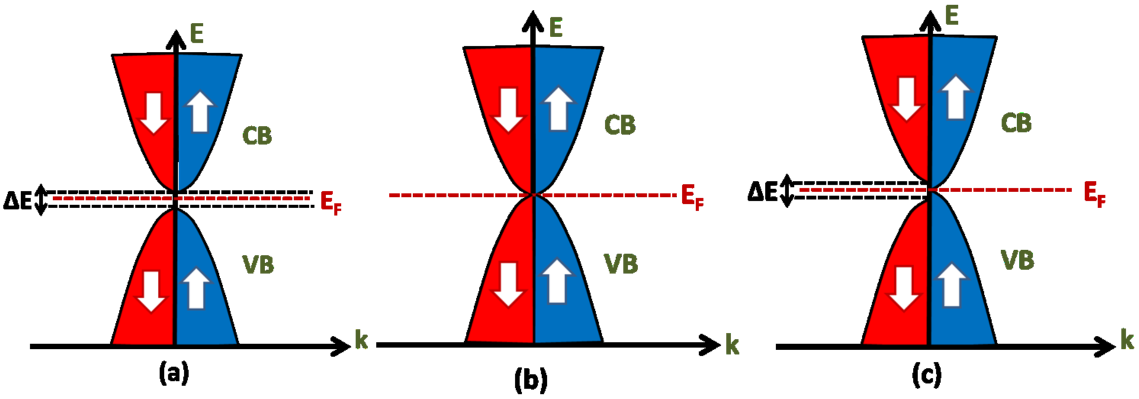

Figure 1.3: Schematic representation of (a) Semiconductor or insulator (depending upon ΔE), (b) metal and (c) half-metal. The Fermi energy (E_F) lies between the valence band (VB) and the conduction band (CB). ΔE represents the band gap.

This half-metallic nature of the nanoribbons can be obtained by other methods also. It is noted that ZGNRs can be tuned to half-metals by a shift in the energy of the two zigzag-edge states differently. Such shifting can be obtained by doping,[73] substitution,[74] or their combinations [75]

1.3 Graphene Quantum Dots (GQDs)

The zero-dimensional (0-D) form of graphene, which may be called graphene nano-flakes (GNFs) or graphene nano-dots (GNDs), are the lowest dimensional graphitic material. It is found that preliminary studies suggest they show some very interesting properties which differ from those of 2-D graphene and 1-D graphene nanoribbons.[79] They have great potential for a variety of applications, principally as electronic and magnetic devices because of their interesting properties.[80-83] These interesting properties arise because GNFs not only have edge states, but also corner states, and also can have mixture of zigzag and armchair edges also. They may also be cut into a much larger variety of different shapes and sizes (figure 1.4). The addition of these structural features may be regarded as giving GQDs yet another degree of engineering freedom over GNRs and twice as many degrees of freedom than 2-D graphene. Examples of corner states can be seen where the edge states meet (figure 1.4), and the different types of corners that can be introduced in a GQD. Furthermore, in contrast to GNRs, GQDs can range in size from molecular to semi-infinite 2-D structures, which means that they are the bridge between poly-aromatic hydrocarbons (PAHs) and 2-D graphene, and consequently their electronic structures would vary from having discrete molecular levels to being band-like as their dimensions are made larger.[84] This leads to the tuning of band-gap ranging from the molecular level to quasi-2D level and also interesting electronic and magnetic properties.[85-88]

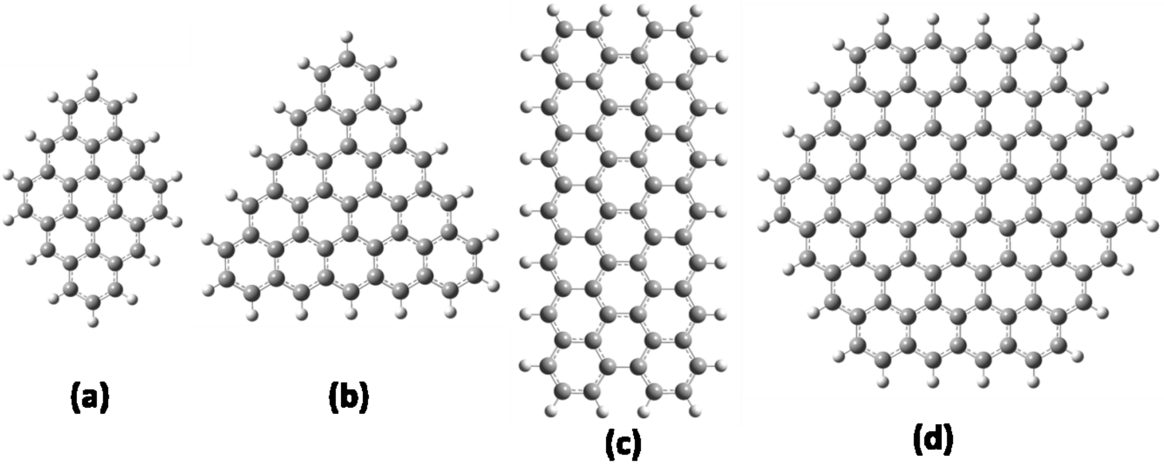

Figure 1.4: GQDs of different shapes and sizes: (a) diamond-shaped (b) triangular (c) rectangular and (d) Hexagonal GQDs.

1.3.1 Experimental Synthesis

Similar to graphene nanoribbons, graphene quantum dots also can be synthesized by two possible approaches, namely, bottom up and top down approaches.

Bottom up approach

Bottom up approaches are essentially the chemical methods to produce aromatic molecule based on the organic chemistry approaches. Small molecular units are reacted together to form large aromatic moieties. The largest such structure produced by these methods reported to date is a 222 ring GNF.[89] The benzene ring edges of the graphene quantum dots can be terminated with different atoms or groups, which may be made by hydrogen, alkyl groups, different functional groups, etc.[90]

Top down approach

Top down approaches start with a large piece of graphene sheet or graphitic material such as graphene oxide or carbon nanotubes (CNTs) and cut GQDs directly from the sheets or tubes. Normally, this method requires that one first produce large graphene sheets and this has been done by a variety of methods, micromechanical cleavable of a graphite single crystal[48] or by chemical means e.g. by chemical vapour deposition[57] or by chemically "unzipping" carbon nanotubes (CNTs)[91]. Presumably some or all of these techniques could be adapted to produce graphene GQDs. Once sheets of 2-D graphene are produced, GQDs have to be cut from them which has been done by a variety of methods, namely, combined e-beam lithography and plasma etching,[92] scanning tunnelling microscope lithography [65] and atomic force microscope lithography,[92] also catalytic cutting by atoms.[93] Also GQDs can be produced via graphite nanotomy process which is recently reported by Mohanty *et al.*,[70] where sharp diamond knife application on graphite produces graphite nanoblocks, which can be exfoliated to produce GQDs with definite shapes and sizes. Small pieces of CNTs can be directly unrolled to produce free-standing GQDs.

1.3.2 Properties of GQDs

GQDs are the lowest dimensional graphitic structures, so they exhibit many interesting properties. Because of lower dimension, most of the properties they show are very different from 2-D graphene or quasi 1-D nanoribbons. Because of quantum confinement effect in all the three directions, GQDs show some really interesting properties.

Solubility in different solvents

Graphene is hydrophobic and is therefore difficult to solubilize or disperse in most liquids, which limits their easy processability and application in many ways. Thus, chemists have spent considerable effort in functionalizing graphenes so that they may be more readily solubilized or dispersed, especially in water. Groups such as carboxyl epoxy and hydroxyl are commonly substituted into GQDs to solubilize them in water and long alkyl chains make GQDs soluble in many organic solvents like tetrahydrofuran.[90]

Electronic properties

Graphene quantum dots are semiconducting. The band-gap or, more precisely, the HOMO-LUMO (H-L) gap depends on the size of the quantum dot and also on the edge and corner states. Similar to the particle in a box analogy, increase in size of the GQD results in the decrement of the H-L gap.[84] GQDs with either zigzag edges or armchair edges have a finite band gap and are semiconducting,[80, 81, 94, 95] although, the origin of the gap is different in each case. Zigzag edges introduce localized states or edge states similar to GNRs.[60] As opposite edges of such a GQD belong to different sublattices, the spin ordering is different on each edge. Zigzag edges can create antiferromagnetic (AFM) ground state.[80] There are no localized states at armchair edges. The zigzag graphene quantum dots (ZGQDs) can also show half-metallicity similar to ZGNRs on the application of a certain critical electric field across the width of the QD.[80]

Magnetic properties

In GQDs, large magnetic moments occur at zigzag edges but there are none for armchair edges. But overall a ZGQD is non-spin-polarized if the number of A and B sublattices are same. In case of triangular GQDs, one type of sublattice is present in excess and in that case the system can have high magnetic moment.[86, 88, 96]

1.4 Inorganic Analogues of Graphene

After the discovery of fullerenes in 1985,[97] it was found that inorganic layered materials such as MoS_2 and WS_2 can also form fullerene-like structures,[98, 99] soon fullerene like structures of BN and other nitrides were also discovered.[100] When carbon nanotubes (CNTs) were discovered,[101] inspired by that similar inorganic analogues of them were discovered also.[102],[103] Similarly, when graphene, the 2-D graphitic material, was exfoliated from 3-D graphite it became a great interest of research in the last few years because of its unique properties and novel phenomena exhibited by it. But graphene is a zero band-gap semi-conductor or semi-metal. So to use graphene in opto-electronic devices opening of band-gap is required. Various methods, like, doping on graphene,[104, 105] reducing the dimensionality (1-D or 0-D) of graphene sheet,[59, 106, 107] molecular charge transfer[108-111] or defect induced opening of band-gap[112, 113] has been well studied. However, the inorganic analogues of graphene can be used in the field of electronics without any modifications in some cases or with little modifications as they are either semi-conductor (transition metal dichalcogenites) or insulator (BN sheet).[47, 48, 114-120] These materials possess graphite-like layered structures in which the layers are held together by weak van der Waals forces unlike graphene, where the force is π-stacking interaction. Also composite materials like BCN hybrid nano sheet has already been prepared and studied to show unique and novel properties.[121] In this thesis BN and MoS_2 systems have been studied. So these materials will be discussed in details.

1.4.1 Single Layer BN Sheet

Boron nitride or BN is a chemical compound which generally has equal numbers of boron and nitrogen atoms. BN lattice is isoelectronic to a similarly structured carbon lattice as B has one electron less and N has one electron more than a carbon atom. Thus BN can exist in various crystalline forms which are similar to carbon systems. The hexagonal form of BN corresponding to graphite is the most stable among all BN polymorphs. Boron nitride (BN) is an insulator or wide band gap semiconductor with interesting properties.[122] It form can nanotubes or fullerene like clusters just as carbon and also similar to graphene, BN nano sheets (figure 1.5) can be synthesized with high purity.

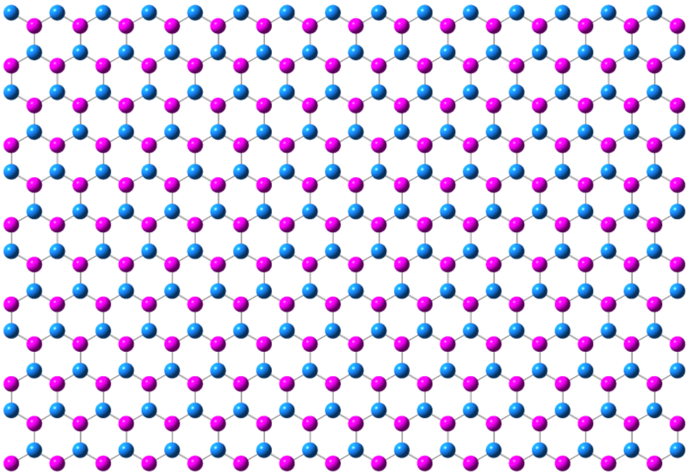

Figure 1.5: Single layer BN sheet, where the pink balls are B atoms and the blue balls are N atoms.

Single layer BN sheet is sp^2 bonded hexagonal network of atoms similar to graphene. While a single layer BN can be synthesized from a bulk BN crystal by micromechanical cleavage or scotch tape technique,[123] a few-layer BN can be made by sonication of BN particles[124] or by using a high-energy electron beam.[125] Also BN sheets can be made by reacting boric acid with different proportions of urea at high temperature by chemical vapour deposition.[122]

Properties of BN sheet

All C atoms in graphene sheet are equivalent with covalent bonding between them making it a bipartite lattice. In contrast, B and N sites in BN sheet are non-equivalent. The charge transfer from B to N makes the bonding between them to be more ionic, thus the properties of a BN sheet becomes highly different from that of graphene system. BN sheet has acquired immense scientific attention because of its unique mechanical, optical, thermal and electronic properties, also with resistance to oxidation over a wide range of temperatures.[126] Unlike graphene, which is a semi-metal, BN sheet is insulator or a large band-gap semi-conductor (band-gap is 4.7 eV).[127] BN sheet is thermally very stable; it can be as it is up to 1000 ^{o}C without any deformation.[128] Also BN sheet is non-magnetic.[129]

1.4.2 Single Layer Molybdenum Sulfide (MoS_2)

MoS_2 is the principal ore from which molybdenum metal is extracted. MoS_2 is relatively unreactive, being unaffected by dilute acids and aerial oxygen. Bulk MoS_2 is a layered structure where each layer contains again three layers of atoms. In this structure each Mo (IV) center occupies a trigonal prismatic coordination sphere, being bound to six sulfide ligands. Each sulfur centre is pyramidal, being connected to three Mo centres. In this way, the trigonal prisms are interconnected to give a layered structure, where molybdenum atoms are sandwiched between layers of sulfur atoms. MoS_2 layers are held together with weak van der waals interactions, unlike graphene π-π stacking interaction. That's why single layer MoS_2 systems are easy to prepare and also it is feasible to apply them in different devices.[130-132] A graphene-like single layer two-dimensional structure of MoS_2 or WS_2 can be obtained by lithium intercalation and exfoliation of bulk MoS_2 or WS_2.[133] Also chemical vapor deposition method can be used to prepare single layer MoS_2 using organic precursors like Mo(S-*t*-Bu)$_4$.[134, 135]

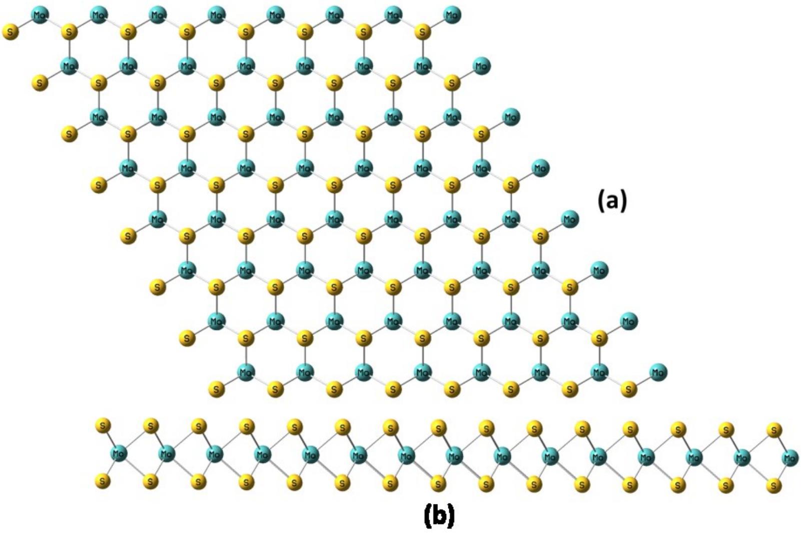

Figure 1.6: Single layer MoS_2 sheet, (a) top view and (b) side view.

Properties of single layer MoS_2

Unlike graphene, which is zero band-gap semi-conductor or semi-metal, single layer MoS_2 is intrinsic semiconductors (single layer MoS_2 has a direct band-gap of ~1.8 eV[116, 130]) as their bulk three dimensional (3-D) counterpart. Single layer MoS_2

sheets have high carrier mobility.[115, 116, 130, 136] Thus, they are already being used as transistors[136, 137] or energy storage devices such as anode for Li or Mg ion batteries. It was found that MoS_2 layer is nonmagnetic.[138] MoS_2 can be used in the field of electronics without any kind of band-gap modifications. Also band-gap tuning of a MoS_2 layer is easily done by doping metal and non-metal adatoms or different molecules on MoS_2 to change the electronic and magnetic properties of MoS_2. Even, electron beam mediated creation of vacancies and adding impurity atoms to these vacancies have been shown to modify the electronic properties of single layer MoS_2.[63, 138, 139],[140-142]

1.5 Methods

In this section, the different theoretical methods, that are used to compute various properties of the low dimensional systems, are discussed in this section briefly. We will first introduce the density functional theory (DFT) –a revolutionary theory to calculate electronic structures of materials. Then some of the different packages what are generally used to calculate these properties outlined above are mentioned.

1.5.1 Density Functional Theory (DFT)

DFT is one of the most widespread quantum mechanical approaches for calculating the ground state properties of wide range of systems: from molecules to bulk materials, from insulators to metals, from diamagnetic to ferromagnetic materials. DFT can predict various ground state properties such as optimized geometry, vibrational frequency, atomization energy, ionization energy, electronic properties, one-particle magnetic states, optical properties, reaction pathways etc. very reliably. With the advancement of this theory, it has also been modified successfully for several kinds of studies including molecular dynamics, spin dependent study, investigation at non-zero temperature, time dependent phenomena etc.

From elementary quantum mechanics, we know that all the information about a system is stored in its wave function, ψ. The total energy of a system having interacting electrons and nuclei, can be calculated by solving time independent Schrödinger equation,

$$\hat{H}\,\Psi = E\,\Psi \tag{1.1}$$

Where, E denotes the total energy eigenvalue and $\hat{H}$ is the Hamiltonian operator of the system. Every system consists of a number of nuclei and electrons. For a system with N_e number of electrons and N_n number of nuclei, the total Hamiltonian of the system can be written as:

$$\begin{aligned}\hat{H} = -\frac{\hbar^2}{2m}\sum_{i=1}^{N_e}\nabla_i^2 - \frac{\hbar^2}{2}\sum_{I=1}^{N_n}\nabla_I^2/M_I \\ -\sum_{i=1}^{N_e}\sum_{I=1}^{N_n}\frac{Z_I e^2}{|r_i - R_I|} + \sum_{i=1}^{N_e}\sum_{j>i}^{N_e}\frac{e^2}{|r_i - r_j|} \\ +\sum_{I=1}^{N_n}\sum_{J>I}^{N_n}\frac{Z_I Z_J e^2}{|R_I - R_J|}\end{aligned} \tag{1.2}$$

Where, m and M are the masses of electrons and nuclei, respectively. The Laplacian operators, $\boldsymbol{\nabla_i^2}$ and $\boldsymbol{\nabla_I^2}$ represent the second order differentiation with respect to the coordinates of the i^{th} electron and the I^{th} nucleus. $\mathbf{Z_I}$ is the atomic number of the nucleus I. $\mathbf{r_i}$ and $\mathbf{R_I}$ represent the spatial coordinates of i^{th} electron and I^{th} nucleus, respectively and **e** is the electronic charge. The first two terms in the equation 1.2 are the kinetic energy operators of electrons and nuclei, respectively. The third term represents the Coulomb attraction between electrons and nuclei. The fourth and fifth terms represent the Coulomb repulsion between the electrons and between the nuclei themselves, respectively. It's very complicated to solve this many-body Schrödinger equation. To simplify the equation, one can use Born-Oppenheimer (BO) approximation which states that as the nuclei are heavier than electrons and also move much slower than the electrons, the motion of electron and nucleus can be separated. It can be assumed that nuclei are fixed in particular positions, while the electrons are moving in a charged field created by the nuclei. Now, entire wave function can be divided into two parts, namely, electronic ($\boldsymbol{\Psi_{electronic}}$) and nuclear ($\boldsymbol{\Psi_{nuclear}}$) parts.

$$\Psi_{Total} = \Psi_{electronic} \times \Psi_{nuclear} \tag{1.3}$$

Now in BO approximation the *electronic* Schrödinger equation is solved, yielding the wavefunction $\boldsymbol{\Psi_{electronic}}$ depending on electrons only. Therefore, the time independent Schrödinger equation corresponding to electronic part can be written as,

$$H_e\,(\boldsymbol{r},\boldsymbol{R})\Psi_e = E_e\,\Psi_e \tag{1.4}$$

Where, electronic Hamiltonian is given as,

$$\hat{\mathrm{H}} = \sum_{i=1}^{N_e} -\frac{\hbar^2}{2m}\nabla_i^2 + \sum_{i=1}^{N_e}\ \sum_{j>i}^{N_e} \frac{e^2}{|r_i - r_j|} + \hat{V}_{ext} \tag{1.5}$$

Here $\boldsymbol{\hat{V}_{ext}}$ acts as the external potential acting on the electrons induced by the nuclei and any other externally applied field.

After introducing Born-Oppenheimer approximation, the total number of degrees of freedom can be reduced, however still it's very difficult to handle electron-electron interactions part of a many electron system. And also electronic wave function depends on the positions of all electrons. A very intelligent approach to treat this situation is to use electron density instead of many-body wave function to describe the system of interest. DFT demands much lesser computational effort and gives a considerably good description of ground state properties of materials.

In 1964, pioneering work by Hohenberg and Kohn considers as the beginning of DFT. [143] There they stated two basic theorems;

- The ground state electron density, $\boldsymbol{\rho_0}$, of a many electron system can uniquely determine the external potential, $\boldsymbol{V_{ext}}$,which is acting on the system. It can be stated in other way also: the external potential, $\boldsymbol{V_{ext}}$, can exactly calculate the ground state electron density $\boldsymbol{\rho_0}$ of the system. Moreover, $\boldsymbol{\rho_0}$ can uniquely determine the ground state expectation values of any observables.
- To be the true ground-state electron density, it has to minimize the total energy functional of the system. And it can be achieved by following variational principle.

The Hohenberg-Kohn theorem[143, 144] can be called as the soul of the DFT. As mentioned earlier, the fundamental concept of DFT is to use electron density as an alternative of complicated many-body wave function to handle interacting systems. According to this, now one can express the Schrödinger equation in the following way;

$$E[\rho] = \hat{F}[\rho] + \int dr\, V_{ext}(r)\rho(\mathrm{r}) \tag{1.6}$$

Where, $\hat{F}[\rho]$ is universal functional of $\boldsymbol{\rho}$, that is the density. One can find the ground state density by minimizing the functional, $\mathbf{E}[\boldsymbol{\rho}]$, with respect to $\boldsymbol{\rho}$. But the minimization of the explicit energy functional is still difficult to solve exactly. In 1965, Kohn and Sham proposed an efficient way to replace original many-body problem into an auxiliary one-electron problem. In this approach, interacting electrons are treated as non-interacting electrons which are moving in the effective potential. The many-body effects are included in this through exchange-correlation functional. According to this approach, the total energy functional can be expressed as,

$$\begin{aligned} E[\rho(r)] = T_s[\rho(r)] + \frac{1}{2}\int \frac{\rho(r)\rho(r')}{\left|r_i - r'_j\right|} dr dr' + E_{xc}[\rho(r)] \\ + \int \rho(\mathrm{r}) V_{ext}(r) dr \end{aligned} \tag{1.7}$$

where $\mathbf{T_s[\rho(r)]}$ is the kinetic energy functional for non-interacting electrons, second term is electrostatic energy, third term is exchange and correlation energy and last is the energy due to external potential caused by nuclei and other externally applied potentials. Among these, first and third terms can't be solved in this form. However, if wave functions $\mathbf{\Psi_i(r)}$ constructs the electron density, $\boldsymbol{\rho}\mathbf{(r)}$, then the first term i.e. the kinetic energy term can be calculated as follows;

$$T_s[\rho(r)] = -\frac{\hbar^2}{2m}\sum_{i=1}^{N}\int \Psi_i^*(r)\nabla^2\Psi_i(r)\, dr \tag{1.8}$$

From equation (1.7) we can get a set of differential equations called as Kohn-Sham equations,

$$[-\frac{\hbar^2}{2m}\nabla^2 + V_H + V_{xc} + V_{ext}]\Psi_i(r) = \epsilon_i\Psi_i(r) \tag{1.9}$$

where, $\mathbf{V_H}$ is Hartree potential, $\mathbf{V_{xc}}$ is exchange-correlation term, $\mathbf{V_{ext}}$ corresponds to external potential and $\mathbf{\Psi_i(r)}$ are the special orbitals called as Kohn-Sham orbitals. The general process to solve these equations is the iterative method and it does continue until self-consistency is reached. Now, we should concentrate on the exchange-correlation potential which can't be found exactly and should be approximated. From equation (1.9), $\mathbf{V_{xc}}$ can be expressed as;

$$V_{xc} = \frac{\delta E_{xc}[\rho(r)]}{\delta\rho(r)} \quad (1.10)$$

With the advancement of DFT, several approximations came forward to approximate the exchange-correlation functional more and more accurately. Here, we will discuss about two approximations which are used most extensively in the literature.

Local Density Approximation (LDA): First and simplest approximation of exchange-correlation potential is LDA.[145] It can be defined as;

$$E_{xc}^{LDA}[\rho(r)] = \int d^3r\varepsilon_{xc}\left(\rho(r)\right).\rho(r) \quad (1.11)$$

where $\boldsymbol{\varepsilon_{xc}(\rho(r))}$ denotes the exchange and correlation energy per electron of the homogeneous electron gas with electron density, $\boldsymbol{\rho(r)}$. Here, the electron density smoothly varies in space. Therefore, any area of space can be locally treated as homogeneous electron gas of density, $\boldsymbol{\rho(r)}$. Now, to obtain the total exchange-correlation energy, one has to perform summation of local exchange-correlation energy for all the electrons in every region of space. These functional works nicely for bulk solids but have a poor performance for the systems where the electron density does not vary smoothly in space.

General Gradient Approximation (GGA): In this approximation, the standard LDA has been extended to inhomogeneous systems where electron density varies non-uniformly. This improved approximation not only considers the local charge densities but also more physical parameter i.e. their gradients. Fundamentally, there are three kinds of GGA:

a. **Ab-initio based:** These functionals are derived from exact results. Here exchange and correlation parts are calculated individually. The typical examples of this are PBE (Perdew-Burke-Ernzerhof) [146], PW91 (Perdew-Wang 1991) [147] etc.
b. **Atom-based**: It has some basic similarities with the previous one such as, these are also based on some exact results and exchange and correlations are treated separately. But for this type, the functional parameters are fitted on close-shell atom properties. Becke's GGA for exchange[148] and Lee Yang and Parr functional for correlation[149] are some example of this.
c. **Empirical:** In this case, exchange and correlation terms are treated as a whole. Functional parameters are obtained by fitting the results on a set of atomic and

molecular properties. Well-known example of this is HCTH (Hamprecht-Cohen-Tozer-Handy) functional.[150]

Basis Set: One of the most important steps to achieve accurate results for electronic structure calculation is to choose suitable basis sets. One needs to expand the one-particle wave functions in the following manner:

$$\Psi_i(r) = \sum_{j=1}^{N_b} C_{i,j}\, g_i(r) \tag{1.12}$$

where $\boldsymbol{C_{i,j}}$ denotes the coefficients of expansion, $\boldsymbol{g_i(r)}$ is the basis functions and $\mathbf{N_b}$ is the size of the basis. In this way, the Kohn-Sham equations convert to one-particle matrix equations. Now, one has to diagonalize this one particle Hamiltonian matrix to obtain the eigenvalues and eignevectors. Here, the Kohn-Sham equations are solved in self-consistent manner. The procedure is to begin with some initial guess of density and keep on improving density and potential in each iteration until the self-consistency is achieved.

Pseudopotentials:

Next, we will focus on another vital concept of DFT, called pseudopotential. Generally it is assumed that, the core electrons are rather unaffected by changes in their chemical environment. A pseudopotential, ($\mathbf{V_{PP}}$) is an effective external potential experienced by valence electrons in an atom when all the core electrons of the atom are frozen. Using this analogy, one can freeze all the core electrons of an atom and can construct an effective external potential which acts on the valance electrons on each atom. Consequently, the oscillatory nature of valance wave function in the core region can be substituted by a smooth wave function. [151, 152] Pseudo wave function and all electron (where core electrons are free) match each other beyond a particular value of radial distance which is chosen to be outside the last node in the all electron wave function; this is called the cutoff radius $\mathbf{r_c}$. If we can use the same pseudopotential to describe different chemical environments then the pseudopotential is said to be transferable. A good pseudopotential needs to fulfil the following conditions:

- The lowest pseudo wave function generated by the pseudopotential should not contain any nodes.
- The normalized atomic radial pseudo wave function with an angular momentum l should be equal to the normalized radial all electron (AE) wave function outside a given cut-off radius $\mathbf{r_c}$ (Fig. 1.7):

$$R_i^{PP}(r) = R_i^{AE}(r); (r > r_c) \tag{1.13}$$

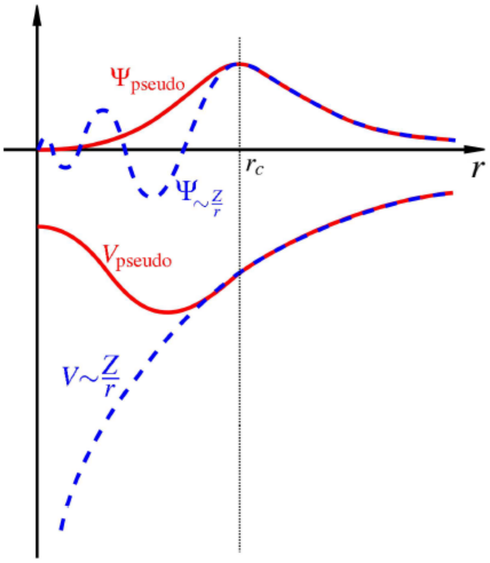

Figure 1.7: Comparison of a wave function in the Coulomb potential of the nucleus (blue) to the one in the pseudopotential (red). The real and the pseudo wave function and potentials match above a certain cutoff radius r_c.

- Norm conservation: The charge inside of $\mathbf{r_c}$ has to be the same for both the wave functions,

$$\int_0^{r_c} |R_i^{PP}(r)|^2 r^2 dr = \int_0^{r_c} |R_i^{AE}(r)|^2 r^2 dr \tag{1.14}$$

- The eigenvalues of both wave functions should be the same.

A large number of packages have been developed in the last few decades where self-consistent calculations for electronic structure using various methods such as Hartree-Fock, post Hartree-Fock and DFT have been implemented. Among all these, some of the packages like Gaussian 09,[153] General Atomic and Molecular Electronic Structure System (GAMESS),[154] Amsterdam Density Functional (ADF)[155] are used extensively for molecular systems. As these packages use localized orbital basis functions, it can't handle large systems. However, the concept of numerical orbitals and pseudopotential come into play to study large periodic systems. Spanish Initiative for Electronic Simulations with Thousands of Atoms (SIESTA)[156] is an example of such kind of packages, where combination of numerical orbitals and norm-conserving pseudopotentials have been implemented successfully. Another way is to use plane augmented wave basis sets for calculations. This approach is implemented in packages like Quantum-Espresso (PWscf), Vienna Ab-initio Simulations Packages (VASP)[157-159] etc.

1.6 Outline of Thesis

As discussed so far, reduction in dimensions of materials gives rise to a number of interesting properties. The experimental developments in this field of research have demonstrated various unique phenomena. The low dimensional graphitic and inorganic graphene-like systems are very much important in this respect. In this thesis, we have mostly focused on electronic, optical and charge transfer properties of a few low dimensional systems, namely, graphene quantum dots and single layer MoS_2.

In the next chapter, we have performed calculations on single layer MoS_2 and organic molecule-MoS_2 adsorbate systems to find out the changes in the electronic properties of single layer MoS_2. We have performed our calculations for Tetracyanoquinodimethane (TCNQ), Tetracyanoethylene (TCNE) and Tetrathiafulvalene (TTF) to calculate the charge transfer and optical conductivity.

In the chapter 3, we have studied the interactions between TTF and TCNQ and graphene and BN quantum dots to find the changes in the electronic, magnetic and optical properties of these systems. We have studied different configurations as well as different sizes of the complex systems.

In the chapter 4, we have calculated electronic, magnetic, optical and charge transfer properties of the rectangular graphene and BN quantum dots. We have studied the effect of size variation, substitution and external electric field on the systems to find that these modifications on the systems change their properties in a significant amount.

In the sixth and final chapter, we have calculated electronic, magnetic and charge transfer properties of the X-shaped graphene and BN quantum dots. We have studied the effect of size variation and substitution of BN in GQD and C in BNQD systems to find the changes in the systems. We have found that some of the systems show very unique properties, like half-metallicity.

Chapter 2

Effect of Organic Molecule Adsorption on Single Layer MoS_2: A Detailed Theoretical Study

2.1 Introduction

Purely two dimensional (2-D) crystals like graphene, transition metal-dichalcogenite (MoS_2, WS_2, VS_2 etc.), Si or Ge 2-D sheets and boron-nitride sheet has become an interesting subject to study now a days because of their possible application in nano devices.[47, 48, 114-120] They are much more promising than bulk materials because of their lower dimensions and easier fabrications. In some of the cases, these materials are used as such, whereas they are modified for some other applications as for opto-electronic devices. For example, graphene, a widely studied two dimensional carbon material is a zero band-gap semiconductor or a semi-metal. So, to use it in electronics devices, opening of band-gap is required. Various methods, like, doping on graphene,[104, 105] reducing the dimensionality (1-D or 0-D),[59, 106, 107] molecular charge transfer[109-111, 160] or defect induced opening of band-gap[112, 113] have been well studied. Among them, adsorption of organic molecules on graphene and adding holes or electrons to the graphene surface and thus introducing a change in electronic structure by charge transfer interactions seems to be the easiest way to open up a band-gap in graphene as these types of systems are easy to fabricate and there is a direct control over the amount of doping also.

However, single layer Molybdenum di Sulfide (MoS_2) can be used in the field of electronics without any modifications, as these layers do not require any band-gap opening like graphene. They are intrinsic semiconductors as their bulk three dimensional (3 D) counterpart and also they have high carrier mobility.[115, 116, 136, 161] Thus, they are already being used as transistors[136, 137] or energy storage devices such as anode for Li or Mg ion batteries.[162-164] Bulk MoS_2 is a layered structure where Mo (IV) centers are sandwiched between sulfur atoms. MoS_2 are held together with weak van der Waals interactions, unlike graphene π-π stacking interaction. In fact, these systems are easy to prepare and also it is feasible to apply them in different devices.[131, 132, 161] Also, it was found that the phonons of the layered MoS_2 have lower energy than the phonons of bulk 3 D MoS_2.[161] Thus from these studies, one can easily predict that modification of band-gap of these systems can make them more versatile towards different device applications and the change in Fermi energy can detect whether they are compatible with a device or not.[165] Previously, many studies were performed by doping metal and non-metal adatoms or different molecules on MoS_2 to see the changes in the electronic and magnetic properties of MoS_2. Even, electron beam mediated creation of vacancies and adding impurity atoms to these vacancies have been shown to modify the electronic properties of single layer MoS_2.[63, 138, 139]'[140-142]

But all these processes require a lot of expensive experimental effort. Whereas, there can be much simpler way to obtain different band-gaps in single layer MoS_2. Herein, we study a simple method to tune the electronic properties of single layer MoS_2 that is organic molecules adsorption on MoS_2. Previously, different types of organic molecules (such as thiophene, benzothiophene, benzene, naphthalene, pyridine, quinoline etc.) were deposited on MoS_2 to study the adsorption energies of these types of systems.[166, 167] Here we have selected three molecules for our study, Tetracyanoquinodimethane (TCNQ), Tetracyanoethylene (TCNE) and Tetrathiafulvalene (TTF), where the first two are electron acceptors, while the last molecule is an electron donor. In fact, TCNQ and TCNE are electron acceptors because of the presence of 4 cyano groups and TTF is an electron donor molecule because of the presence of S lone pairs of electrons. From our study, we can suggest that all the three molecules get physisorbed on the single layer MoS_2 via π stacking interactions. Also, we have calculated the charge transfer interaction and the modification of the band-gap of MoS_2 single layer in our study.

2.2 Computational Details

In the present study, first-principle calculations have been performed, to obtain all the electronic and optical properties of the systems, using the density functional theory (DFT) method as implemented in the SIESTA package.[168] Generalized gradient approximation (GGA) in the Perdew–Burke–Ernzerhof (PBE) form[169] has been contemplated for accounting the exchange-correlation function. Double ζ polarized (DZP) numerical atomic-orbital basis sets have been used for Mo, S, C, N and H atoms. Norm-conserving pseudo-potentials[170] are considered with the $4d^5$ $5s^1$, $3s^2$ $3p^4$, $2s^2$ $2p^2$, $2s^2$ $2p^3$, $1s^1$ valence electrons for Mo, S, C, N and H, respectively in the fully nonlocal Kleinman–Bylander form.[171] A reasonable mesh cut-off of 400 Ry is used for the grid integration to represent the charge density. All the structures are considered to be optimized if the magnitude of the forces acting on all atoms is less than 0.04 eV/Å. We have sampled the Brillouin zone by 5 × 5 × 1 k-points using the Monkhorst-Pack scheme for structural optimization. Whereas, for electronic property calculations, we have sampled the Brillouin zone by 10 × 10 × 1 k-points. Periodic boundary condition and the supercell approximation are taken in such a way so that the distance between an absorbate molecule and its periodic image is more than 10 Å so that any interaction between adsorbates can be avoided. The MoS_2 supercell contains 64 Mo atoms and 128 S atoms. We have kept a 15 Å vacuum along the z axis and found that this is sufficient to get the energy convergence and optimized configurations. The optical conductivity measurement is also done by sampling the Brillouin zone by 10 × 10 × 1 k-points.

2.3 Results and Discussion

In our present study, at first, we have examined the interaction between single layer MoS_2 and Tetracyanoquinodimethane (TCNQ), Tetracyanoethylene (TCNE) and Tetrathiafulvalene (TTF) molecules (figure 2.1). We have considered our MoS_2 layer to be nonmagnetic as suggested in a previous study.[138]

Here, we have found that all the molecules, that is, TCNE, TCNQ and TTF are physisorbed on the MoS_2 layer. In order to figure out the relative stabilities of the systems, we have calculated the adsorption energies of the molecules on MoS_2. The system with higher adsorption energy (i.e. more negative value) is more strongly adsorbed on the MoS_2 layer. We have calculated the adsorption energy using the following equation,[160]

$$\Delta E_{\mathrm{adsorption}} = E_{\mathrm{molecule+MoS_2}} - E_{\mathrm{MoS_2}} - E_{\mathrm{molecule}} \tag{2.1}$$

where $\Delta\mathbf{E}_{\mathbf{adsorption}}$, $\mathbf{E}_{\mathbf{molecule+MoS_2}}$, $\mathbf{E}_{\mathbf{MoS_2}}$ and $\mathbf{E}_{\mathbf{molecule}}$ are the adsorption energies, total energies of the optimized molecule-MoS_2 systems, total energy of the MoS_2 layer and total energies of the absorbate molecules, respectively.

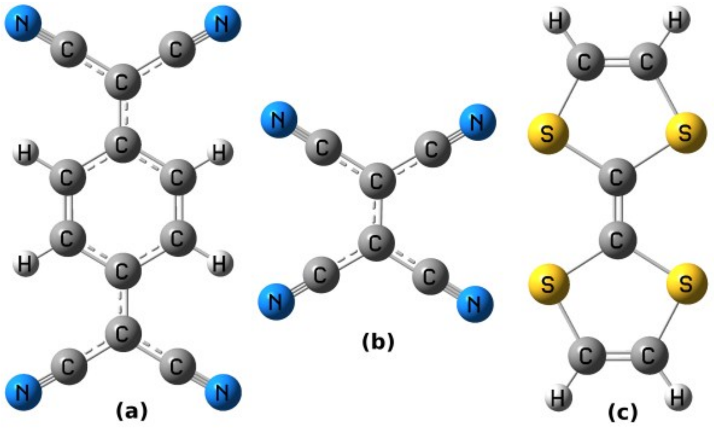

Figure 2.1: Molecular structure of (a) Tetracyanoquinodimethane (TCNQ) (b) Tetracyanoethylene (TCNE) and (c) Tetrathiafulvalene (TTF) molecules.

From the optimized structures (as given in Figure 2.2), we have calculated the distance between the molecules and the MoS_2 layer and also the orientation of the molecules on single layer MoS_2. We have found that TCNQ molecule is absorbed on the MoS_2 layer at about 3.17 Å above the layer. Similarly, TCNE and TTF molecules are stable at distances of 3.12 Å and 3.42 Å, respectively. These are the shortest distance between the adsorbate molecules and the sulfur surface of the single layer MoS_2.

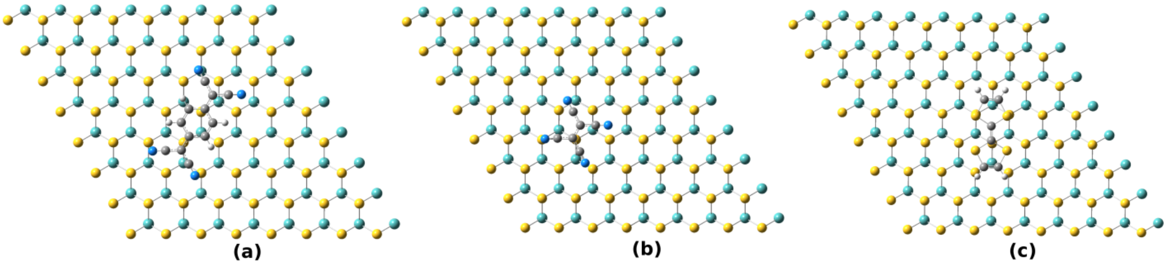

Figure 2.2: Optimized geometries of (a) TCNQ (b) TCNE (c) TTF on MoS_2 single layer (Sky blue balls, yellow balls, grey balls, dark blue balls and white balls are Mo, S, C, N and H atoms respectively).

From the optimized geometries, we have found that, in the case of TCNQ and TCNE, the molecules are on top of the S atoms of MOS_2 layer, and TTF is aligned in such a way so that two S atoms of TTF sit on top of the two S atoms of MoS_2 layer. So electron transfer from TTF S atom to MoS_2 S atom is feasible. Also, all the molecules are almost parallel on the upper sulfur surface of the single layer MoS_2 that means there is no indicative amount of bending in the molecules (figure 2.3).

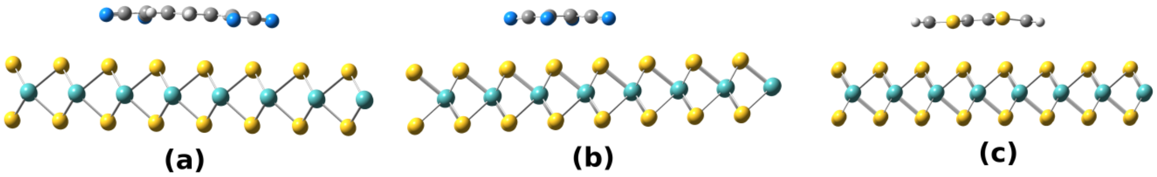

Figure 2.3: Side-view of (a) TCNQ (b) TCNE (c) TTF molecules on MoS_2 single layer.

There is no chemical bond formation between the molecules and the MoS_2 layer as the distance between them is too long to form a chemical bond. The physisorbed molecules are stable because of the π stacking interactions between the molecules and the MoS_2 layer. In fact, the adsorption energy values also prove the same. There is van der Waals interaction present between the molecules and MoS_2 similar to that of graphene system.[160] We have found that TCNQ has the highest adsorption energy (most stable) on MoS_2 and TCNE has the lowest adsorption energy (least stable). This trend is analogous to the molecular surface of TCNQ, TCNE and TTF. The molecular surface area varies in the order: TCNQ > TTF > TCNQ (as can be seen in figure 2.1). So it is apparent that larger the surface area, higher the π interaction and more stable is the molecule on MoS_2 layer in contrast to graphene, where charge transfer interaction gives the stability to the system.[160] To make this point clear, we have done the Mülliken population analysis and have found out that there is a negligible amount of electron transfer (0.02 e and 0.04 e respectively) from the S atoms of MoS_2 layer to TCNQ and TCNE (as these molecules are electron acceptors), respectively. In fact, there is relatively higher amount of electron transfer (0.14 e) from TTF to the S atoms of MoS_2 layer. We have investigated the effect of concentration of absorbed molecules on the MoS_2 and have found that in case of TCNE and TCNQ change of concentration does not change the charge transfer in any significant amount, but in case of TTF when we have decreased the size of the supercell size from 192 atoms to 96 atoms, charge transfer increased by a small amount (from 0.14 e to 0.39 e) but the system becomes unstable (adsorption energy increases). But further increase in supercell size from our original 192 atoms containing supercell to 288 atoms containing supercell, charge transfer does not change.

So it is evident that the interaction between the π surface of the molecules and the p orbital on S is responsible for the stable physisorption. In Table 2.1, we have given all the data for the MoS_2-molecule systems.

Table 2.1: Adsorption energies, distances and charge transfers between the molecules and single layer MoS_2. In case of TTF, the data correspond to 96/192/288 atoms containing supercells (we have not given data for other systems as there are no significant chages).

Molecule	$\Delta E_{adsorption}$ (eV)	Distance (Å)	Charge Transfer (e)
TCNQ	-1.76	3.17	-0.02
TCNE	-1.09	3.12	-0.04
TTF	-1.27/-1.42/-1.6	3.47/3.42/3.42	+0.39/+0.14/+0.14

We have plotted the wave functions of the adsorbate -MoS_2 systems and we have found that the highest occupied molecular orbital (HOMO) for TTF and the lowest unoccupied molecular orbital (LUMO) for TCNQ and TCNE remain localized on the molecules. These plots also indicate that the interaction between the molecules and the MoS_2 layer is purely non-covalent interaction as there is no significant overlap between the molecular wave functions and the MoS_2 layer wave functions (figure 2.4 and figure 2.5).

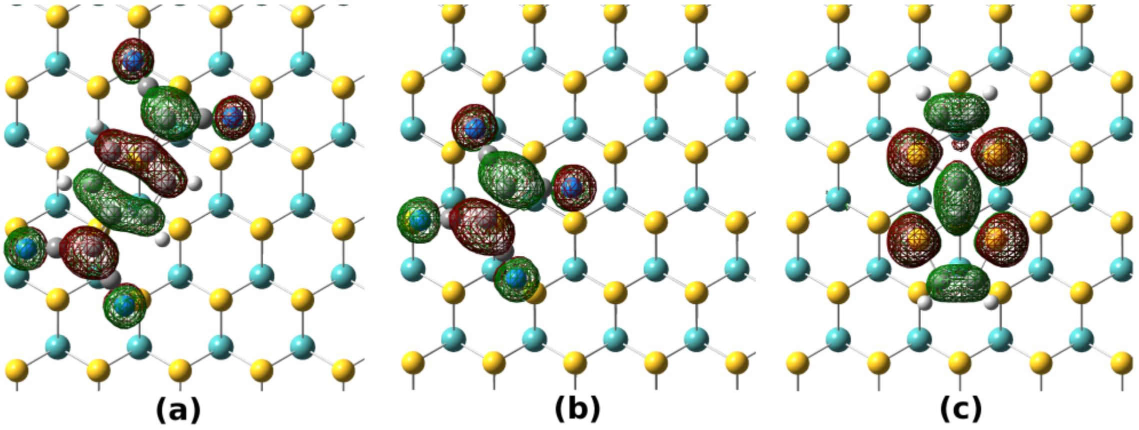

Figure 2.4: Wave function plots of (a) TCNQ, (b) TCNE and (c) TTF on MoS_2 layer (isovalue is 0.02 e/Å^3 for all the cases).

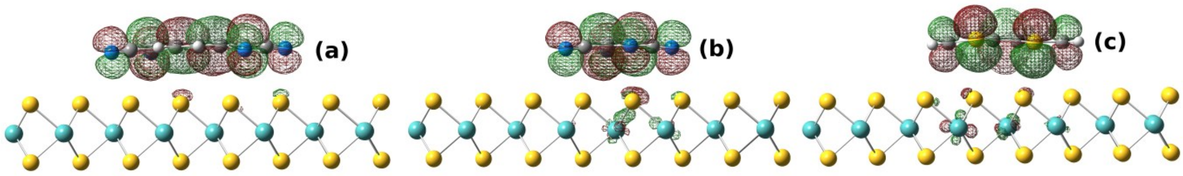

Figure 2.5: Side-view of the wave function plots of (a) TCNQ, (b) TCNE and (c) TTF on MoS_2 layer (isovalue is 0.02 e/Å^3 for all the cases).

Next, in order to find out the effects in the electronic properties of the MoS_2 layer, we plotted the band structure, Density of States, as well as projected density of states (pDOS) of the pure single layer MoS_2 and the MoS_2-molecule adsorbed systems. We have found that MoS_2 has a direct band-gap of 1.809 eV (which is comparable with previous results [116, 130]) at high symmetry K point (0.667, 0.333, 0.000) which does not change much upon adsorption of TCNQ and TCNE (1.81 and 1.807 eV) that indicates that there is no significant charge transfer in the systems. But a localized molecular state appears in between this energy range. For both the cases, the molecular level appears above Fermi level. Because of the electron deficient nature of TCNQ and TCNE, they provide one extra localized acceptor level below the conduction band of the MoS_2 layer. In the case of TTF adsorption on the layer, there is a minute change in the band gap of MoS_2 which is about 1.804 eV. This indicates that there is a minute amount of charge transfer present between the TTF molecule and the MoS_2 layer. In this case, one localized molecular level appears below the Fermi level. This is expected because of the electron rich nature of TTF.[160] TTF acts as electron donor and thus provides an extra localized level above the valence band of the MoS_2 layer.

In figure 2.6, we have plotted the band structures of the MoS_2 layer as well as the adsorbate-MoS_2 systems. From the figure, the presence of a flat band (red line) is recognizably visible in all the cases. This flat state corresponds to isolated non-dispersive mid-gap molecular state. In the case of TCNQ and TCNE, this band appears above the Fermi level, and in case of TTF this flat band appears below the Fermi level because of the fact discussed previously. Gamma point wave function analysis also supports this argument as we have found a localized wave function for the molecule (figure 2.4).

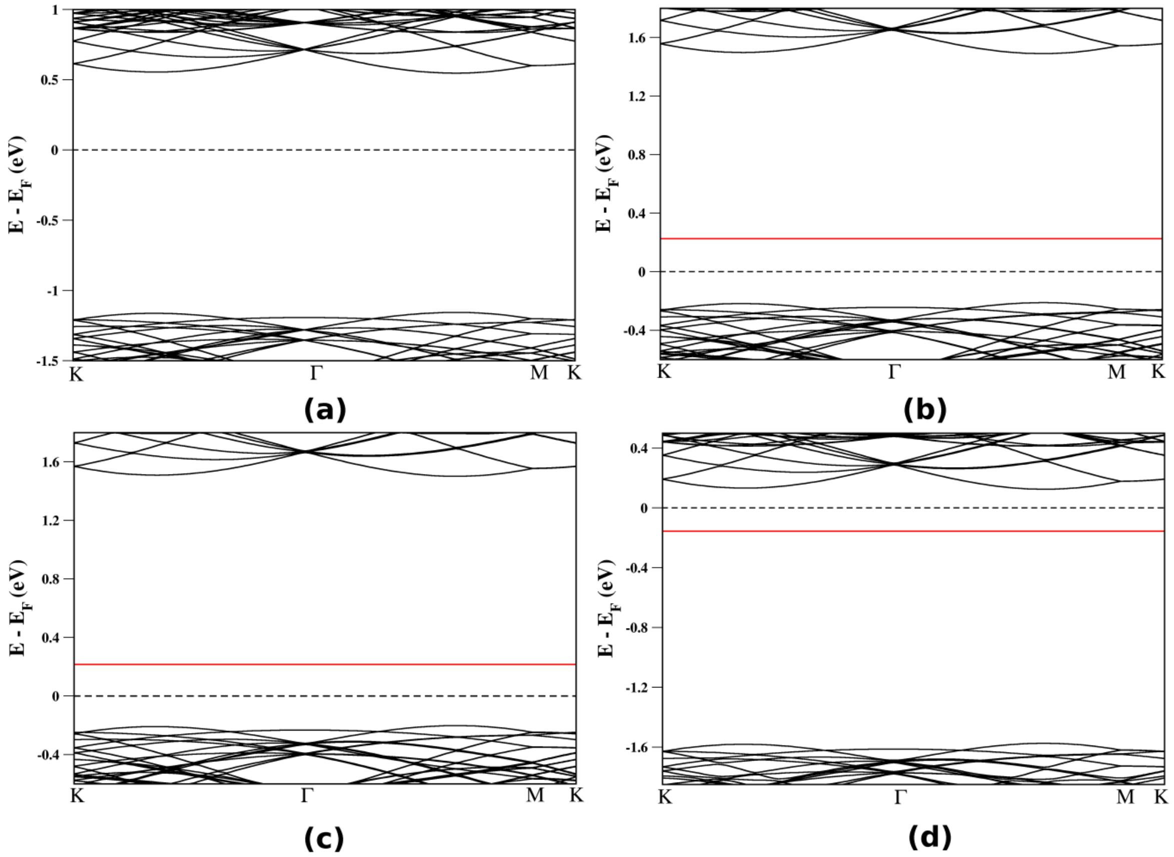

Figure 2.6: Band structure plots of (a) single layer MoS_2, (b) MoS_2-TCNQ, (c) MoS_2-TCNE and (d) MoS_2-TTF. The red line corresponds to the mid-gap molecular level. The Fermi level is set to zero the K, M and Γ point have the coordinates (0.667, 0.333, 0.000), (0.5, 0.5, 0.5) and (0.0, 0.0, 0.0) respectively.

Next, in order to confirm our findings, we have plotted the Density of States (DOS) and the projected density of states (pDOS). Here, from plot of the total density of states (black line), Mo and S atoms contributions (blue and orange lines respectively) to the DOS and the Mo *d*-orbital and S *p*-orbital contributions (red and green lines respectively) to the DOS it is clear that near the Fermi level Mo *d*-orbital contribution is maximum. This is found in previous studies also.[116] From the figure it is evident that in all of the molecule-MoS_2 systems, there is a localized molecular level present. In case of TCNQ and TCNE, this level is above Fermi level and in case of TTF, this localized level is below Fermi level. These levels do not have any contribution from the MoS_2 sheet.

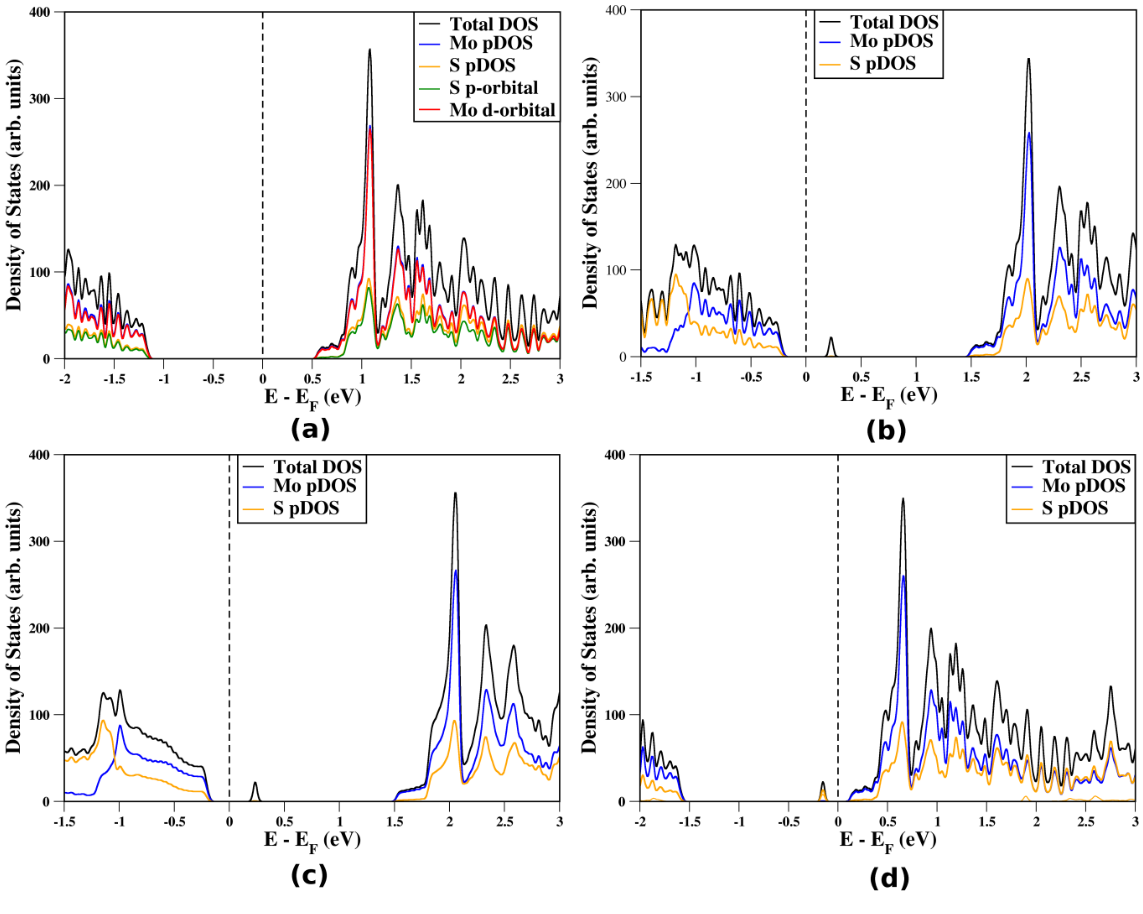

Figure 2.7: pDOS plots of (a) single layer MoS_2, (b) MoS_2-TCNQ, (c) MoS_2-TCNE and (d) MoS_2-TTF. The Fermi level is set to zero. The Gaussian broadening parameter used is 0.025 eV.

Fermi levels of the systems also have been shifted form the pure MoS_2 layer Fermi level (-3.45 eV). For TCNQ and TCNE adsorption, the Fermi level has been shifted down (-4.41 eV and -4.42 eV respectively). However, for the case of TTF adsorption, Fermi level shifts to higher energy value (-3 eV). This clearly suggests that electron donor molecule can shift the Fermi level up to higher energy by electron donation and electron acceptor molecules can shift the Fermi level down to lower energy value. The actual reason behind this is can be explained in the following way, that, adsorption of TTF on the MoS_2 sheet introduces an extra donor level in the system, as a consequence Fermi level shifts up. The opposite trend is observed in case of a acceptor molecule.

Finally, we have analyzed the low frequency region of the optical conductivity, as this quantity helps to understand the extent of electron transfer from the top of the valence band to the bottom of the conduction band with the change in the energy. So, from this, we have calculated the charge transfer interactions present between the molecules and MoS_2 layer because these types of charge transfer generally occurs between the extra donor or acceptor level and the sheet.

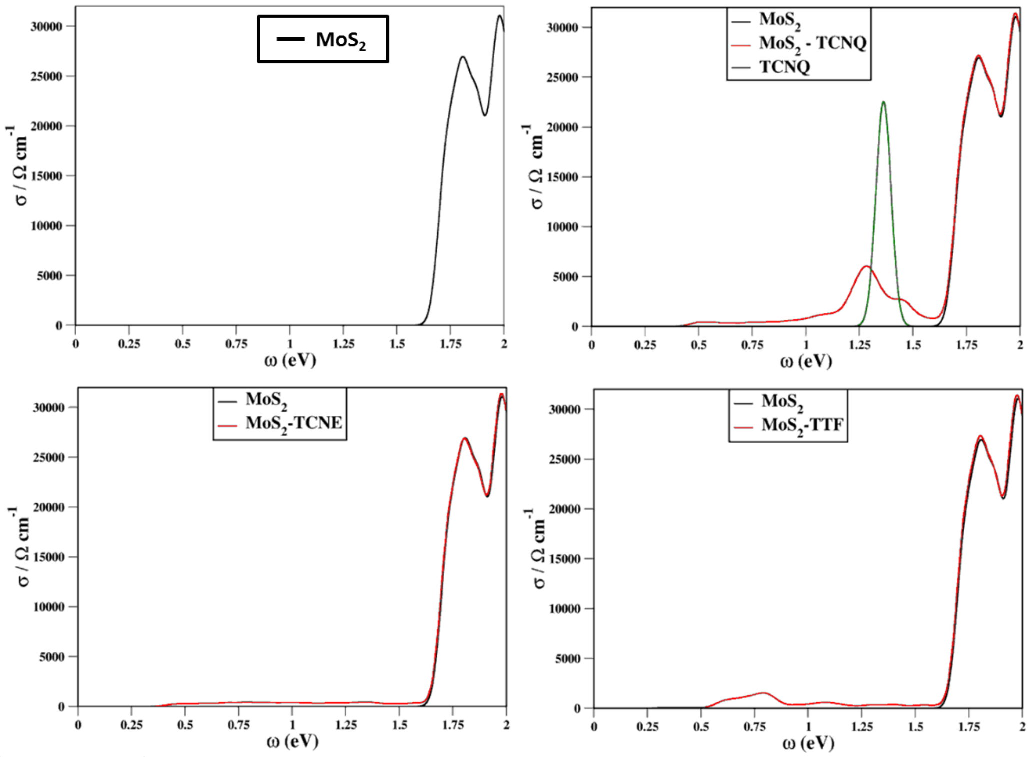

Figure 2.8: Low frequency region of optical conductivity plots for pure MoS_2 single layer and MoS_2-molecule composites. The Gaussian broadening parameter used is 0.05 eV.

From the plot of optical conductivity, we have found that the lowest peak for single layer MoS_2 comes at about 1.8 eV, which corresponds to its band-gap. For pure TCNQ, the peak appears at about 1.37 eV, but TCNE or TTF does not show any peak in this energy region. MoS_2-TCNQ system shows that the molecular peak is little red shifted and flattened; this is because of the MoS_2-TCNQ interaction and the presence of intra-band electronic transition. MoS_2-TCNE does not show any significant change in low frequency optical conductivity, a clear evidence of absence of any charge transfer. In Case of MoS_2-TTF composite system, there is an extra peak coming at lower frequency region. This is because of the charge transfer from TTF to MoS_2. Therefore, from this study also, we make it clear that there is no significant charge transfer for TCNQ and TCNE but TTF can donate charge (although small) to MoS_2 layer.

2.4 Conclusion

In this study, we have shown that organic donor molecule (TTF) and acceptor molecules (TCNQ and TCNE) can add extra holes and electrons, respectively, to the MoS_2 single layer and as a consequence can modify the electronic properties of the single layer MoS_2. We find that all the composite systems are stable as they have negative adsorption energies and the molecules are physisorbed on the MoS_2 layer. The physisorbed molecules are stable because of the π stacking interactions between the molecules and the MoS_2 layer. Our Mülliken population analysis shows that, when the adsorbed molecule is an electron-donor then there is a minute amount of charge transfer from the molecule to MoS_2. On the other hand, when the adosrbate is an electron-acceptor molecule then there is no significant charge transfer. We have found that the concentration of doping does not affect the charge transfer in the case of TCNQ or TCNE, whereas in the case of TTF, increase in molecular doping concentration results in more charge transfer. The above conclusions regarding the charge transfer have also been confirmed with the low-frequency optical-conductivity calculations. Band structure, DOS and pDOS plots evidently showed that there is a presence of isolated localized energy level near the Fermi-energy, which arise from the adsorbed molecule. In case of TCNQ and TCNE, this localized energy level is the acceptor level above the Fermi-energy, and in the case of TTF, it is the donor level below the Fermi-energy.

Chapter 3

Molecular Charge Transfer Interactions to Tune the HOMO-LUMO Gaps of Graphene and BN Quantum Dots

3.1 Introduction

Since the experimental discovery of graphene in 2004,[48] it has become a potent candidate for the application in nano devices because of its unique properties.[105, 172-177] But, pure graphene is a zero band-gap semiconductor or semi-metal. So, it cannot be used into opto-electronic devices without any modification. Unlike graphene, its low-dimensional graphitic sisters, namely, 1-D nanotubes, 1-D nanoribbon and 0-D quantum dots can be used directly in opto-electronic devices because they have an intrinsic band-gap.[61, 71, 80, 81, 178] Band-gap of a graphene nanoribbon depends upon its width, passivation and edge geometries.[60, 61, 76, 179] Similarly, graphene quantum dots (GQDs) are also found to possess unique electronic properties depending upon their size, edge passivation and shape.[80, 81] Because of their tunable energy gaps, GQDs have been shown to be used in solar cells [82] or LEDs [83].

Two dimensional inorganic (2-D) crystals like boron-nitride (BN) sheet, transition metal-dichalcogenites (MoS_2, WS_2, and VS_2 etc.) and Si or Ge 2-D sheet also have become interesting subjects for study due to their possible application in different nano devices. [115-118, 180] These materials are either semiconductors (e.g. MoS_2 [115, 116]) or insulators (e.g. BN sheet [117]). So, these materials can be used in the opto-electronic devices, without any further modification, because of their finite band-gap.

Molecular charge transfer interactions in these low dimensional systems can fine-tune their band-gaps as well as it can open up a band-gap in graphene.[96, 108-111, 181] Depending upon the electronic donor or acceptor natures of the dopant molecules, these systems can be n or p-doped because of molecular charge transfer interactions.[96, 108-111, 181] So, for the purpose of modulating the band-gaps in these systems, different organic molecules are used.[96, 108-111, 181]

Two such types of molecules are Tetracyanoquinodimethane (TCNQ) and Tetrathiafulvalene (TTF), where the first molecule is an electron acceptor and the second molecule is an electron donor. The electron accepting properties of TCNQ is because of the presence of 4 cyano groups and TTF is an electron donor molecule because of the presence of sulfur lone pairs of electrons. Previously, doping of these molecules on graphene,[108] carbon nanotubes,[181] BN sheet and BN nanoribbons[96] have been well studied. It was found that TCNQ can add extra holes to these systems, whereas TTF can add extra electrons.[96, 108, 181]

In this present study, we have calculated the charge transfer interaction between graphene or BN quantum dots (QDs) and TCNQ or TTF. From the results we have got, we can suggest that both the molecules are physisorbed on the GQDs or BNQDs. Also, we have calculated the amount of charge transfer present between the molecules and the QDs.

3.2 Computational Details

All the electronic and optical properties of the systems have been calculated using the density functional theory (DFT) method as implemented in the SIESTA package.[168] Generalized gradient approximation (GGA) in the Perdew–Burke–Ernzerhof (PBE) form[169] has been used to account for the exchange-correlation function. Double-ζ-polarized numerical atomic-orbital basis sets have been used for the C, N, S and H atoms.

Norm-conserving pseudo-potentials[170] in the fully nonlocal Kleinman–Bylander form have been used for all the atoms.[171] A mesh cut-off of 400 Ry is used for the grid integration to represent the charge density. All the structures are considered to be optimized if the magnitude of the forces acting on all atoms is less than 0.04 eV/Å. As the systems are zero-dimensional, all the calculations are performed only at the gamma (Γ) point of the Brillouin zone. A vacuum of 20 Å has been maintained in all the three directions to avoid any unwanted interactions between the systems and their periodic images.

3.3 Results and Discussion

Structure and Stability:

In this work, we have considered both graphene and boron-nitride quantum dots of rectangular geometry and studied the effect of organic molecular doping to them. These rectangular quantum dots have a zigzag edge along their length direction and an armchair edge along their width direction. Following the convention of the graphene nanoribbons,[179] we represent these QDs as (21, 8)-QDs. Here, 21 and 8 are the number of atoms along the zigzag-edge (length, ~2.2 nm) and the armchair-edge (width, ~1.8 nm), respectively. Tetracyanoquinodimethane (TCNQ) and Tetrathiafulvalene (TTF) (figure 3.1) have been considered as the dopants.

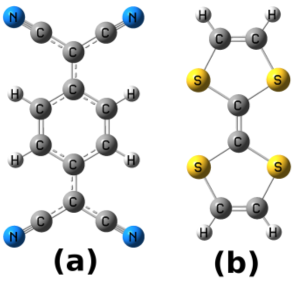

Figure 3.1: (a) Tetracyanoquinodimethane (TCNQ) and (b) Tetrathiafulvalene (TTF)

molecules

Table **3.1**: Energies of the GQD-dopant complexes with a variation in the position of the dopant on QD. Energies are scaled to the most stable conformation.

QD-dopant Complex	Energy of the structure in Figure 3.2/3.3 (eV)	Energy of the structure in Figure 3.4 (eV)
GQD-TCNQ	0.00	0.06
GQD-TTF	0.00	0.04
BNQD-TCNQ	0.00	0.05
BNQD-TTF	0.00	0.04

From the previous studies on the interaction of TCNQ and TTF with graphene [108] and boron-nitride, [96] we know that both the TCNQ and TTF are physisorbed on these systems, and they are stabilized at a distance of ~ 3.2 Å over graphene and at a distance of ~ 3.5–3.6 Å over boron-nitride sheet. So, for the optimization calculations, we chose the initial distances of 3.2 Å and 3.5 Å for the dopants on top of the GQDs and BNQDs, respectively. Also, while choosing the initial arrangement of the dopant on top the QDs we followed the references 29 and 31(similar to figures 3.2 and 3.3 of this article), respectively, for GQDs and BNQDs. But, to check the universality of these arrangements we have also considered the other configurations, namely, the reported stable arrangement for “TTF on BN-sheet” as an initial arrangement for “TTF on GQD” and the reported stable arrangement for “TCNQ on graphene” as an initial arrangement for “TCNQ on BNQD” etc. as shown in figure 3.4. From these studies we recognized that (see table 3.1) the most stable arrangements of dopants didn’t change with dimensionality, for example, they are same for BN-sheet and BNQD.

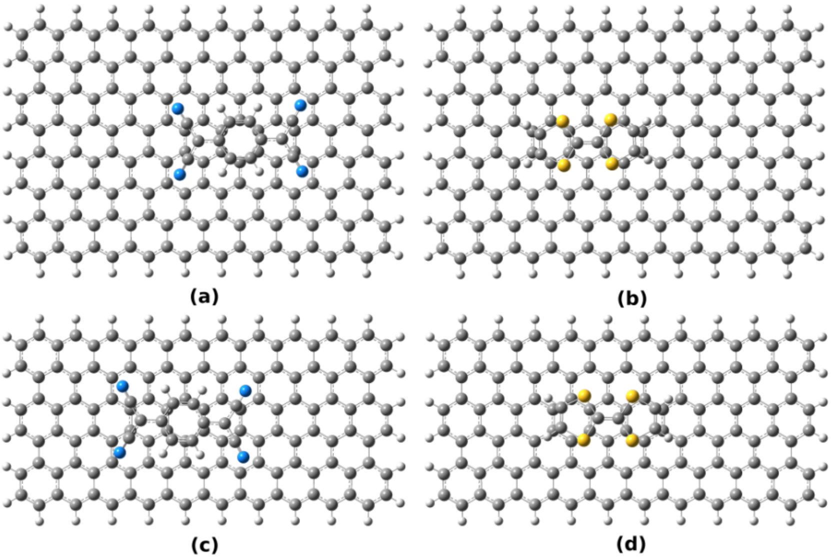

Figure 3.2: (a) TCNQ adsorbed on (21, 8) GQD, (b) TTF adsorbed on (21, 8) GQD, (c) TCNQ adsorbed on (21, 6) GQD and (d) TTF adsorbed on (21, 6) GQD.

.

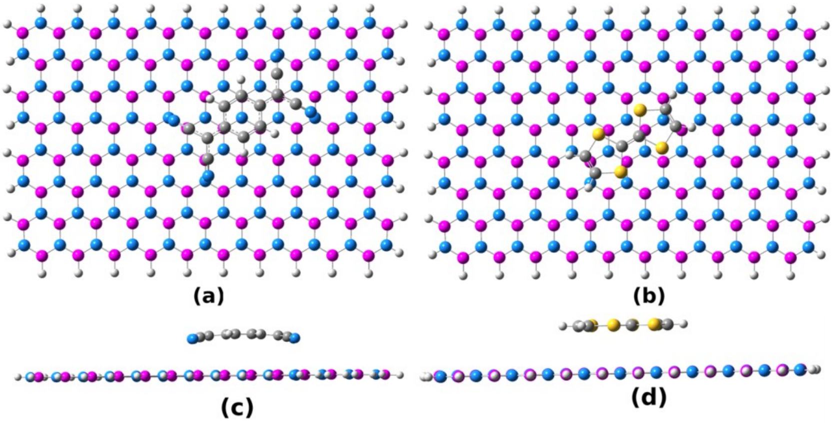

Figure 3.3: (a) TCNQ-(21, 8) BNQD, (b) TTF-(21, 8) BNQD, and side-view of (c) TCNQ-(21, 8) BNQD, (d) TTF-(21, 8) BNQD

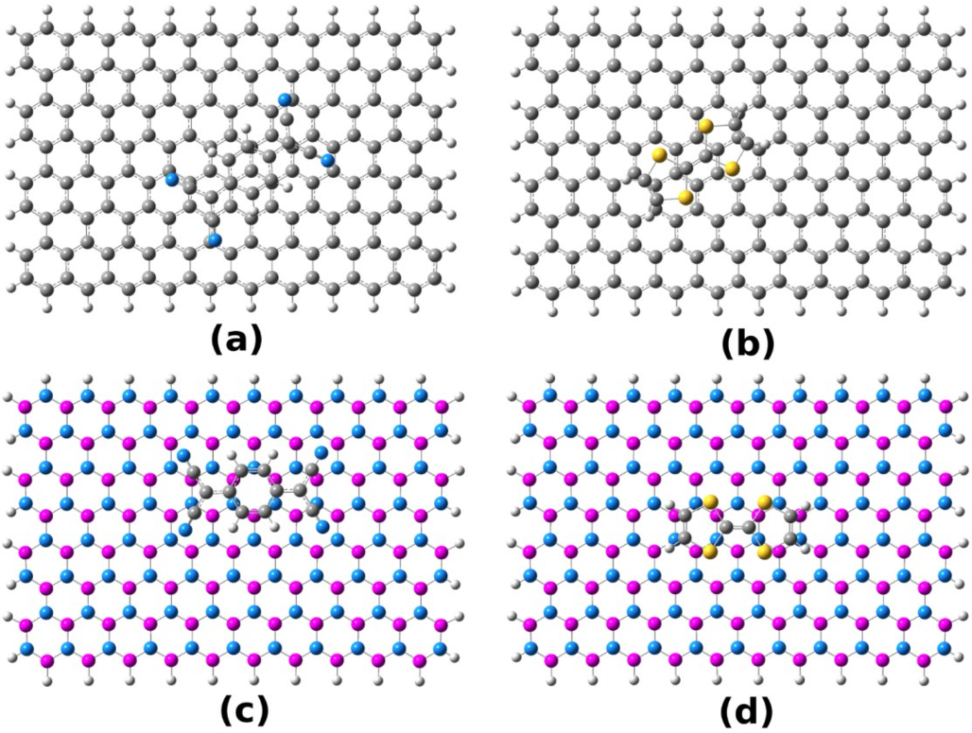

Figure 3.4: (a) TCNQ adsorbed on (21, 8) GQD, (b) TTF adsorbed on (21, 8) GQD, (c) TCNQ adsorbed on (21, 8) GQD and (d) TTF adsorbed on (21, 8) GQD. In this figure, the positions of the TCNQ and TTF on GQD are swapped with their positions on BNQD in the figure 3.2, and vice-a-versa for BNQD.

Table 3.2: Energies of the complexes in different spin states (with respect to their ground-state) are given.

Molecule	AFM (meV)	FM (meV)	NM (meV)
GQD-TCNQ	0	20	750
GQD-TTF	0	90	770
BNQD-TCNQ	10	–	0
BNQD-TTF	10	–	0

Next, as both graphene and boron-nitride nanoribbons are shown to be spin-polarized, [78, 182] under different conditions, we have also considered the spin-polarization in all our studies and the energies of the complexes in different spin-states, with respect to their ground-states, are given in table 3.2. From these spin-polarized calculations, we find that the GQD-dopant complexes are anti-ferromagnetic (AFM) in their ground state, whereas, the BNQD-dopant complexes are nonmagnetic (NM) in their ground state. Next, the stability of each complex in its ground-state has been calculated and the formation energy (E_{form}) values of all the (21, 8) complexes are given in the table 3.3.

Table 3.3: Formation energy of the complexes, optimum-distance of dopants above QDs and the amount of charge-transfer between dopants and QDs for (21, 8) QDs are given.

Molecule	E_{form} (eV)	Distance (Å)	Charge-transfer (e)	E_{form} (kcal/mol)
GQD + TCNQ	-2.01	3.11	-0.43	-46.35
GQD + TTF	-1.45	3.15	+0.12	-33.44
BNQD + TCNQ	-1.66	3.38	-0.18	-38.28
BNQD + TTF	-1.34	3.41	+0.21	-30.90

Formation energy is calculated using the equation "$E_{form} = E_{complex} - E_{dopant} - E_{QD}$", where E_{form} is the formation energy of the complex and $E_{complex}$, E_{dopant} and E_{QD} are the absolute energies of the complex, dopant and quantum-dot, respectively. It is known that, [108] greater the formation energy of the complex stronger the interaction between the dopant and the substrate (here, QDs). From table 2, it is apparent that the dopants are strongly adsorbed on GQDs than on BNQDs. Presence (absence) of a π-surface through which a GQD (BNQD) can (cannot) interact with its dopant's π-surface could be the main reason for the strong (weak) interaction between GQDs (BNQDs) and the dopants. Values of formation energy are clearly reflected in the distances between the dopants and the QDs–greater the distance lesser is the formation energy–in their optimized structures (see columns 3 and 5 of table 3.3). In what follows, first we will discuss the properties of the GQD-dopant complexes and then we will switch to the BNQD-dopant complexes.

GQDs + Dopants:

Optimized structures of the GQD-dopant complexes, from which the distance between dopants and GQDs are calculated, are given in figure 3.2. In their minimum energy configurations, TTF's C=C bond is exactly on top of the center of a benzenoid ring of GQD and TCNQ's benzenoid ring is exactly on top of the benzenoid ring of GQD in staggered position. From the optimized geometries we find that, TCNQ is stable at a distance (this is the least distance between GQD plane and dopant) of ~ 3.11 Å and TTF is stable at a distance of ~ 3.15 Å on top of the (21, 8) GQDs. Also, both the dopants and GQD have bent from their planar structures, but in opposite directions (i.e. dopant has bent in convex manner and GQD in a concave manner). Among the dopants, TCNQ has bent more when compared to TTF (as shown in figures 3.2a, 3.2b), and in the GQD, bent has occurred mainly in the area below the dopant.

We have also calculated the E_{form} values of the GQD-dopant complexes (see table 2), and we find that these values are comparable (with in 2 kcal/mol) to the E_{form} values of the graphene-dopant complexes, [108] suggesting that the dopants interact with the graphene and GQDs in a similar manner. The lesser E_{form} values (< 50 kcal/mol) also suggest that dopants are just physisorbed on the GQDs. The argument regarding the physisorption is further supported by the large distance of separation–a distance (> 3 Å) at which a chemical bond formation has not been shown till date between a carbon atom and any other atom present in the study[183]–between the dopant and the GQDs (see table 2). Importantly, a larger value of distance separation, a lesser value of bending and a lesser E_{form} value of TTF when compared to TCNQ clearly indicates that there is a strong (weak) interaction between TCNQ (TTF) and GQD.

BNQDs + Dopants:

Optimized structures of the BNQD-dopant complexes are given in figure 3.3. The BNQD-TCNQ and BNQD-TTF distances, in their optimized structures, are 3.38 Å and 3.41 Å, respectively. Similar to the GQD-dopant complexes, BNQD-dopant complexes have also deviated from their planarity. Again, TCNQ has bent more compared to the TTF, proving its stronger interaction with BNQD (as shown in figures 3c, 3d). Bending of TCNQ on top of BN-sheet has been observed previously [96] and the reason is predicted as the weak dipolar interaction between the TCNQ and BN-sheet. This is different from the case of graphene-TCNQ, where, the interaction was predicted to be mainly through π-surfaces of dopant and graphene. [108] So, we also expect that the nature of interaction between BNQD and dopants as the weak dipole–dipole and/or electrostatic, similar to its 2-D counterpart. [96, 108] Finally, we noticed that in their optimized structures, TTF's middle C=C bond is on top of the hexagonal ring of the BNQD and TCNQ's benzenoid ring is on top of the BNQD's hexagonal rings in a manner such that three of its six carbon atoms are top of the hollow sites of the BNQD's hexagonal rings (exactly similar to the Bernald-stacking of graphite [177]). Again, the absence of any chemical bonds between BNQD and the dopants suggests that these molecules are physisorbed.

Electronic properties:

In this section, first we will explain the charge-transfer between the dopant-QD complexes. Then we will describe the changes in the H-L gap for all the systems, and finally, we will try to explain some of these results based on the density of states (DOS) and projected-DOS (pDOS) plots.

Charge-transfer: In order to find out the amount of charge-transfer between QDs and dopants, we have performed the Mülliken population analysis and this charge-transfer data is given in table 3.3 for all the (21, 8)-GQD/BNQD-dopant complexes. Population analysis shows that these QDs have the ability to both give and take the charges from the dopants depending on their nature. From table 2 we can also find that, among the QDs, GQD can give electrons to the dopant easily rather than taking from it and exactly the opposite behavior is exhibited by the BNQD. Now comparing the dopants, there is a significant amount of charge-transfer (see table 3.2) from GQD to TCNQ and a relatively less amount of charge-transfer from TTF to GQD. The latter is mainly due to the electron-rich nature of the GQD. On the other hand, the electron poor nature of the BNQD could be the reason for the larger charge-transfer from TTF to BNQD compared to the charge-transfer from BNQD to TCNQ.

HOMO–LUMO gap: As mentioned earlier, it is known that the low-dimensional graphene and BN systems can be spin-polarized. So, we have calculated the spin-polarized HOMO–LUMO (H-L) gaps for all the systems and their values for (21, 8)-QD-complexes are given in table 3.4. From table 3.4 we can notice that, pure (21, 8)-GQD is a semi-conductor with an H-L gap of 0.54 eV and pure (21, 8)-BNQD is an insulator with an H-L gap of 4.03 eV, for both the spin channels. Interestingly, H-L gap of both the QDs have decreased to more than half of their original H-L gap (though the decrement is huge for BNQDs) with the addition of dopants. In addition to the decrement in the H-L gap, we have also found a spin-dependent H-L gap in the TCNQ-GQD system. But, this spin dependent H-L gap in not observed for the case of TTF. Finally, it is known that the chemical reactivity of a molecule is dependent on the H-L gap in an inverse manner–that is, higher the gap, lower the reactivity. [184] Assuming that the charge-transfer will occur only when a system is chemically reactive, we find that our results on charge-transfer also reflects the same–larger the H-L gap, greater the charge-transfer (please compare columns 2/3 and 4 of table 3.4)–though, not quantitatively.

Table 3.4: Spin-polarized H-L gaps of TCNQ and TTF adsorbed (21, 8)-QDs. Charge-transfer values are given, again, for comparison.

System	H-L gap		Charge-transfer (e)
	α-spin (eV)	β-spin (eV)	
Pure GQD	0.54	0.54	-
TCNQ-GQD	*0.21*	*0.09*	-0.43
TTF-GQD	0.22	0.22	+0.12
Pure BNQD	4.03	4.03	-
TCNQ-BNQD	0.73	0.73	-0.18
TTF-BNQD	1.98	1.98	+0.21

DOS and pDOS:

In order to further understand the reasons behind the decrement in the H-L gap in QD-dopant complexes and spin-polarized H-L gap in TCNQ-GQD system we have plotted the DOS and pDOS of all the (21, 8) complexes, as shown in figure 4. From this figure it is apparent that, (a) the DOS of a QD-dopant complex is nearly equal to the sum of the individual DOS of the QD and the dopant and the minor changes are due to the complex formation. This observation shows that the interaction between the dopant and the QD is weak in nature. Also, this proves that the dopant is just physisorbed on QDs; (b) there is a shift in the Fermi-level towards the HOMO or LUMO depending on whether the dopant is an electron-acceptor (TTF) or electron- donor (TCNQ), respectively; (c) major amount of the dopant levels are concentrated near the Fermi-level and are in between the HOMO and LUMO levels corresponding to the un-doped QDs; (d) the position of these major amount of dopant levels is dictated by the electron-accepting/donating nature of the dopant. Thus, for TCNQ–being an electron acceptor–it is just below the LUMO of the QD, and for TTF–being an electron donor–it is just above the HOMO of the QD.

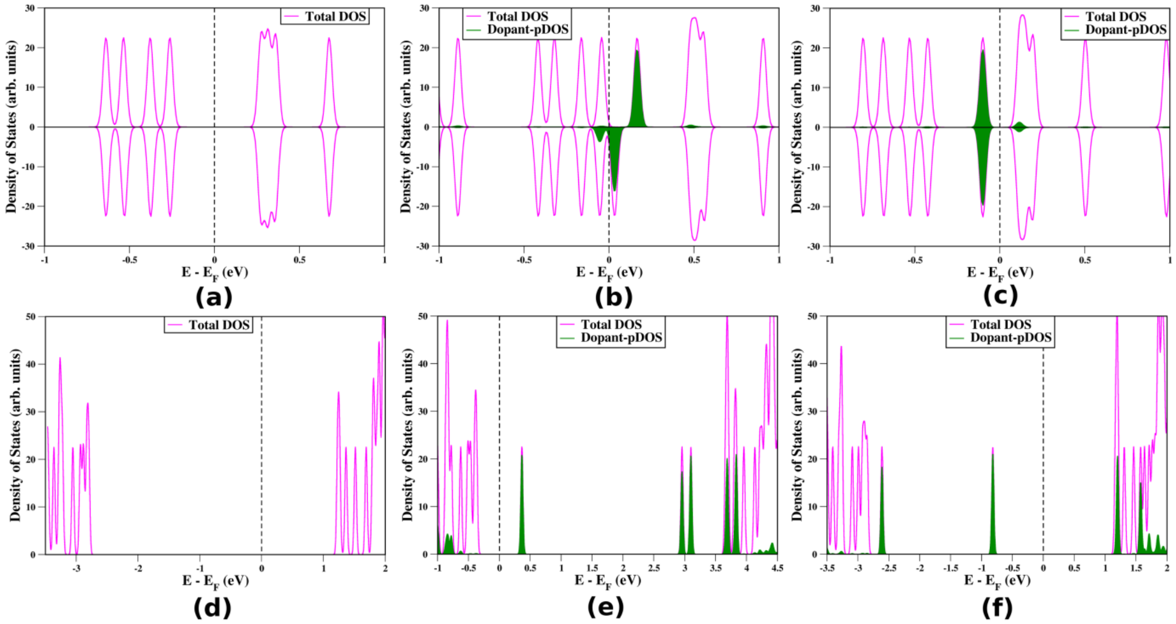

Figure 3.5: Projected density of states (pDOS) plots for (a) (21, 8) BNQD, (b) TCNQ-BNQD and (c) TTF-BNQD systems. The Fermi level is set to zero. The pDOS lines are broadened with Gaussian functions of width 0.025 eV.

Based on the above observations, we understood that the reason for the decrement in the H-L gap of QDs after the physisorption of a dopant is mainly because of the presence of the dopant-levels near the Fermi-level of the complexes. Despite of our efforts, we *couldn't* understand the exact reason for the generation of spin-dependent H-L gap in the TCNQ-GQD system. But, we are sure that it is arising because of the combined effect of the GQD and TCNQ and not because just one of them. We are sure about this because, if GQD (TCNQ) alone can create the spin-polarization irrespective of the dopant (QD), then, obviously, one would expect the same spin-polarization for the TTF-GQD (TCNQ-BNQD) complex. But, none of the above two cases were observed in our study. Furthermore, none of the above molecules– that is, neither the dopants nor the QDs–are spin-polarized individually (see figure 3.6, give the DOS plots for all the individual molecules). All these above reasons prove that, there is a combined effect of both GQD and TCNQ which is generating the spin-polarized H-L gap in TCNQ-GQD complex. Also, we believe that the large amount of charge-transfer between TCNQ and GQD will play a key role in lifting the spin-degeneracy of the TCNQ-GQD complex.

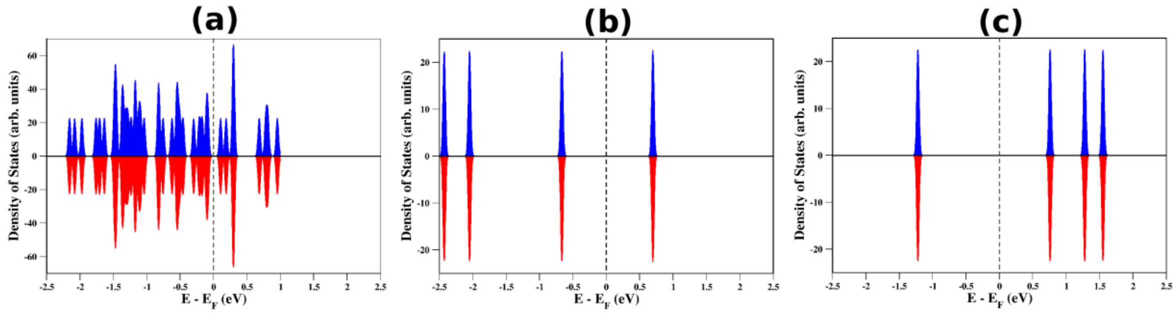

Figure 3.6: DOS plots of (a) (21, 8) GQD, (b) TCNQ and (c) TTF. The DOS lines are broadened with Gaussian functions of width 0.025 eV.

Optical-Conductivity:

It is known that molecular charge-transfer can affect the optical-conductivity in the low-frequency region. [108] As our Mülliken population analysis shows that there is a charge transfer between the dopants and the QDs (see table 3) in the QD-dopant complexes, we have calculated the optical-conductivity of all the (21, 8) complexes and are shown in figure 3.7. The low-frequency optical-conductivity of GQD is given in figure 5a, and it has a single peak situated at 0.54 eV. This energy is exactly equal to the H-L gap of the GQD (see table 3.4). Thus, this peak corresponds to the electronic transition from HOMO to LUMO. Also, it should be noted that there no peaks below this energy.

Now, when a dopant is adsorbed on the GQD, new peaks below 0.54 eV are observed. For the TCNQ-GQD complex, these new peaks are situated at 0.21 eV and 0.09 eV (exactly equal to the spin-polarized H-L gaps of TCNQ-GQD complex) for the majority and minority spin-channels, respectively. Adsorption of TCNQ on GQD gives rise to an asymmetry in the population of majority and minority spins near the Fermi-level (see figure 4b) which leads to the difference in conductivity for different spins in the low-frequency regime. But, for the TTF-GQD complex system there is no spin-polarization, and hence, the optical conductivity is also same for both the spins. For pure BNQD, the calculated H-L gap is 4.03 eV. For the complex systems, we have found that, multiple numbers of peaks appears below 4 eV. These peaks correspond to the electronic excitations between the molecular-molecular and molecular-BNQD energy levels– a clear reflection of the pDOS plots of (21, 8) BNQD-dopant complexes.

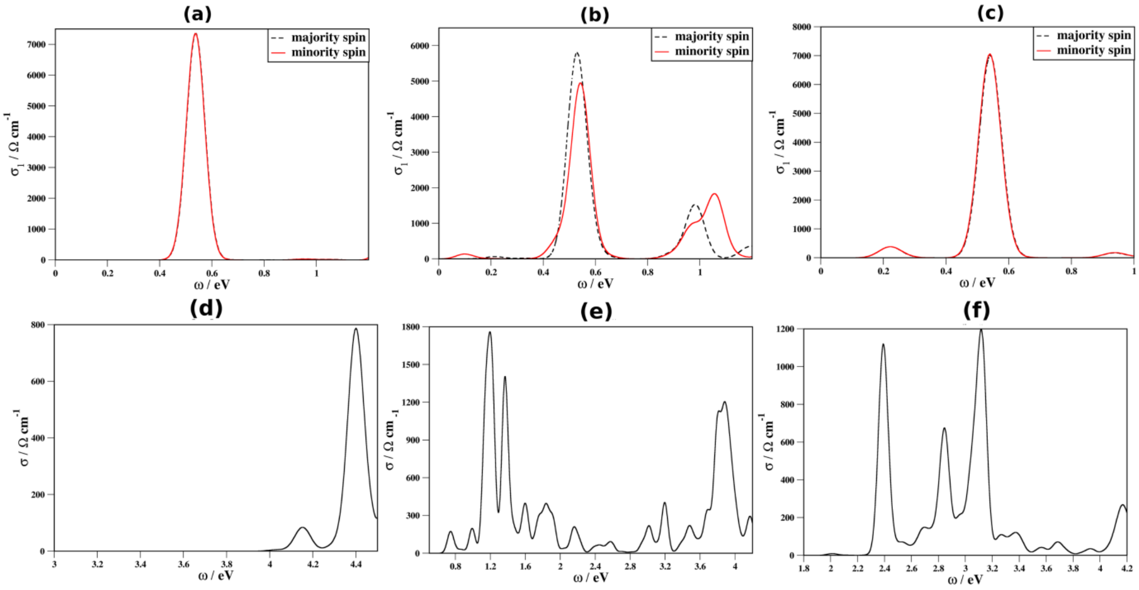

Figure 3.7: Low-frequency region of optical conductivity for (a) (21, 8) BNQD, (b) TCNQ-(21, 8) BNQD, and (c) TTF-(21, 8) BNQD. The lines are broadened with Gaussian functions of width 0.05 eV.

Effects of size:

To find the effect of the size of the graphene quantum dots on the interaction between the molecules and the GQD, we have considered GQDs of smaller size–length of ~2.2 nm and a width of ~1.4 nm–which according to the notation are (21, 6)-GQDs. Compared to the pure (21, 8) GQDs, the H-L gap of pure (21, 6) GQDs has increased by ~ 0.14 eV, that is, they have ~ 0.68 eV gap. Also, as expected, the amount of charge-transfer has decreased. For TCNQ molecule, it has decreased from ~ 0.43 e to ~ 0.37 e with a decrease in the size of the GQD from (21, 8) to (21, 6). On the other hand, TTF don't show any appreciable change. Interestingly, there is no change in the position and distance of the dopants from the GQD plane even after the reduction of size. Thus, decrement in the size of GQD doesn't have any direct impact on the position of the dopant, but, because of the increment in the H-L gap, it does have an effect on the charge-transfer.

Table 3.5: Spin-polarized H-L gaps of TCNQ and TTF adsorbed (21, 6)-QDs.

System	H-L gap		Charge-transfer (e)
	α-spin (eV)	β-spin (eV)	
Pure GQD	0.68	0.68	-
TCNQ-GQD	*0.22*	*0.1*	-0.37
TTF-GQD	0.23	0.23	+0.11
Pure BNQD	4.16	4.16	-
TCNQ-BNQD	0.76	0.76	-0.18
TTF-BNQD	2.0	2.0	+0.20

3.4 Conclusion

In the present study, we have calculated the effects of organic donor or acceptor molecule doping on the rectangular graphene or BN quantum dots. We have shown that the organic donor molecule (TTF) and acceptor molecule (TCNQ) can add extra holes or electrons to the GQDs as well as to the BNQDs and as a consequence can modify the H-L gap and the electronic properties of them. We have found that all the complex systems are stable as they all have negative adsorption energies. The interaction between the molecules and the GQD is the interaction between the π surfaces of them, whereas, the interaction between the BNQD and the molecules is governed by the weak dipole–dipole and electrostatic forces. From the DOS and pDOS plots we have found that there are extra donor or acceptor levels present in the systems because of the presence of the TTF or TCNQ. The discrete molecular levels change the H-L gaps of the systems. By the Mülliken population analysis, we have found that there is a significant amount of charge-transfer present from GQD to TCNQ and a relatively less amount of charge-transfer present from TTF to GQD. Just the opposite trend is observed in the case of a BNQD. In case of TCNQ, because of this charge-transfer, a finite spin polarization is observed near the Fermi energy. The low energy region of the optical conductivity plot also proves our result.

Chapter 4

Structural Stabilities, Electronic, Magnetic and Optical Properties of Rectangular Graphene and Boron-nitride Quantum Dots: Effect of Size, Substitution and External Electric Field

4.1 Introduction

Since the experimental discovery of graphene in 2004,[185] it has become a subject of intense interest for scientists. Graphene is two dimensional (2-D) honeycomb lattice of sp^2 bonded carbon atoms having C-C bond distance as 2.41 Å. Graphene has the combination of many unique properties.[172-175] But graphene is a zero band-gap semiconductor or semi-metal. It has almost zero density of states at Fermi level which is the main problem for using it into semiconducting devices. So for the application in electronics finite band-gap should be introduced in graphene system. So, when quasi one dimensional graphene nanoribbons were discovered, this problem was partly solved. Finite termination of infinite graphene sheet introduces a band-gap in graphitic materials. Band-gap of graphene nanoribbons depend on length and width. Also passivation and edge geometry of a graphene nanoribbon changes the electronics, optical and magnetic properties.[179] According to first principles calculations, both zigzag and armchair graphene nanoribbons are semiconducting.[71] Armchair GNRs are non-magnetic whereas zigzag GNRs have ferromagnetic arrangement of spin along one edge and antiferromagnetic arrangement of spin along opposite edges. Upon application of electric field along cross ribbon width zigzag graphene nanoribbons show half-metallicity, that is conducting for only one spin channel, upon application of electric field.[78]

The boron-nitrogen (BN) analogue of graphene, the 2-D BN sheet is a large band-gap insulating material.[127] So, by substituting B and N atoms in graphene sheet, properties can be tuned. For example, doping the edge carbon atoms of a zigzag graphene nanoribbon with boron atoms, changes the system into an intrinsic half-metal without application of any external electric field.[73] Intrinsic half-metallicity in GNRs are also observed when the systems are doped with B and N atoms in different ratios.[75]

Zero dimensional graphene quantum dots (GQDs) or nano-flakes (QNFs) are the bridge between small poly aromatic hydrocarbon (PAH) molecules and bulk 2-D graphene sheets. They are much easier to synthesize experimentally but theoretically they are not studied as much as bulk graphene or GNRs. GQDs are found to possess unique optical,[186-188]electronic[80, 81, 94, 95] and magnetic properties[81] already. By changing the shape and size, these properties can be tuned. For example, smaller nano-flakes have discrete energy levels but considerably large nano-flakes will have continuous energy bands[81] and triangular nano-flakes will have finite magnetic moment.[86, 88, 96] The properties of BN nano-flakes also can be modulated by varying shape and size. So, by combining both of them, properties of a hybrid graphene-BN nano-flake can be fine-tuned. Preparation of the hybrid nano-flake is already reported, so if controlled doping is possible, band-gap modulation can be an easy thing.

In this present study, we carry out our calculations on rectangular graphene (G), BN and graphene-BN hybrid quantum dots (QDs). We have substituted BN on GQDs and also carbon on BNQDs to investigate the changes in electronic and magnetic properties. All these studies are done on nano-flakes which have zigzag edge along the edge and armchair edge along the width. We have done width and length variation of the systems to find out the dependency of these factors on the properties of the QDs.

We have found that pure graphene nano-flakes are non-magnetic and semiconducting and pure BNQDs are non-magnetic and insulating as expected from earlier studies.[127] The BNQD having all the edge atoms substituted by carbon are also non-magnetic and semiconducting. Our systems having substitution of edge carbon atoms of graphene nano-flakes partially with BN at opposite edges, or substitution of all the carbon atoms at edges, shows half-metallic property.

For all the systems, finally we have done width and length variation studies. Such studies show that increase in width or length reduces the band-gap for both the spin channels. Finally we have done the magnetic property analysis of the QDs. We found out that none of the system has any significant spin polarization.

4.2 Computational Details

Spin polarized first-principles calculations have been performed, to obtain all the electronic and magnetic properties of the systems, using the density functional theory (DFT) method as implemented in the SIESTA package.[168] Generalized gradient approximation (GGA) in the Perdew–Burke–Ernzerhof (PBE)[169] form has been considered for accounting the exchange-correlation function. Double ζ polarized (DZP) numerical atomic-orbital basis sets have been used for H, B, C, and N atoms. Norm-conserving pseudo-potentials in Kleinman-Bylander form[171] with 1, 3, 4 and 5 valence electrons for H, B, C, and N, respectively, have been considered. A reasonable mesh cut-off of 400 Ry for the grid integration has been used to represent the charge density and a vacuum of 20 Å has been maintained, around the quantum-dots, in all directions to avoid any spurious interactions. Systems are considered to be optimized if the magnitude of the forces acting on all atoms is less than 0.04 eV/Å. As the systems are zero-dimensional, all the performed calculations are only at the gamma (Γ) point of the Brillouin zone. Finally, optical properties have been calculated, for the optimized structures obtained from the SIESTA calculations, using the time dependent density functional theory (TDDFT) method as implemented in the Gaussian 09[189] package with hybrid B3LYP (Becke exchange with Lee, Yang and Parr correlation) functional[149, 190, 191] in unrestricted form (i.e. uB3LYP) and with the basis-set 6-31+g(d).

4.3 Results and Discussion

Systems under consideration and Stability: In this work, we have considered rectangular quantum-dots (QDs) of graphene (G), boron-nitride (BN) and their hybrids [i.e. GQDs with BN substitution and BNQDs substituted with C] with a zigzag edge along the direction of the length and an armchair edge along the width direction. Following the convention of the graphene nanoribbons,[179] we have assigned them as (n, m) to represent the length and width of the QDs. Here ‘n’ represents the number of atoms along the zigzag-edge (length) and ‘m’ represents the number of atoms along the armchair-edge (width), as shown in figure 1. In the present study, we have considered two values, namely, 21 (~ 2.2 nm) and 33 (~ 4.2 nm) for ‘n’ and three values, namely, 4 (~ 1 nm), 6 (~ 1.4 nm) and 8 (1.8 nm) for ‘m’. Thus, we have varied the length X width from ~ (2.2X1) nm^2 to ~ (4.2 X1.8) nm^2. We have substituted the zigzag edges of the QDs either completely or partially.

We have kept the initial spin ordering as antiferromagnetic for all of the system as predicted in case of a bipartite lattice by Lieb’s theorem.[77]

We found that all the systems under study are non-magnetic in nature.

Formation energies (E_{Form}) of all the systems are calculated using the following equation:

$$E_{\mathrm{Form}} = (E_{\mathrm{tot}} - N_C E_C - N_H E_H - N_B E_B - N_N E_N) \ldots\ldots\ldots(4.1)$$

where, E_{tot}, E_H, E_B, E_C and E_N are the total energy of the system, energy of a H atom (calculated from hydrogen molecule), energy of a B atom (calculated from alpha-boron), energy of a C atom (calculated from a 8 X 8 graphene super-cell) and energy of a N atom (calculated from nitrogen molecule), respectively and N_H, N_B, N_C and N_N are the number of H, B, C and N atoms present in the system, respectively. E_{Form} of the systems (21, 4), (21, 6) and (21, 8) are listed in table 1. Formation energies of all the systems are negative (see table 1), which indicates that all these systems are thermodynamically feasible.

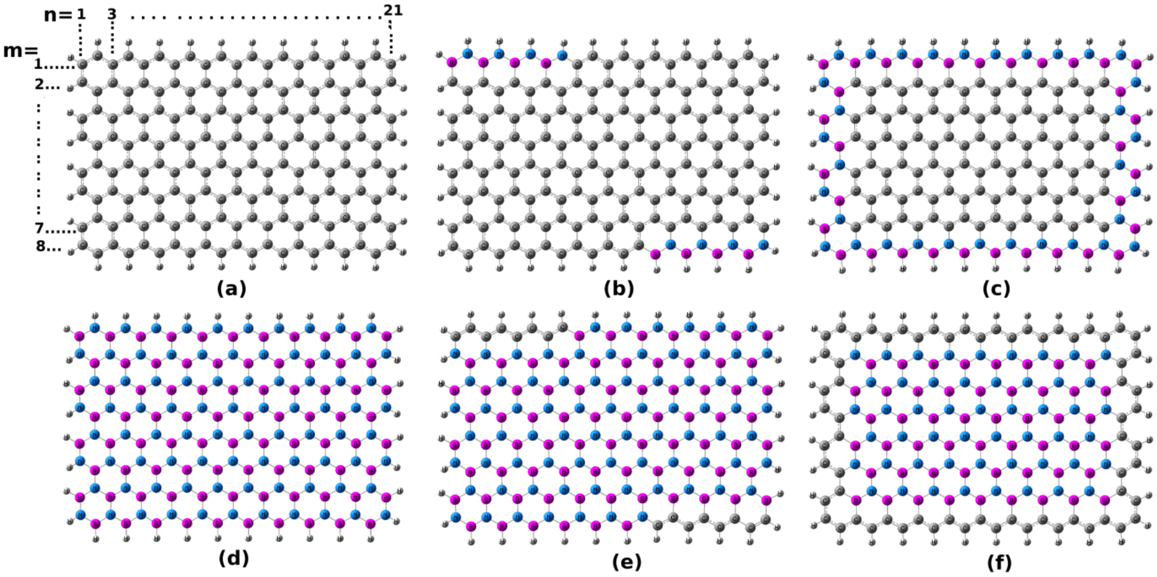

Figure 4.1: Optimized geometries of all the (21, 8) nano-flakes under our study. (a) GQD, (b) GQD with the edge atoms partially substituted with BN atoms, (c) GQD with all the edge atoms substituted with BN atoms, (d) BNQD (e) BNQD with all the edge atoms substituted with C atoms (f) BNQD with the edge atoms partially substituted with C atoms.

Table 4.1: Formation energies (eV) of the systems (21, 4), (21, 6) and (21, 8). Numbers inside the brackets (in bold-italics) are the $(N_B + N_N) : (N_C)$ ratios.

System Name	**(21, 4)**	**(21, 6)**	**(21, 8)**
GQD	-61.60 (***0 : 84***)	-70.62 (***0 : 126***)	-79.56 (***0 : 168***)
BN-partial-ed- GQD	-79.52 (***16 : 68***)	-88.48 (***16 : 110***)	-97.92 (***16 : 152***)
BN-full-ed- GQD	-126.56 (***50 : 34***)	-143.78 (***58 : 68***)	-163.81 (***66 : 102***)
C-full-ed-BNQD	-107.52 (***34 : 50***)	-170.64 (***68 : 58***)	-234.55 (***102 : 66***)
C-partial-ed-BNQD	-166.88 (***68 : 16***)	-244.44 (***110 : 16***)	-322.32 (***152 : 16***)
BNQD	-196.12 (***84 : 0***)	-274.92 (***126 : 0***)	-352.92 (***168 : 0***)

E_{Form} values also show that, BNQDs are more stable than GQDs and the stability of the QDs in the increasing order is: GQD > BN-partial-ed-GQD > BN-full-ed-GQD > C-full-ed-BNQD > C-partial-ed-BNQD > BNQD. This trend is observed for all the systems except for the (21, 4), where, we have observed the order: "C-full-ed-BNQD > BN-full-ed-GQD" instead of the expected order: "BN-full-ed-GQD > C-full-ed-BNQD". This is not an anomalous behaviour and can be explained as follows: As BNQDs are more stable than GQDs, it is obvious that, the stability of a system which has both BN and C (i.e. either full-ed or partial-ed systems) will be more if it has more number of B and N atoms than the C atoms. In table 1, we have shown the ratio between the total number of boron and nitrogen atoms ($N_B + N_N$) and the number of carbon atoms (N_C) for each system. From the table 1 it is clear that, among the C-full-ed-BNQD systems the ratio ($N_B + N_N$): (N_C) is less than one (i.e. $N_B + N_N < N_C$) only for the case of (21, 4) system, and hence, this system is found to be less stable than BN-full-ed-GQD.

Electronic and magnetic properties:

Graphene Quantum Dots (GQD): Rectangular GQDs are semiconducting in nature. (21, 4) GQD has a band-gap of 0.69 eV. As the width of the GQD is increased to 6 and then 8, band-gap is decreased to 0.67 and 0.53 respectively. The same trend is observed when the length of the ribbon is increased. The reason for the above changes is because of the decrease in the energy-level spacing as the system's length and/or width increases (similar to the particle in a box problem[192]) We have given the H-L gaps of all the systems in table 4.2 and 4.3. We have plotted the projected density of states of the systems and found out that the zigzag edge C atoms have maximum contribution near fermi level (figure 2).

Table 4.2: HOMO-LUMO gap (eV) for the systems (21, 4), (21, 6) and (21, 8) in both α- and β-spins.

System Name	**(21, 4)**		**(21, 6)**		**(21, 8)**	
	α-spin	**β-spin**	**α-spin**	**β-spin**	**α-spin**	**β-spin**
GQD	0.71	0.71	0.68	0.68	0.54	0.54
BN-partial-ed-GQD	0.81	0.16	0.04	0.54	0.04	0.43

BN-full-ed- GQD	0.71	0.71	0.41	0.11	0.09	0.34
C-full-ed-BNQD	0.28	0.28	0.44	0.44	0.48	0.48
C-partial-ed-BNQD	1.35	1.35	1.08	1.08	0.91	0.91
BNQD	4.32	4.32	4.16	4.16	4.03	4.03

Table 4.3: HOMO-LUMO gap (eV) for the systems (33, 4), (33, 6) and (33, 8) in both α- and β-spins.

System Name	**(33, 4)**		**(33, 6)**		**(33, 8)**	
	α-spin	**β-spin**	**α-spin**	**β-spin**	**α-spin**	**β-spin**
GQD	0.70	0.70	0.60	0.60	0.54	0.54
BN-partial-ed-GQD	0.05	0.51	0.32	0.04	0.01	0.19
BN-full-ed- GQD	0.62	0.62	0.32	0.06	0.22	0.03
C-full-ed-BNQD	0.05	0.23	0.16	0.16	0.19	0.19
C-partial-ed-BNQD	0.79	0.79	0.52	0.52	0.36	0.36
BNQD	4.32	4.32	4.16	4.16	4.06	4.06

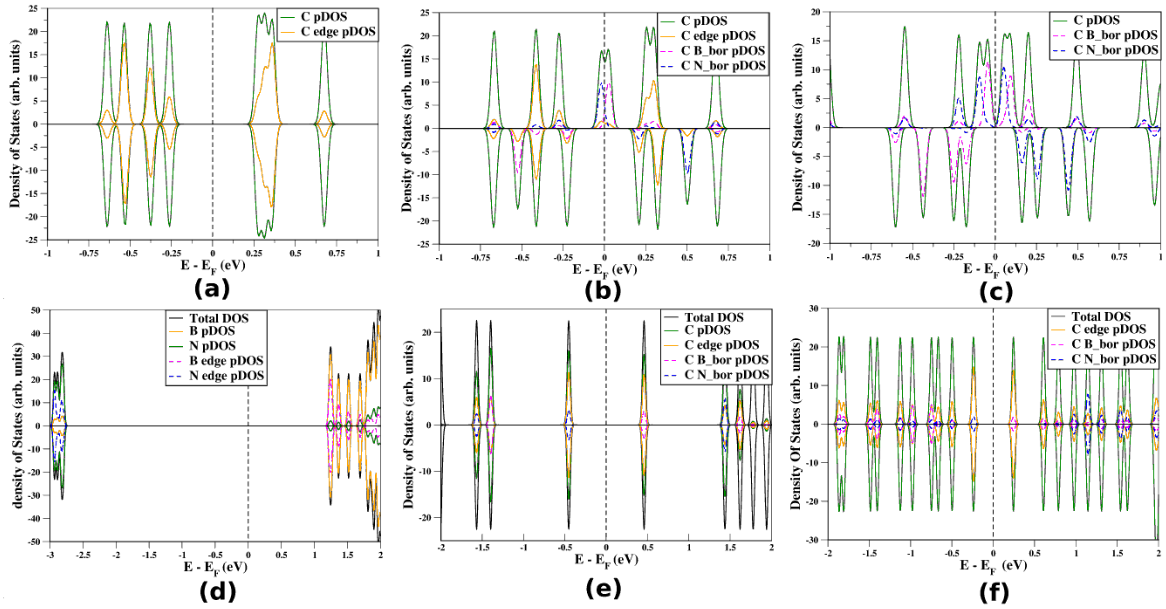

Figure 4.2: Density of states plots of (a) GQD, (b) GQD with the edge atoms partially substituted with BN atoms, (c) GQD with all the edge atoms substituted with BN atoms, (d) BNQD (e) BNQD with all the edge atoms substituted with C atoms (f) BNQD with the edge atoms partially substituted with C atoms. Fermi level is set to zero. Gaussian broadening parameter is 0.025 eV.

We have plotted both the HOMO and LUMO of (21, 8) GQD and the result shows that the wave-functions are localized at the zigzag-edges. One notable point is HOMO and LUMO are localized at two different edges for each spin, and also, the edge where the wave-function is localized for the α-spin's HOMO is the same as the β-spin's LUMO and vice-a-versa.

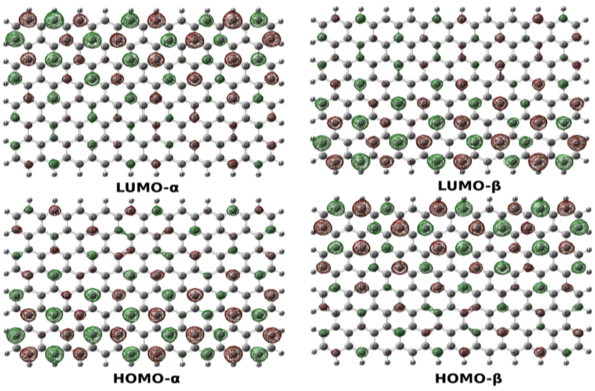

Figure 4.3: HOMO and LUMO plots for the (21, 8) GQDs. Isovalue is 0.02 e/Å^3 for all the cases.

Graphene quantum dots with all the edge atoms substituted with BN atoms: Rectangular graphene nano-flakes with all the edge atoms substituted with B and N atoms are semiconducting in nature. For the smaller width systems, (21, 4) or (33, 4) QDs, it has same band-gap for both the spin channels that is purely semiconducting. But for the larger systems than these, e.g. (21, 6) or (21, 8) so on, the systems have less band-gap for one spin channel and more band-gap for another spin channels, still for both the spin channels the system remains semiconducting. This is because of the fact that applying an external electric field along a zigzag nano ribbon induces half-metallicity in the system[80] and so a zigzag graphene ribbons which have one edge carbon atoms attached with N and another edge attached with B shows half-metallicity because the potential gradient along the system acts as an external electric field applied to the system[193]. The amount of electric field needed to turn the system half-metallic reduces with increase in ribbon width. So, for the same amount of electric field gradient inside our GQDs, the band-gap for only one spin channel starts to close when the ribbon width increases. In figure 3, we plotted pDOS of (21, 4) (21, 6) and (21, 8) systems to compare all of them.

For 0-D graphene quantum dots with all the edge carbons substituted with BN, edge-states which arise at zigzag edges get modified. In this case we have one zigzag N edge and another edge as B edge. HOMO gets localized at zigzag N edge but on the C atoms which are attached to B atoms and LUMO gets localized at zigzag B edge on the C atoms attached to N atoms, both for α spin and β spin for all the systems though HOMOs and LUMOs for α spin and β spin do not behave similarly as the system is spin polarized around the Fermi level.

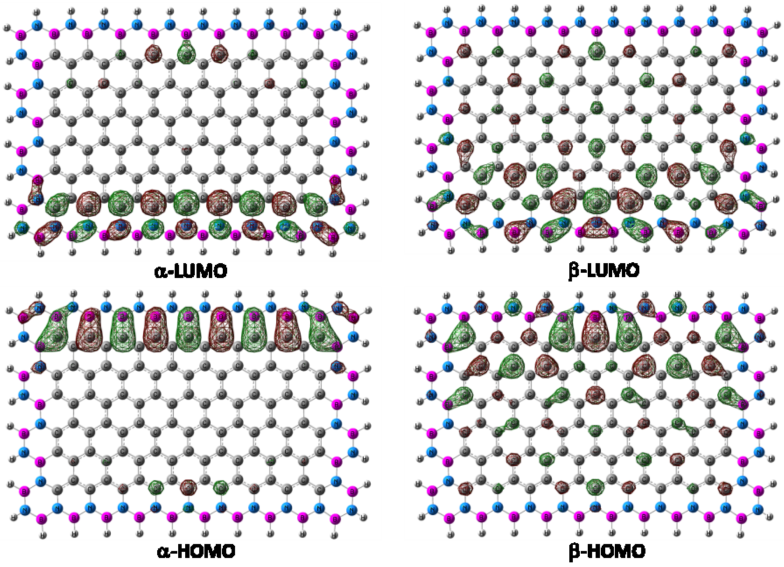

Figure 4.4: HOMO and LUMO diagrams for α spin and β spin of (21, 8) system. Isovalue is 0.02 e/Å^3 for all the cases.

Graphene quantum dots with the zigzag edges partially substituted with BN: The systems which have the zigzag edge atoms partially substituted by B and N atoms, are also semiconducting for both the spin channel but it has different H-L gap for different spin channels. As GQDs with partial edge substitution with BN have the presence of localized edge-states due to edge carbon-atoms, presence of passivated B/N edge-atoms which can supress the half-metallicity and presence of border carbon atoms which strongly contribute to the states near the Fermi-level, the reason for their spin-dependent H-L gap could be either because of a combined effect of some/all of them or because of any one of them. As each edge of these systems possesses both the carbon atoms and B/N atoms, we have first checked for the presence of any intrinsic electric-field in these systems along the diagonal of the rectangular GQD. Unlike the BN-full-ed-GQDs, if any intrinsic electric-field is there, that can act only along the diagonal of the rectangular QDs. So, we have applied an electric-field (from 0.1 to 1V/Å) across the diagonal of the GQDs and we find that all the systems are indeed spin-non-degenerate (see “Effect of external electric field on GQDs” section for further details). This shows that, if an electric-field is applied along the diagonal direction, then the spin-degeneracy of the GQD can be lifted. But as we know that it should be width dependent, which is not observed in this case, we suggest that this semi-half-metallicity is because of the presence

of both the edge and border carbon atoms.
The projected density of states plots also shows that the C-B or C-N border carbon atoms mainly contribute to the density of states near Fermi level.

From the HOMO-LUMO diagrams, we found out that for both the spin channels, HOMO is mainly localised over the C atoms attached to N atoms in the partially substituted nano-flake and LUMO is mainly localised over the C atoms bonded with B atoms. In figure 4.5 HOMO and LUMO for (21, 8) graphene nano-flake with the zigzag edge partially substituted with BN atoms is plotted.

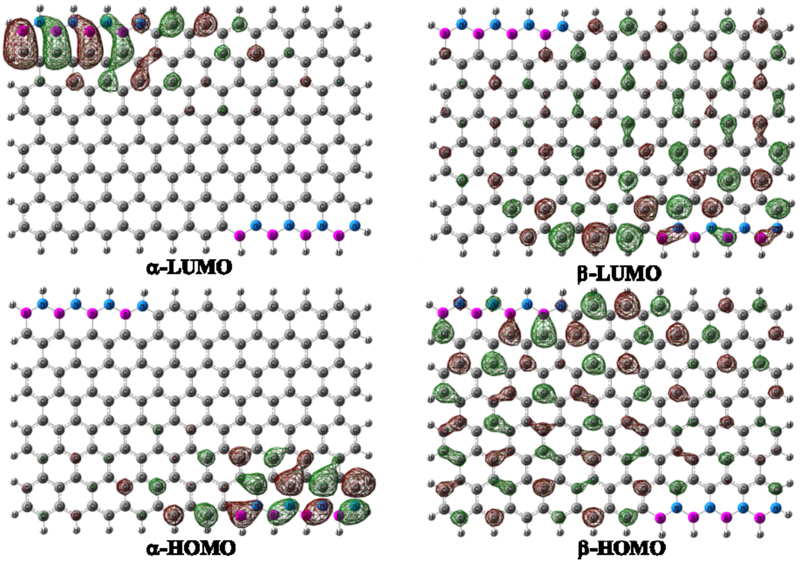

Figure 4.5: HOMO and LUMO diagram for α spin and β spin (21, 8) system. Isovalue is 0.02 e/Å^3 for all the cases.

BN Quantum Dots (BNQD):

Rectangular BN nano-flakes are large band-gap insulators in nature as that of bulk BN sheet. (21, 4) BN nano-flake has a band-gap of 4.32 eV. In case of BN nano-flakes also band-gap reduces with increase in width or length similar to pure GQD. When we plotted the projected density of states of these systems, we found out that mainly the zigzag edge atoms are contributing towards the density of states near Fermi level, as depicted in figure 4.2. Also, Nitrogen atoms contribute more to the HOMO as they are electron rich and Boron atoms contribute more to the LUMO as they are electron deficient.

From HOMO and LUMO plot, it is evident that the HOMO is localised over the

N-zigzag edge of the flake and LUMO is localised over B-zigzag edge of the flake (figure 4.6). HOMO and LUMO for both the spin channels are exactly same in this case.

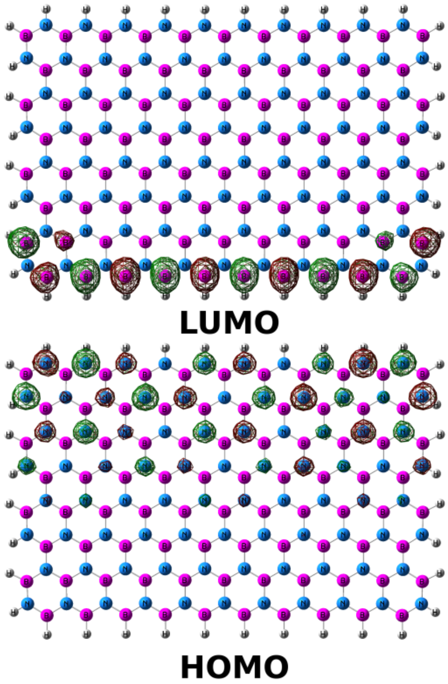

Figure 4.6: HOMO and LUMO diagram for α spin and β spin (21, 8) BNQD. Isovalue is 0.02 e/Å^3 for all the cases.

BNQD with All the edge Atoms Substituted with Carbon Atoms: BNQDs with all the edge atoms substituted with carbon atoms are semiconducting in nature. If we compare these QDs with their pure graphene analogues of them, they have less band-gap than graphene nano-flakes of same size. H-L gap of these systems increases with the increase in size, opposite to that of pure GQDs/BNQDs. This is because as the width of the ribbon increases, in C-full-ed-BNQD, the number of carbon atoms present at the edge increases, which in-turn increases the delocalization of electrons (because B, N atoms are replaced with carbon-atoms). This delocalization will bring stability mainly to the HOMO (leaving the LUMO almost unchanged, see figure 4.7), and hence, the increment in the H–L gap with an increment in the width of the ribbon.

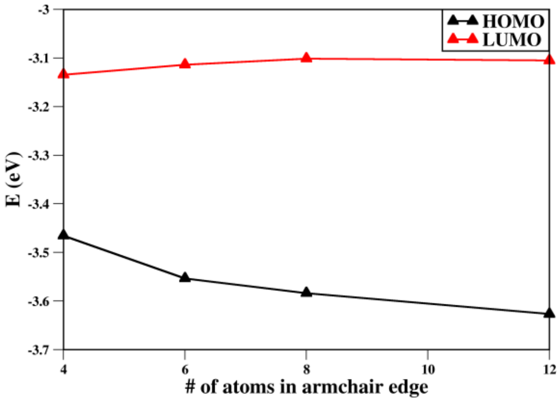

Figure 4.7: HOMO and LUMO Energies for α spin and β spin (21, 8) of BNQD with all the edge BN atoms substituted with carbon with the change in width.

We have found that the HOMO is localised on the carbon atoms attached with N atoms and the LUMO is localised on the C atoms bonded with B atoms. This is because of electron donating nature of N atoms and electron withdrawing nature of B atoms as discussed in earlier section in this case, Both α spin and β spin have HOMO and LUMO levels at same position.

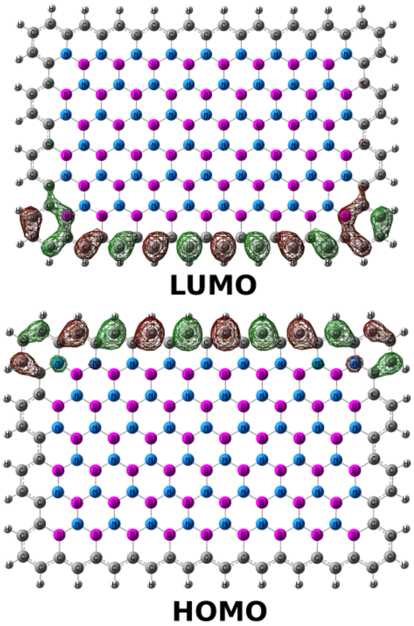

Figure 4.8: HOMO and LUMO diagram for α spin and β spin (21, 8) system. Isovalue is 0.02 e/Å^3 for all the cases.

BN quantum dots with the zigzag edges partially substituted with carbon atoms: BN quantum dots with the zigzag edge atoms partially substituted with carbon atoms are semiconducting in nature. If we compare the semiconducting quantum dots with the pure graphene analogues of them, they have less band-gap than graphene nano-flakes of same size. From the projected density of states plots of the systems it is clear that the C atoms have maximum contribution towards the energy levels near Fermi level as they are present at the edges.

It is found that the HOMO is localized on the edge carbon atoms which are attached with the N atoms and the LUMO is localized on the C atoms bonded with B atoms. Both α spin and β spin have HOMO and LUMO levels at same position for this case also.

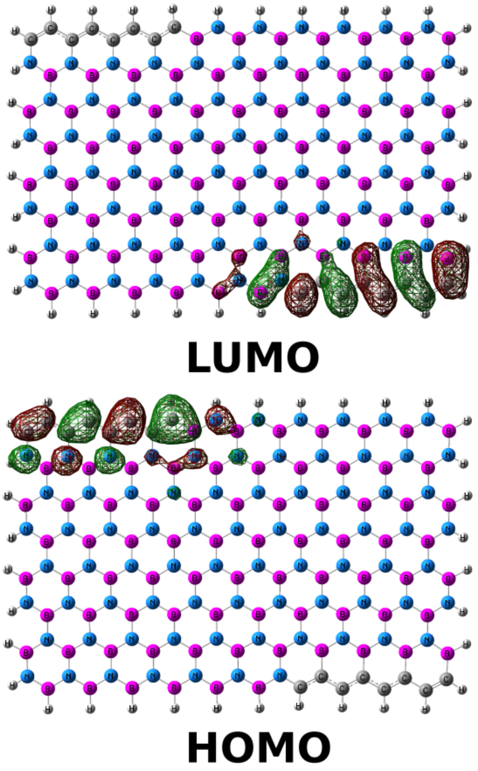

Figure 4.9: HOMO and LUMO diagram for α spin and β spin (21, 8) system. Isovalue is 0.02 e/Å^3 for all the cases.

Effect of external electric field on GQDs: In the previous section we have found out that partial opposite edge BN substitution on GQDs induces semi half-metallic properties in the systems. So we tried to find out if that is because of an intrinsic electric field generated inside the system across the diagonal of the rectangle. In order to find this out we have applied an external electric field on the system across the diagonal of the rectangular (21, 8) GQD. We have applied the electric-field (from 0.1 V/Å to 1 V/Å) across the diagonal of the GQDs and we find that all the systems are indeed spin-non-degenerate In a previous study[194] it was proposed by TB theory that when electric field along different direction and of different strength was applied, oscillatory behavior of band-gap was obtained. We varied the electric field from 0.1V/Å to 1V/Å along the diagonal of a (21, 4) GQD and observed that band-gap starts to reduce for one spin channel, and there is a oscillatory behavior in band-gap with field strength, that is, depending upon the field strength applied along the diagonal band-gap of α and β spins increases and decreases in a oscillatory fashion.

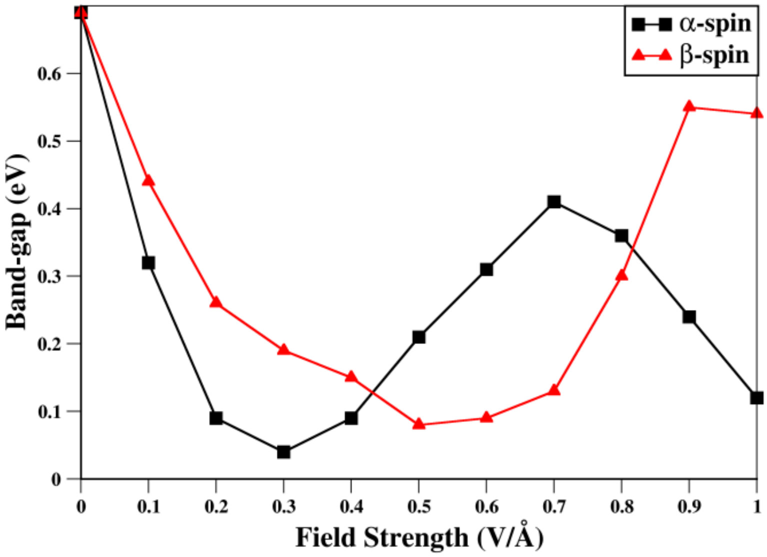

Figure 4.10: HOMO-LUMO gaps of the (21, 4) GQD depending upon the external electric field strength.

Optical absorption properties of all the systems: We have studied the optical absorption properties of all the pure GQD/BNQD and hybrid (21, 4) systems. For pure GQD we found out that though it has a small peak at visible energy range, it has λ_{max} at IR region (1878.38 nm) which corresponds to HOMO to LUMO+1 and HOMO-1 to LUMO doubly degenerate transitions. GQD with complete edge BN substitution shows multiple peaks. Absorption maximum in this case is at 863.16 nm which arises from

HOMO to LUMO+1 and HOMO-1 to LUMO doubly degenerate transitions. The other smaller peak 863.16 nm has major contributions from the HOMO-1 to LUMO+2 and HOMO-2 to LUMO+1 doubly degenerate transitions. Partial edge BN substituted GQD also has many peaks but λ_{max} is at 879.12 nm. This also arises from HOMO to LUMO+1 and HOMO-1 to LUMO transitions. For all the cases it is π - π^* transition. Pure BNQD has λ_{max} at 220.52 nm, but the oscillator strength is very less in this case. BNQD with edge atoms substituted by C atoms both completely and partially absorb in visible energy range ($\lambda_{max} = 618.30$ nm and 427.42 nm respectively).

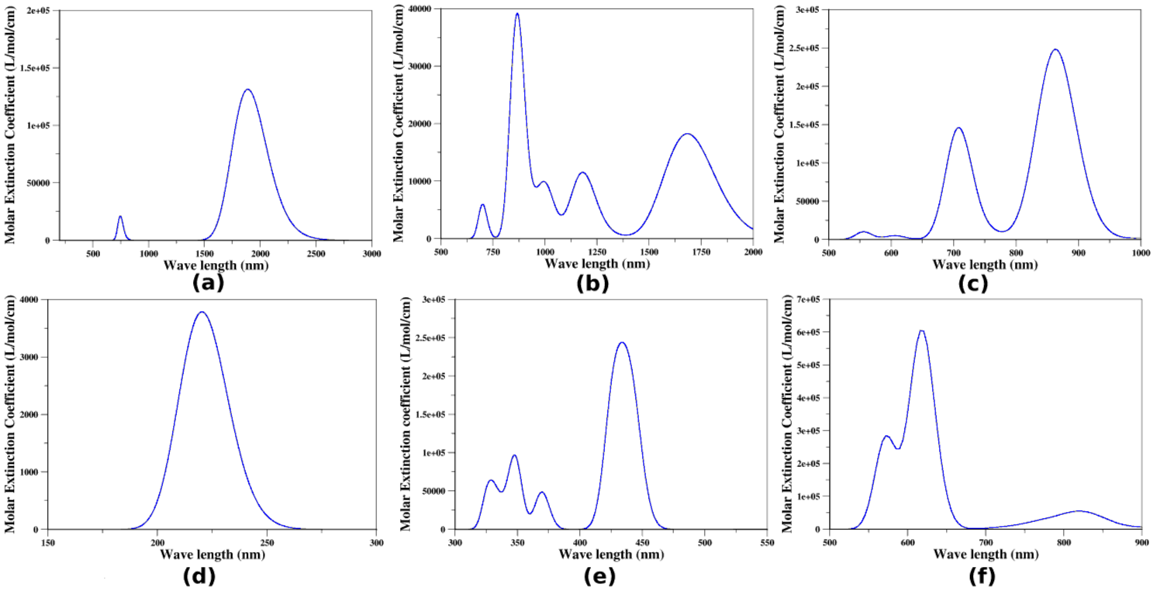

Figure 4.11: Absorption profile plots for (a) GQD, (b) GQD with all the edge atoms substituted with BN atoms, (c) GQD with the zigzag edges partially substituted with BN atoms and (d) BNQD, (e) BNQD with all the edge atoms substituted with C atoms and (f) BNQD with zigzag edges partially substituted with BN atoms.

4.4 Conclusion

In this study we have considered graphene, BN, and graphene-BN hybrid nano-flakes. We have shown that by varying width, length and extent of substitution, properties of a nano-flake can be tuned to generate suitable material for application in device.

We have found out that among all the systems under study, graphene nano-flakes are semiconducting with tunable band-gap. BN nano-flakes are insulating in nature. Graphene nano-flakes with edge atoms completely or partially substituted with BN atoms shows semi-half-metallic behavior. BNNFs with edge atoms completely substituted with C atoms are again semiconducting with least band-gap among all the systems. In case of partially BN substituted graphene nano-flakes, even for the 1nm X 1.8 nm nano-flakes, that is the smallest system under study, we found out that it is semiconducting for both the spin channels but with smaller band-gap for one and larger band-gap for another one. GQDs with all the edge C atoms substituted by BN atoms show this type of property after a certain size limit.

We observed as a general result that in all the systems HOMO is mainly localized on either N atoms or on the C atoms which are attached with the N atoms. LUMO is mainly localized on either B atoms or the C atoms bonded with B atoms.

All the systems under our study are overall non-spin polarized. But near the Fermi levels, the semi-half-metallic systems are spin polarized, that is, both the spin channels do not have similar property.

So, we can say that by changing the type of substitution in GQDs or in BNQDs, the properties can be changed. Though none of the systems are spin polarized, electronic nature of the system is completely changed with variation in substitution. Also we calculated the optical absorption properties of the systems and found out that completely edge substituted BNQD is a potent material to use in LEDs.

Chapter 5

Electronic and Magnetic Properties of X-shaped Graphene, BN and hybrid CBN Quantum Dots

6.1 Introduction

Graphene, since its discovery in 2004,[185] has attracted huge scientific interest in several areas of science because of its several interesting properties which include electrical, magnetic, optical, mechanical etc.[172-175] Although graphene is the host for exciting electronic properties like ballistic conductance,[47] charge fractionalization etc.[172] its use in semiconductor industry in its pristine form is not possible because of its zero band-gap near the Fermi-level. However, this disability of graphene has been overthrown by its low-dimensional material graphene nanoribbon (GNR).

Specifically, density functional theory calculations, with both LDA and GGA exchange correlation functionals, on GNRs showed that GNRs with a zigzag edge (ZGNRs) possess a finite gap (~0.4 eV) for narrow width ribbons (< 5nm) and zero-gap if the width of the ribbon is large.[71, 179] On the other hand, AGNRs have been shown to oscillate between the semiconducting and metallic with an increase in the ribbon width.[71, 179] Although, both AGNRs and ZGNRs are interesting, ZGNRs have attracted huge scientific interest over AGNRs, because of their finite magnetic moment due to the spin-localization at the edges.[60] ZGNRs are also shown to be the promising candidates for the future spintronics because of the fact that this finite magnetic moment can be tuned to bring half-metallicity in ZGNRs.[72, 78] In fact, half-metallicity in

ZGNRs has been achieved in several ways viz., the application of electric field, doping, introducing defects etc.[73-75]

Enlightened with these facts, research groups have started studying, theoretically, more complex devices based on GNRs, like, GNR-FETs,[195] p-n junctions,[196] spin-filters[197] etc. and some of them have already been realized experimentally.[198] Recently, researchers started focusing on the shaped nanoribbon junctions which could be the plausible building blocks for the 2D-nano-networks.

Several shaped nanoribbon junctions viz., L-shaped,[199] T-shaped,[200] cross-shaped[201-203] and Z-shaped[204] nanoribbon junctions have been studied and most of these studies have concentrated on the conduction properties of these junctions. L-shaped GNRs shows low reflectance to the electrons for a large included angle and high reflectance for low included angle when the L-shaped-junction is made of an AGNR and a ZGNR, and, an opposite effect has been observed when the L-shaped-junction is made of two ZGNRs.[199] Similar spin-polarized calculations on the in-plane conductance of the GNR-cross points at different angles have shown large-scattering for quantum transport, except when two ZGNR ribbons meet at 60° angle. At this angle, quantum transport exhibits low-scattering, and also, a spin-polarized transmission probability is observed. Studies on the T-shaped junctions showed that, these systems are metallic and their conduction properties are sensitive to the height of the stem and on the doping position, i.e. on the stem or the shoulder.[200] Similar results were reported for the cross-shaped ribbons.[201, 202] Spin-polarized-conductance calculations on a cross-shaped junction show a transverse spin current with zero charge-current.[201] A Z-shaped GNR junction has been shown as a promising candidate to confine the electronic states completely i.e. a quantum dot (QD) can be realized at the junction.[204]

Motivated by the above mentioned interesting spin-polarized conducting properties of cross-shaped ribbon networks obtained from the theoretical calculations[201-203] and by the recent experimental realization of the alphabetical character QDs,[66] we have performed the spin-polarized density functional theory (DFT) calculations to understand the electronic and magnetic properties of the X-shaped (or cross-shaped) graphene and Boron-Nitride QDs (not GNRs) which can be visualized as the QDs formed by the intersection of a ZGNR and an AGNR ribbon as shown in fig 1. Graphene nanoribbons of sub-5-10 nm size and of controlled shape have been realized experimentally through top-down approaches using lithographic patterning followed by gas-phase etching chemistry[66] and through bottom-up approaches by coupling the molecular precursors by de-halogenation followed by cyclo-de-hydrogenation.[63] Apart from the above experimental methods, standard lithography and catalytic cutting techniques, in principle, are able to produce QDs of larger size.[70, 92, 93]

To our knowledge, there is no work on X-shaped graphene QDs, and in particular, the substitutional effects on the electronic and magnetic properties of X- shaped graphene QDs. In this work, we have investigated the electronic and magnetic properties of X-shaped QDs of both graphene and boron-nitride (BN). As the electronic and magnetic properties of the QDs will be highly sensitive to the edges,[73, 75, 78] we have considered the substitution, of these pristine dots, at the edges. For graphene-QD (GQD), edges are substituted with boron and nitrogen and for BN-QD (BNQD), edges are substituted with carbon. Thus, the systems are isoelectronic before and after the substitution.

Substitution has been performed in two ways: (i) complete replacement of the edge atoms with the substituent atoms and (ii) replacement of the edge atoms present at the V and inverted-V-shape of the X-shaped QDs with the substituent atoms. Thus, the other systems under consideration are complete edge substituted GQD (com-ed-sub-GQD), V-edge substituted GQD (V-ed-sub-GQD), complete edge substituted BNQD (com-ed-sub-BNQD) and V-edge substituted BNQD (V-ed-sub-BNQD). In order to see the size effects of the wings on the calculated properties, we have considered 3 different sizes of the wings, without changing the size of the central / junction region of the QDs. The size of the ribbon is indicated by (A, Z), where ‘A’ and ‘Z’ are the lengths of the armchair and zigzag-edged-wings, respectively, in nm. We have considered 3 sizes of QDs in this work, viz., (2.44 nm, 2.48 nm), (4.16 nm, 3.97 nm) and (5.79 nm, 5.39 nm). In all the 3 sizes, we have maintained equal numbers of zigzag (armchair) edges on both sides of the junction, in order to keep track on the important changes which will occur only because of the substitutional effects rather than the asymmetry across the junction.

All the six systems of the medium size, (4.16 nm, 3.97 nm), are shown in figure 5.1 and all of them have a total number of 240 atoms (308 atoms by including the hydrogen atoms), among which, 130 atoms are always at the edges of the QD and the remaining 110 atoms at the center, which makes these systems suitable for studying the edge effects.

6.2 Computational Details

All the first-principles calculations have been performed using spin-polarized density functional theory (DFT) as implemented in the SIESTA package.[168] The generalized gradient approximation (GGA) with the Perdew-Burke-Ernzerhof (PBE) form[169] is chosen for the exchange-correlation functional. Interaction between the ionic cores and the valence electrons is accounted by the norm conserving pseudo-potentials in the fully nonlocal Kleinman-Bylander form.[171] The pseudo-potentials are constructed from 3, 4 and 5 valence electrons for the B, C and N atoms, respectively. To expand the wave-functions, numerical localized combination of atomic orbitals with double-ζ basis sets are used. To represent the charge density, a reasonable mesh-cut-off of 400 Ry is used for the grid integration. As the systems under consideration are quantum dots, we have sampled the Brillouin-zone by 1 × 1 × 1 k-points using the Monkhorst-Pack scheme for both the electron properties calculations and for the full-relaxation of the systems. Systems are considered to be optimized only when the forces acting on all the atoms are less than 0.04 eV / Å. Unit-cells of 45 × 45 × 25, 45 × 45 × 25 and 85 × 85 × 25 $(\text{Å})^3$ have been taken for the systems of sizes (2.44, 2.48), (4.16, 3.97) and (5.79, 5.39) nm, respectively, to avoid any spurious interactions between the quantum-dots and their periodic images. For all the DOS and pDOS plots, a broadening parameter of 0.05 eV has been used. For plotting charge and spin density 100 × 100 × 100 grid points have been considered and isovalues of 0.001e / $(\text{Å})^3$ and 0.015e / $(\text{Å})^3$ have been used for the charge and spin-densities, respectively, for all the systems using the XCRYSDEN software.

5.3 Results and Discussion

In this section, we will explain the stability, electronic and magnetic properties of the considered systems.

1) Structural Stability

First, in order to find the ground state of the systems, we have performed the spin polarized calculations with both anti-ferromagnetic (AFM) and ferromagnetic (FM) spin configurations. The energy difference between the spin configurations for the systems with sizes (2.44, 2.48), (4.16, 3.97) nm are given in the third columns of the tables 5.1 and 5.2, respectively. From the values it can be seen that, all BNQDs are stabilized in FM state and all GQDs are stabilized in the AFM state irrespective of the size of the system. We can see that the energy by which a particular spin-configuration is stabilized over the other is far below the room temperature (~ 0.025 eV) for certain systems. However, as the DFT calculations are performed at 0 K, we will consider only those spin-configurations which are more stable (irrespective of the amount of stabilization) at 0 K (rather than considering how they will be at room temperature) for our further studies like DOS and wave-function analysis.

Next, to account for the stability, we have calculated the formation energy per atom, E_{form}, of all the systems in their ground state spin configurations using equation 5.1. The formation energy per atom, E_{form}, is defined as:

$$E_{form} = [E_{tot} - N_H (E_H) - N_B (E_B) - N_C (E_C) - N_N (E_N)] / N \text{ ---- } (5.1)$$

where, E_{tot} is the total energy of the system in its ground state spin configuration and E_H, E_B, E_C and E_N are the energies of the hydrogen, boron, carbon and nitrogen in hydrogen molecule, α-rhombohedral boron, graphene and nitrogen molecule, per atom, respectively. N is the total number of atoms in the system and N_H, N_B, N_C and N_N are the number of hydrogen, boron, carbon and nitrogen atoms in the system, respectively.

Table 5.1: Formation energy, Fermi-energy, magnetic moment, band-gap of the systems in both ferro and anti-ferro magnetic spin configurations for (2.44, 2.48) nm ribbon.

Ferro-Magnetic (FM) (2.44, 2.48) nm ribbon= total 176 atoms					
System	**E_{FM} - E_{AFM} (meV)**	**Formation Energy per atom, E_{form} (eV/ atom)**	**Spin-polarization (Spin-up - Spin-down) μβ**	**Band-gap (eV)**	
				Majority Spin	**Minority Spin**
Pristine-X-shaped-GQD	0.04	-2.986	0.00	-	-
com-ed-sub-GQD	6.94	-2.186	0.00	-	-
V-ed-sub-GQD	13.34	-2.639	0.80	-	-
Pristine-X-shaped-BNQD	-0.16	-1.746	0.00	4.05	4.05
com-ed-sub-BNQD	-0.44	-2.342	0.00	0.56	0.56
V-ed-sub-BNQD	-2.68	-1.968	1.08	0.00	0.00
Anti-Ferro Magnetic (AFM) (2.44, 2.48) nm ribbon					
System	**E_{FM} - E_{AFM} (meV)**	**Formation Energy per atom, E_{form} (eV/ atom)**	**Spin-polarization (Spin-up - Spin-down) μβ**	**Bandgap (eV)**	
				Majority Spin	**Minority Spin**
Pristine-X-shaped-GQD	0.04	-2.986	0.00	0.78	0.78
com-ed-sub-GQD	6.94	-2.186	0.00	0.90	0.90
V-ed-sub-GQD	13.34	-2.639	-0.80	0.00	0.00
Pristine-X-shaped-BNQD	-0.16	-1.746	0.00	-	-
com-ed-sub-BNQD	-0.44	-2.342	0.00	-	-
V-ed-sub-BNQD	-2.68	-1.968	1.08	-	-

Table 5.2: Formation energy, Fermi-energy, magnetic moment, band-gap of the systems in both ferro and anti-ferro magnetic spin configurations for (4.16, 3.97) nm ribbon.

<table>
<tr><th colspan="6">Ferro-Magnetic (FM) (4.16, 3.97) nm ribbon = total 308 atoms</th></tr>
<tr><th rowspan="2">System</th><th rowspan="2">E_{FM} - E_{AFM} (meV)</th><th rowspan="2">Formation Energy per atom, E_{form} (eV/ atom)</th><th rowspan="2">Spin-polarization (Spin-up - Spin-down) μβ</th><th colspan="2">Band-gap (eV)</th></tr>
<tr><th>Majority Spin</th><th>Minority Spin</th></tr>
<tr><td>Pristine-X-shaped-GQD</td><td>92.24</td><td>-2.988</td><td>4.00</td><td>0.51</td><td>0.44</td></tr>
<tr><td>com-ed-sub-GQD</td><td>0.67</td><td>-2.187</td><td>0.00</td><td>0.52</td><td>0.52</td></tr>
<tr><td>V-ed-sub-GQD</td><td>47.16</td><td>-2.615</td><td>2.15</td><td>0.00</td><td>0.00</td></tr>
<tr><td>Pristine-X-shaped-BNQD</td><td>-6.96</td><td>-1.743</td><td>0.00</td><td>3.90</td><td>3.90</td></tr>
<tr><td>com-ed-sub-BNQD</td><td>-0.82</td><td>-2.336</td><td>0.00</td><td>0.27</td><td>0.27</td></tr>
<tr><td>V-ed-sub-BNQD</td><td>-4.43</td><td>-1.996</td><td>0.73</td><td>0.00</td><td>0.00</td></tr>
<tr><th colspan="6">Anti-Ferro Magnetic (FM) (4.16, 3.97) nm ribbon</th></tr>
<tr><th rowspan="2">System</th><th rowspan="2">E_{FM} - E_{AFM} (meV)</th><th rowspan="2">Formation Energy per atom, E_{form} (eV/ atom)</th><th rowspan="2">Spin-polarization (Spin-up - Spin-down) μβ</th><th colspan="2">Band-gap (eV)</th></tr>
<tr><th>Majority Spin</th><th>Minority Spin</th></tr>
<tr><td>Pristine-X-shaped-GQD</td><td>92.24</td><td>-2.988</td><td>0.00</td><td>3.74</td><td>3.74</td></tr>
<tr><td>com-ed-sub-GQD</td><td>0.67</td><td>-2.187</td><td>0.00</td><td>0.52</td><td>0.52</td></tr>
<tr><td>V-ed-sub-GQD</td><td>47.16</td><td>-2.615</td><td>0.00</td><td>0.00</td><td>0.24</td></tr>
<tr><td>Pristine-X-shaped-BNQD</td><td>-6.96</td><td>-1.743</td><td>0.00</td><td>3.90</td><td>3.90</td></tr>
<tr><td>com-ed-sub-BNQD</td><td>-0.82</td><td>-2.336</td><td>0.00</td><td>0.27</td><td>0.27</td></tr>
<tr><td>V-ed-sub-BNQD</td><td>-4.43</td><td>-1.996</td><td>0.02</td><td>0.00</td><td>0.03</td></tr>
</table>

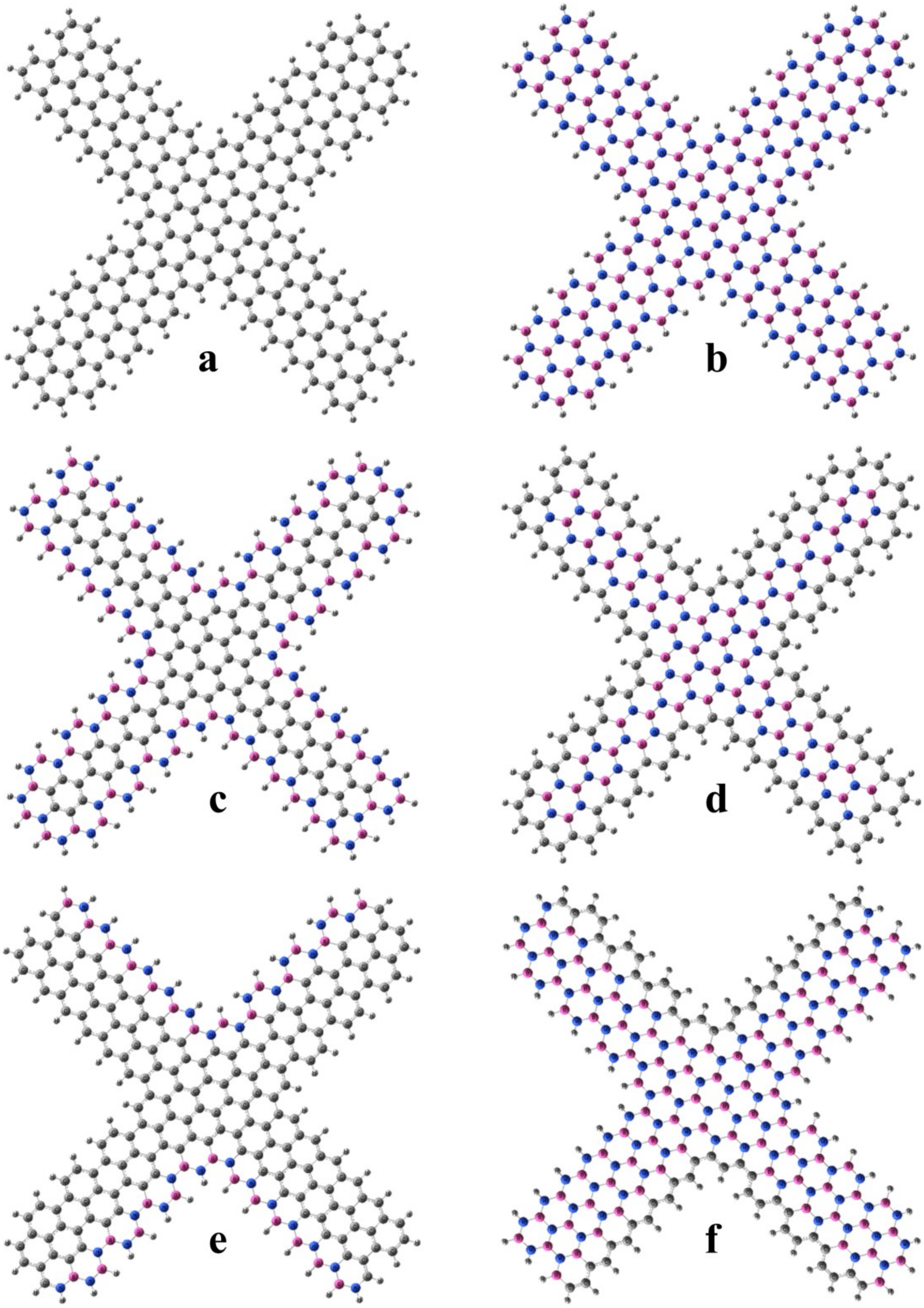

Figure 5.1: X-shaped quantum dots (a) Pristine-X-shaped-GQD, (b) com-ed-sub-GQD, (c) V-ed-sub-GQD, (d) Pristine-X-shaped-BNQD (e) com-ed-sub-BNQD (f) V-ed-sub-BNQD.

In tables 5.1 and 5.2, the formation energy values (per atom) of all the systems along with their magnetic moments and band-gap values are given. As is well known, negative E_{form} value indicates a thermodynamically stable system and higher the negative

E_{form} value, higher the stabilization of the system. Clearly, from tables 5.1 and 5.2, all the systems possess negative E_{form} values, and hence, thermodynamically stable. It is also important to mention here that, the formation energies of these systems are much below the formation energies of pristine graphene (-8.65 eV/atom) and h-BN sheet (-7.79 eV/atom),[205] but, their negative E_{form} values (much above the room temperature) assure that they are thermodynamically feasible, and hence, could be prepared experimentally.

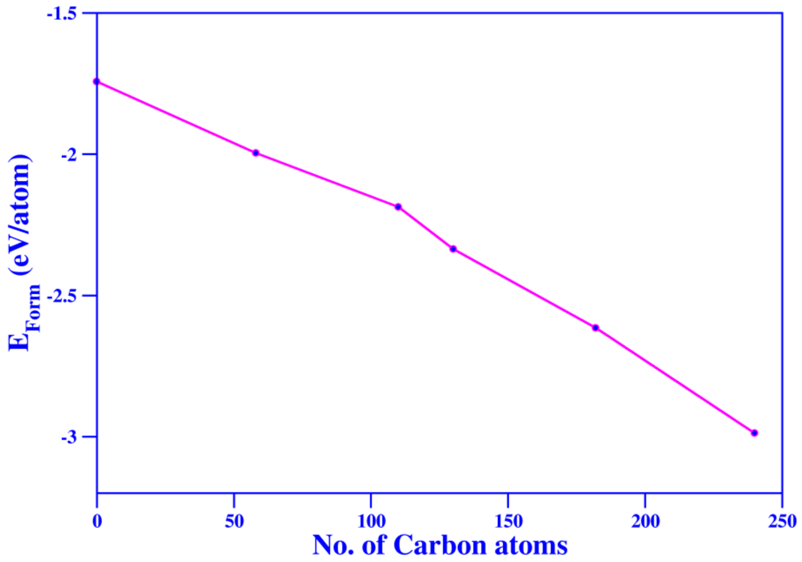

Figure 5.2: Variation of E_{form} with number of carbon atoms.

If we observe the E_{form} values of tables 5.1 and 5.2, we can also unveil that (among the systems considered) systems which have more number of carbon atoms are thermodynamically more stable than the systems with boron and nitrogen atoms (also see figure 5.2) which is just opposite to rectangular quantum dots.[206] This can be explained by comparing the formation energies of pristine graphene (-8.65 eV/atom) and h-BN (-7.79 eV/atom). These values indicate that, the formation of graphene is thermodynamically more feasible than h-BN. Thus, as we go from a system with a lower number of carbon atoms (i.e. BN rich) to a higher number (i.e. carbon rich), we are allowing the system to stabilize thermodynamically, and hence, the observed trend.

2) Electronic and Magnetic properties:

In this section we will explain the electronic and magnetic properties of all the QDs considered in this work.

To understand the edge effects on the electronic and magnetic properties of QDs, we have plotted the density of states (DOS) and projected density of states (pDOS) of all the QDs (see figure 5.3 and figure 5.4). Before explaining the reasons for the observed changes in electronic and magnetic properties, let us list some of the interesting results.

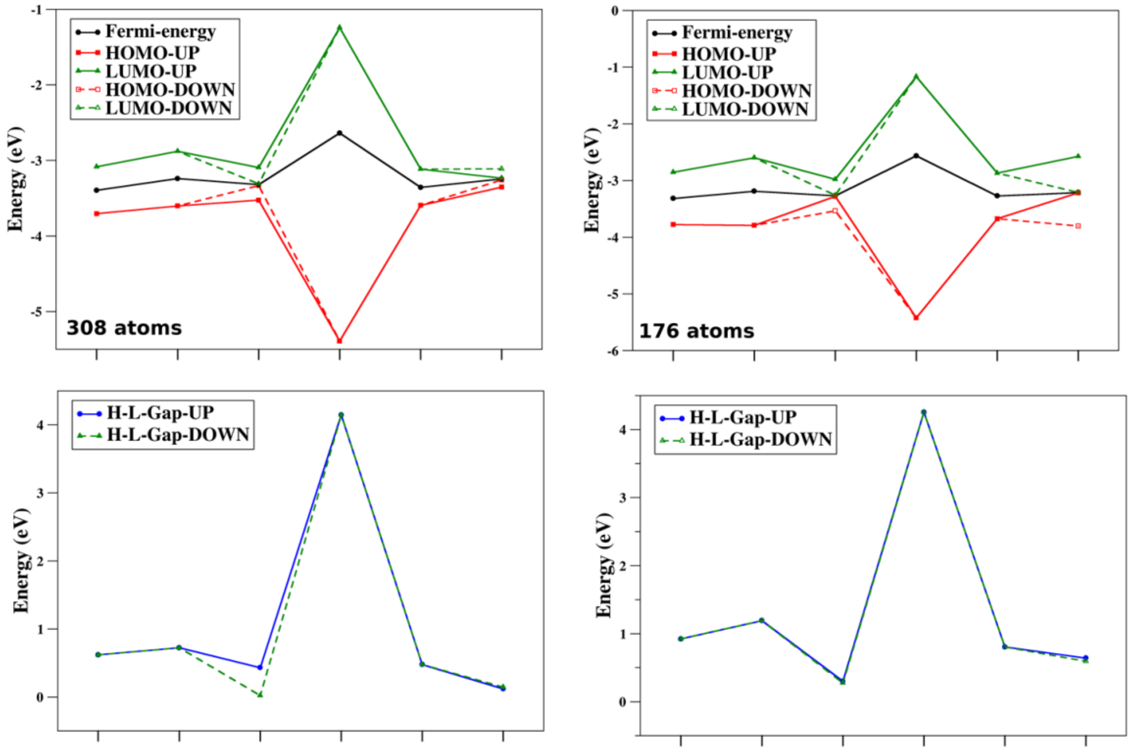

Figure 5.3: Variations of HOMO-LUMO gaps with substitution and size of the systems considered.

(i) Band gap:

By observing the tables 5.1 and 5.2, it can be noticed that the change in the band-gap from pristine-BNQD (pristine-GQD) to com-sub-BNQD (com-sub-GQD) is as large (low) as 3.63 eV (0.03 eV), for both the sizes. In fact, the band-gap of com-sub-BNQDs is even lesser than that of pristine-GQDs (the similar trend was found in case of rectangular quantum dots also [206]), and the order of the band-gap for the systems considered in this work is pristine-BNQDs > com-sub-GQDs > pristine-GQDs > com-sub-BNQDs > V-edge-sub-QDs. Also, if we observe the substitution at V-edge for both the dots, it can be realized, for both the sizes, that pristine-QDs turn from semiconducting to metallic when the substitution is done only at V-shape, and there is an opening of the band-gap again, when the QDs are completely substituted. Thus, there is a semiconducting (insulating) → metallic → semiconducting transition in both graphene and h-BN QDs as one goes from pristine-QDs → V-edge-sub-QDs → completely-sub-QDs. Clearly, in contrast to the formation energy, there is no relation between the band-gap and the number of carbon atoms. But, one plausible reason for the above trend could be the change in the symmetry of the quantum dot with the substitution, which follows the trend, symmetric → asymmetric → symmetric when the systems changes from pristine-QDs → V-edge-sub-QDs → completely-sub-QDs.

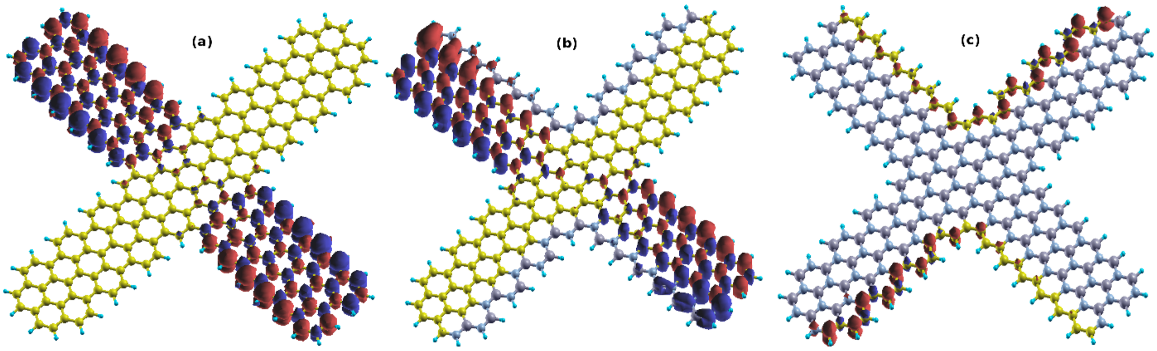

Figure 5.4: (spin-up) – (Spin-down) density of the spin-polarized systems with 308 atoms. (a) Pristine-X-shaped-GQD (b) V-ed-sub-GQD and (c) V-ed-sub-BNQD.

(ii) Spin-polarization:

Similar to the band-gap, there is also a transition in the spin-polarization (see table 5.1) from un-polarized → spin-polarized → un-polarized, when one goes from pristine-QDs → V-edge-sub-QDs → completely-sub-QDs, for both the sizes. So, V-edge-substituted QDs exhibits some interesting properties when compared to other QDs, and hence, need a special attention. From the figures 5.4 and 5.5, one can easily notice that, with a change in the size of the systems there is no change in the position of the total-spin (spin-up – spin-down) in the systems, for example, in the case of V-ed-sub-BNQD total-spin is mainly localized at the substituted edges only, for both the sizes. Thus, one can conclude that those properties which are related to the total-spin will not change with the size of the systems, for the systems considered here. Although, the systems are spin-polarized, as the total-spin is localized one would expect there will be no spin-conductance in these systems.

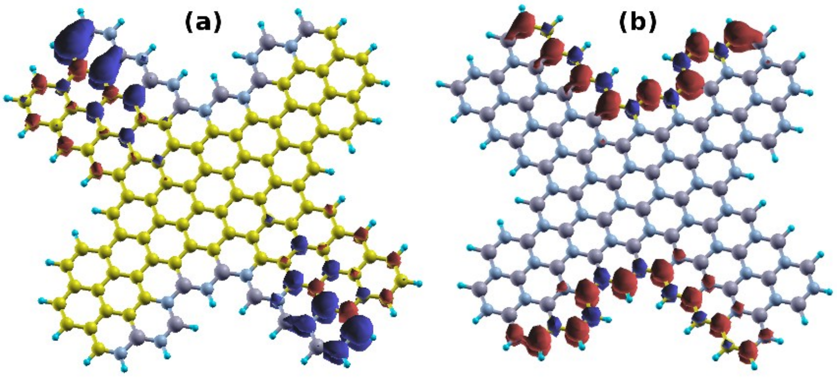

Figure 5.5: (Spin-up) – (Spin-down) density of the spin-polarized systems with 176 atoms.

(iii) DOS and p-DOS:

Interestingly, DOS plots show that for V-ed-sub-GQD, of width (4.16, 3.97) nm, is a half-metallic system, i.e. majority spin is conducting and minority spin is semi-conducting with a gap of ~ 0.24 eV. But, this phenomena is not global i.e. half-metallicity is not retained for all the sizes of V-ed-sub-GQD, and indeed, systems show metallicity for both up- and down-spins, for other widths. However, by observing the DOS of these V-ed-sub-QDs it seems that, there is a possibility to tune the Fermi-level of these systems, under the application of external electric-field, to make them half-metallic. Also, interestingly, we observed that DOS near the Fermi-level for the V-ed-sub-QDs have S_2-point group type symmetry, which is essentially the symmetry of the C-atoms of these systems in the real space. To check whether the symmetry of the C-atoms in the real space is the reason for the observed symmetry of the DOS near the Fermi-level, we did some more calculations by changing the symmetry of the GQDs by varying the substituents positions [To prove the symmetry effects of the system on the DOS of V-ed-doped-GQDs we substituted boron and nitrogen atoms only at the zigzag-wing in opposite sides, to resemble the V-ed-sub-GQD, and we found that symmetry in the DOS is retained, but this time, only very near the Fermi-level. This indicates that the symmetry of the DOS near the Fermi-level has impact from the whole system rather than a particular wing, although the zigzag wing is contributing more near the Fermi-level].

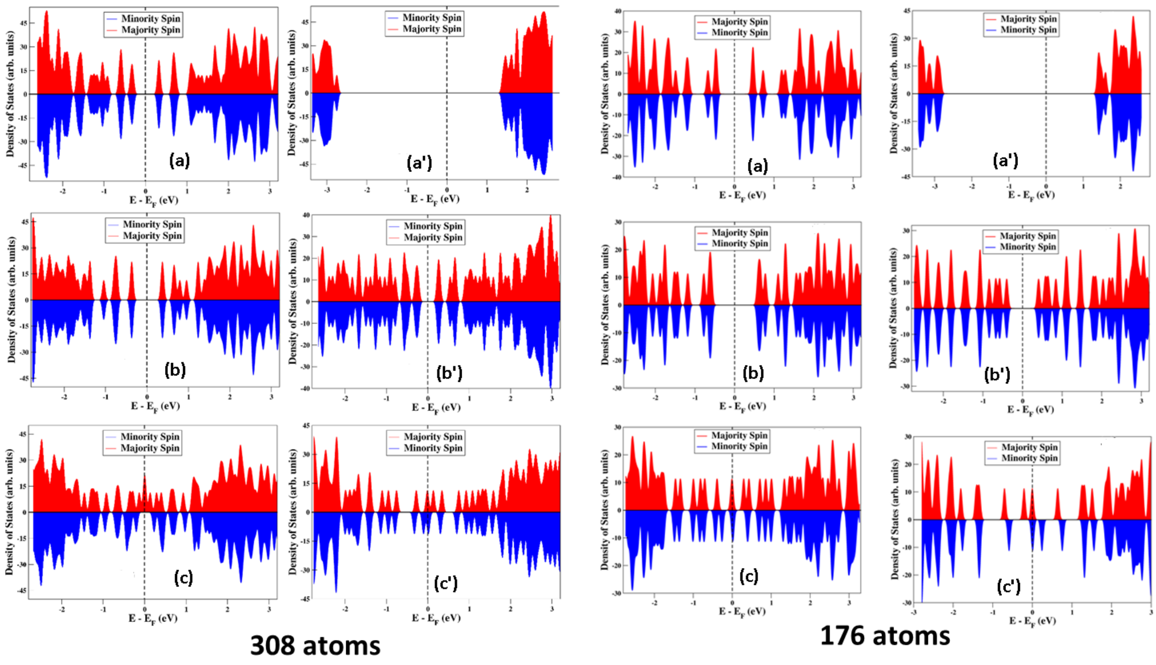

Figure 5.6: Density of States (DOS) plots for (a) Pristine-X-shaped-GQD, (b) com-ed-sub-GQD, (c) V-ed-sub-GQD, (a') Pristine-X-shaped-BNQD (b') com-ed-sub-BNQD (c') V-ed-sub-BNQD with 308 and 176 atoms.

p-DOS plots shows that, the main contribution for the DOS near the Fermi-level is mainly from the C-atoms for all the systems, except the pristine-BNQD which doesn't have any carbon atoms, and when the carbon atoms are at both edge and center of the system, then the former ones are contributing more than the latter ones near the Fermi-level and the reverse is true when we go away from the Fermi-level. When only carbon atoms are present at the edges, they are the major contributors to the DOS near the Fermi-level. These findings support our choice of substitution, i.e. substitution at the edge rather than at the centre of the quantum dot, because of which we got huge changes in the DOS of the systems.

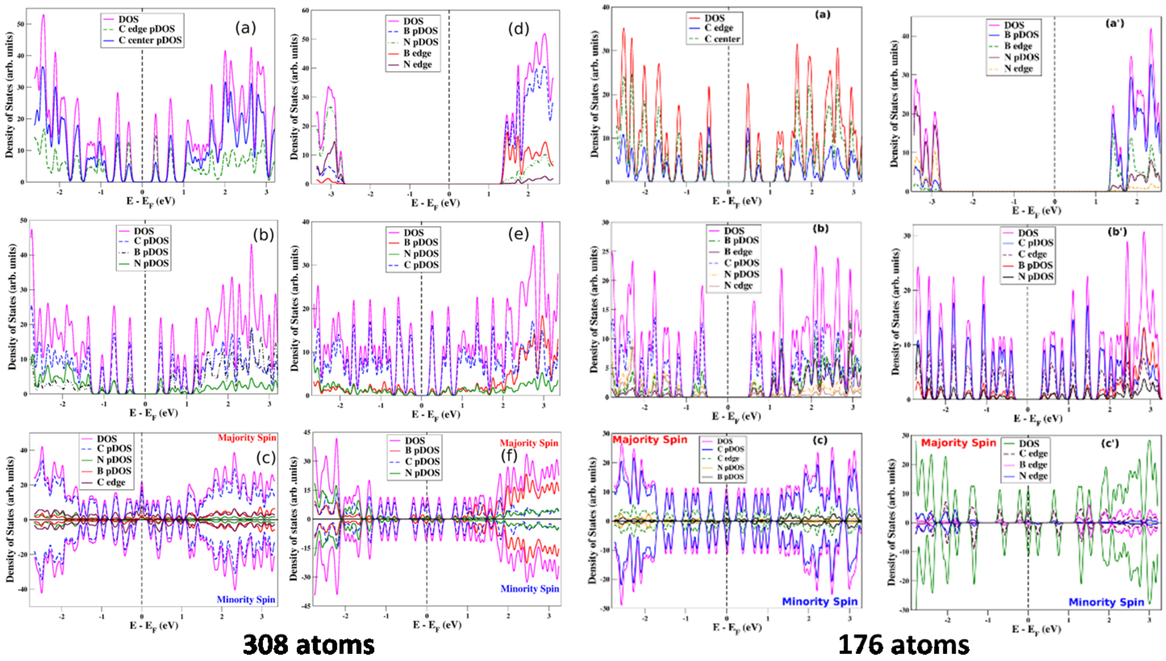

Figure 5.7: Projected Density of States (p-DOS) plots for (a) Pristine-X-shaped-GQD, (b) com-ed-sub-GQD, (c) V-ed-sub-GQD, (a') Pristine-X-shaped-BNQD (b') com-ed-sub-BNQD (c') V-ed-sub-BNQD with 308 and 176 atoms.

From the p-DOS of pristine-BNQD one can notice that the main contributions to the valence band are the nitrogen atoms of the system and for the conduction band boron atoms are the main contributors, as expected. But, when the systems contain carbon atoms, then the contributions got reversed near the Fermi-level. This can be explained on the basis of the border atoms (like a carbon atom in V-ed-sub-GQD which is connected to both an edge-boron atom and a center-carbon atom). When a boron (or nitrogen) atom is attached to a carbon atom then it will get (give) some charge from the carbon atom and thus the property of this atom will be opposite to what it should exhibit. As the border atoms (not shown here) and/or edge atoms are mainly contributing to the DOS near the Fermi-level for these systems (containing C, B and N atoms), we are observing an opposite effect in the DOS compared to the pristine-BNQD.

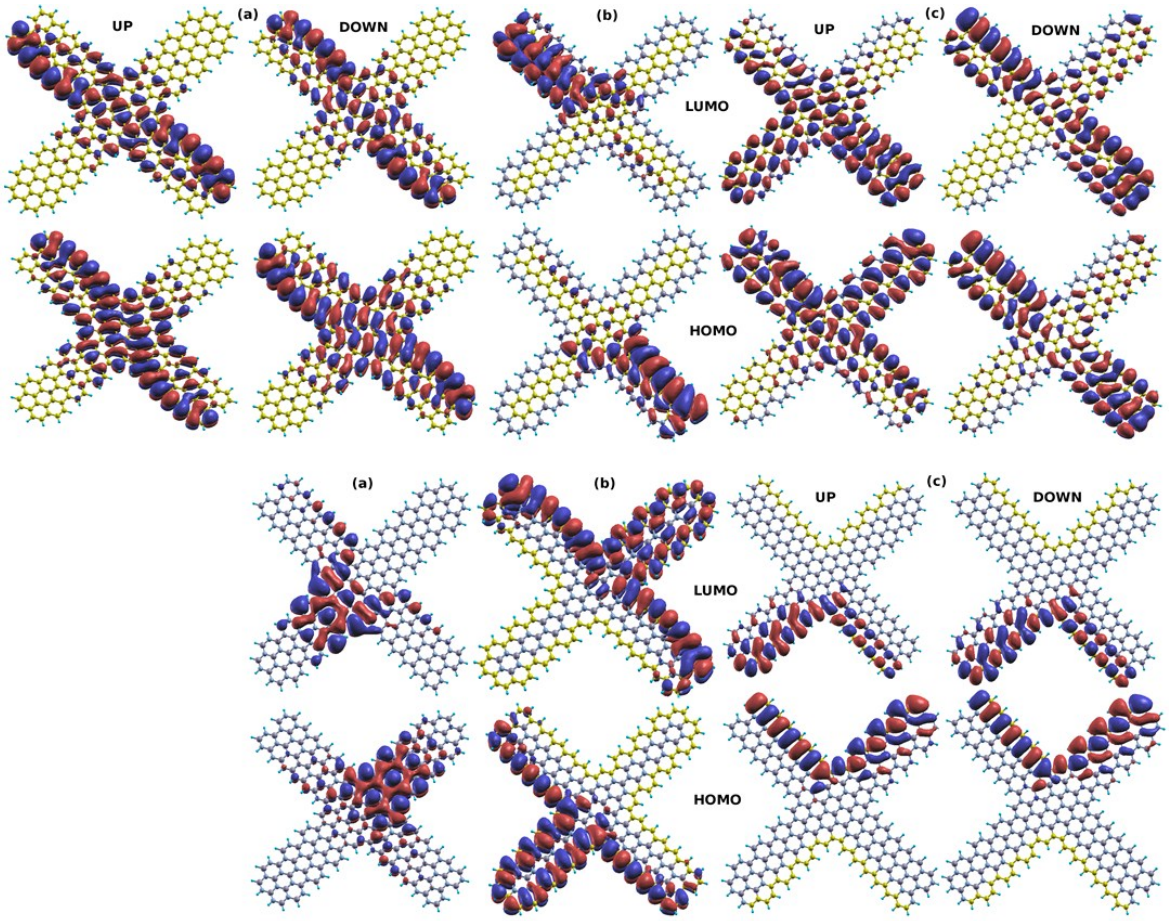

Figure 5.8: Top panel corresponds to: HOMO and LUMOs of (a) Pristine-X-shaped-GQD, (b) com-ed-sub-GQD, (c) V-ed-sub-GQD; Bottom panel corresponds to: HOMO and LUMOs of (a) Pristine-X-shaped-BNQD (b) com-ed-sub-BNQD (c) V-ed-sub-BNQD with 308 atoms.

By closely observing the p-DOS, we find that, although the symmetry in the DOS near the Fermi-level has a main contribution from the edge-carbon atoms, other border atoms are also possess the same kind of symmetry near the Fermi-level, as does the carbon atoms. In fact, the contribution from the boron atom to the valence band in majority spin is equal to the contribution of the nitrogen atom to conduction band in minority and thus related to each other in S_2 symmetry, as can be seen in the p-DOS of any of the V-ed-sub-QDs. The plausible reason for the above effect could be the symmetry of the system in real space, where an S_2 symmetry operation will impose the boron atoms of the V-ed-sub-QDs on to the nitrogen atoms of the system and we are able to observe it only near the Fermi-level because of the border atoms.

(iv) HOMO and LUMO orbitals:

Figures 5.8 and 5.9 show the Highest Occupied Molecular Orbital (HOMO) and Lowest Unoccupied Molecular Orbital (LUMO) plots, with an iso-contour value of 0.015e / $(\text{Å})^3$, for all the systems considered in this study. As can be seen from the plots, the nature of the plots didn't change much as one vary the size of the system for the BNQDs, which has been already reflected in the spin-density profiles of these systems. Thus, one can safely conclude, for the BNQD systems considered here, that variation of the size is not going to influence the properties related to the charge conduction (because the HOMO and LUMO will take main part for the conduction near the Femi-level, the only region which will be generally important for the conduction properties). But, in the case of GQDs, some clear changes can be noticed. Although, these changes seems to be because of the size changes, but close observation leads us to conclude that the changes are mainly because of the extended de-localization in GQDs which is absent in BNQDs. Hence, although the size changes seem to affect GQDs, they might get seized for little longer sizes than what have been considered here.

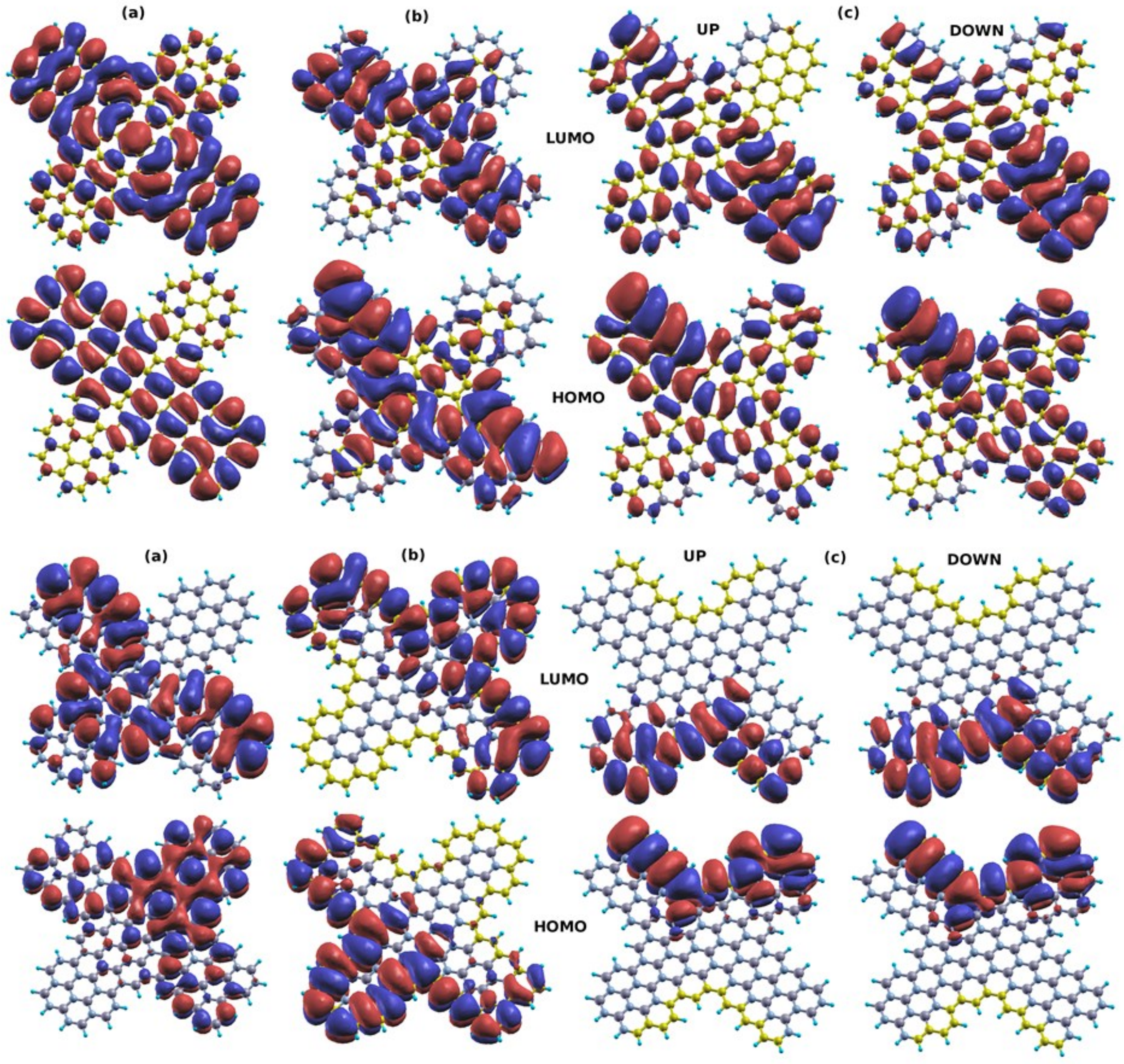

Figure 5.9: (Spin-up) – (Spin-down) density of the spin-polarized systems with 308 atoms. (a) Pristine-X-shaped-GQD (b) V-ed-sub-GQD and (c) V-ed-sub-BNQD.

6.4 Conclusion

In our study, we have calculated the electronic and magnetic properties of X-shaped GQD, BNQD and the effect of BN/carbon atom substitution on GQDs/BNQDs. We have found that the GQDs are stable in AFM and the BNQDs are stable in FM ground state. A semiconducting (insulating) → metallic → semiconducting transition is found in both graphene and h-BN QDs as the systems are substituted from pristine-QDs → V-edge-sub-QDs → completely-sub-QDs. Also, the systems change to un-spin polarized → spin polarized → un-spin polarized ground states under these conditions. V-edge-sub-QDs are found to show a unique property, the half-metallicity.

References

1. Degiorgi, L., *Strong interactions in low dimensions*. 2004: Springer.
2. Kelly, M.J., *Low-dimensional semiconductors:*

materials, physics, technology, devices. 1995.

3. Crommie, M.F., C.P. Lutz, and D.M. Eigler, *Confinement of electrons to quantum corrals on a metal-surface.* Science, 1993. **262**(5131): p. 218-220.
4. Stucky, G.D. and J.E. Macdougall, *Quantum confinement and host guest chemistry - Probing a new dimension.* Science, 1990. **247**(4943): p. 669-678.
5. Takagahara, T. and K. Takeda, *Theory of the quantum confinement effect on excitons in quantum dots of indirect-gap materials.* Physical Review B, 1992. **46**(23): p. 15578-15581.
6. Delley, B. and E.F. Steigmeier, *Quantum confinement in si nanocrystals.* Physical Review B, 1993. **47**(3): p. 1397-1400.
7. Bryant, G.W., *Excitons in quantum boxes - correlation-effects and quantum confinement.* Physical Review B, 1988. **37**(15): p. 8763-8772.
8. Krishna, M.V.R. and R.A. Friesner, *Quantum confinement effects in semiconductor clusters.* Journal of Chemical Physics, 1991. **95**(11): p. 8309-8322.
9. Einevoll, G.T., *Confinement of excitons in quantum dots.* Physical Review B, 1992. **45**(7): p. 3410-3417.
10. Wiegmann, P.B., *Superconductivity in strongly correlated electronic systems and confinement versus deconfinement phenomenon.* Physical Review Letters, 1988. **60**(9): p. 821-824.
11. Si, Q.M., et al., *Locally critical quantum phase transitions in strongly correlated metals.* Nature, 2001. **413**(6858): p. 804-808.
12. Dagotto, E., *Complexity in strongly correlated electronic systems.* Science, 2005. **309**(5732): p. 257-262.
13. Capone, M., et al., *Strongly correlated superconductivity.* Science, 2002. **296**(5577): p. 2364-2366.
14. Chakravarty, S., M.P. Gelfand, and S. Kivelson, *Electronic correlation-effects and superconductivity in doped fullerenes.* Science, 1991. **254**(5034): p. 970-974.
15. Voskoboynikov, O., et al., *Interband magneto-optical transitions in a layer of semiconductor nano-rings.* Europhysics Letters, 2005. **70**(5): p. 656-662.
16. Matveev, K.A., A.I. Larkin, and L.I. Glazman, *Persistent Current in Superconducting Nanorings.* Physical Review Letters, 2002. **89**(9): p. 096802.
17. Miao, F., et al., *Phase-coherent transport in graphene quantum billiards.* Science, 2007. **317**(5844): p. 1530-1533.
18. Waser, R. and M. Aono, *Nanoionics-based resistive switching memories.* Nature Materials, 2007. **6**(11): p. 833-840.
19. Coronado, E., et al., *Coexistence of ferromagnetism and metallic conductivity in a molecule-based layered compound.* Nature, 2000. **408**(6811): p. 447-449.
20. Wang, X.F., et al., *Superconductivity at 5 K in alkali-metal-doped phenanthrene.* Nature Communications, 2011. **2**.
21. Jeong, H., A.M. Chang, and M.R. Melloch, *The Kondo effect in an artificial quantum dot molecule.* Science, 2001. **293**(5538): p. 2221-2223.

22. Liang, W.J., et al., *Kondo resonance in a single-molecule transistor.* Nature, 2002. **417**(6890): p. 725-729.
23. Nygard, J., D.H. Cobden, and P.E. Lindelof, *Kondo physics in carbon nanotubes.* Nature, 2000. **408**(6810): p. 342-346.
24. Park, J., et al., *Coulomb blockade and the Kondo effect in single-atom transistors.* Nature, 2002. **417**(6890): p. 722-725.
25. Lyo, I.W. and P. Avouris, *Field-induced nanometer-scale to atomic-scale manipulation of silicon surfaces with the stm.* Science, 1991. **253**(5016): p. 173-176.
26. Dhirani, A.A., et al., *Self-assembly of conjugated molecular rods: A high-resolution STM study.* Journal of the American Chemical Society, 1996. **118**(13): p. 3319-3320.
27. Jung, T.A., R.R. Schlittler, and J.K. Gimzewski, *Conformational identification of individual adsorbed molecules with the STM.* Nature, 1997. **386**(6626): p. 696-698.
28. Zhou, C., et al., *Microfabrication of a mechanically controllable break junction in silicon.* Applied Physics Letters, 1995. **67**(8): p. 1160-1162.
29. Fernandez-Seivane, L., V.M. Garcia-Suarez, and J. Ferrer, *Predictions for the formation of atomic chains in mechanically controllable break-junction experiments.* Physical Review B, 2007. **75**(7).
30. Giessibl, F.J., *Atomic-resolution of the silicon (111)-(7x7) surface by atomic-force microscopy.* Science, 1995. **267**(5194): p. 68-71.
31. Rief, M., et al., *Single molecule force spectroscopy on polysaccharides by atomic force microscopy.* Science, 1997. **275**(5304): p. 1295-1297.
32. Meyer, G. and N.M. Amer, *Novel optical approach to atomic force microscopy.* Applied Physics Letters, 1988. **53**(12): p. 1045-1047.
33. Carpick, R.W. and M. Salmeron, *Scratching the surface: Fundamental investigations of tribology with atomic force microscopy.* Chemical Reviews, 1997. **97**(4): p. 1163-1194.
34. Rugar, D. and P. Hansma, *Atomic Force Microscopy.* Physics Today, 1990. **43**(10): p. 23-30.
35. Reetz, M.T., et al., *VISUALIZATION OF SURFACTANTS ON NANOSTRUCTURED PALLADIUM CLUSTERS BY A COMBINATION OF STM AND HIGH-RESOLUTION TEM.* Science, 1995. **267**(5196): p. 367-369.
36. Wang, Z.L., *Transmission electron microscopy of shape-controlled nanocrystals and their assemblies.* Journal of Physical Chemistry B, 2000. **104**(6): p. 1153-1175.
37. Schrieffer, J.R. and A.P. Kampf, *ARPES: Novel effect in the energy and momentum distributions.* Journal of Physics and Chemistry of Solids, 1995. **56**(12): p. 1673-1677.
38. Olson, C.G., et al., *Superconducting gap in bi-sr-ca-cu-o by high-resolution angle-resolved photoelectron-spectroscopy.* Science, 1989. **245**(4919): p. 731-733.
39. Wallace, P.R., *The Band Theory of Graphite.* Physical Review, 1947. **71**(9): p. 622-634.
40. McClure, J.W., *Diamagnetism of Graphite.* Physical Review, 1956. **104**(3): p. 666-671.

41. Slonczewski, J.C. and P.R. Weiss, *Band Structure of Graphite.* Physical Review, 1958. **109**(2): p. 272-279.
42. Peierls, R., *Quelques propriétés typiques des corps solides.* Ann. Inst. Henri Poincare, 1935. **5**(3): p. 177-222.
43. Landau, L., *Zur theorie der phasenumwandlungen II. Phys.* Z. Sowjetunion, 1937. **11**: p. 26-35.
44. Mermin, N.D., *Crystalline Order in Two Dimensions.* Physical Review, 1968. **176**(1): p. 250-254.
45. Venables, J.A., G.D.T. Spiller, and M. Hanbucken, *Nucleation and growth of thin films.* Reports on Progress in Physics, 1984. **47**(4): p. 399.
46. Evans, J.W., P.A. Thiel, and M.C. Bartelt, *Morphological evolution during epitaxial thin film growth: Formation of 2D islands and 3D mounds.* Surface Science Reports, 2006. **61**(1–2): p. 1-128.
47. Geim, A.K. and K.S. Novoselov, *The rise of graphene.* Nature Materials, 2007. **6**(3): p. 183-191.
48. Novoselov, K., et al., *Electric field effect in atomically thin carbon films.* Science, 2004. **306**(5696): p. 666-669.
49. Su, C.-Y., et al., *High-Quality Thin Graphene Films from Fast Electrochemical Exfoliation.* ACS Nano, 2011. **5**(3): p. 2332-2339.
50. Reina, A., et al., *Large Area, Few-Layer Graphene Films on Arbitrary Substrates by Chemical Vapor Deposition.* Nano Letters, 2008. **9**(1): p. 30-35.
51. Chae, S.J., et al., *Synthesis of Large-Area Graphene Layers on Poly-Nickel Substrate by Chemical Vapor Deposition: Wrinkle Formation.* Advanced Materials, 2009. **21**(22): p. 2328-2333.
52. Lotya, M., et al., *High-Concentration, Surfactant-Stabilized Graphene Dispersions.* ACS Nano, 2010. **4**(6): p. 3155-3162.
53. Sutter, P.W., J.-I. Flege, and E.A. Sutter, *Epitaxial graphene on ruthenium.* Nature Materials, 2008. **7**(5): p. 406-411.
54. Pletikosić, I., et al., *Dirac Cones and Minigaps for Graphene on Ir(111).* Physical Review Letters, 2009. **102**(5): p. 056808.
55. Li, X., et al., *Evolution of graphene growth on Ni and Cu by carbon isotope labeling.* Nano Letters, 2009. **9**(12): p. 4268-4272.
56. Bae, S., et al., *Roll-to-roll production of 30-inch graphene films for transparent electrodes.* Nature Nanotechnology, 2010. **5**(8): p. 574-578.
57. Li, X., et al., *Large-area synthesis of high-quality and uniform graphene films on copper foils.* Science, 2009. **324**(5932): p. 1312-1314.
58. Novoselov, K., et al., *Two-dimensional gas of massless Dirac fermions in graphene.* Nature, 2005. **438**(7065): p. 197-200.
59. Dutta, S. and S.K. Pati, *Novel properties of graphene nanoribbons: a review.* J. Mater. Chem., 2010. **20**(38): p. 8207-8223.
60. Nakada, K., et al., *Edge state in graphene ribbons: Nanometer size effect and edge shape dependence.* Physical Review B, 1996. **54**(24): p. 17954.
61. Barone, V., O. Hod, and G.E. Scuseria, *Electronic structure and stability of semiconducting graphene nanoribbons.* Nano Letters, 2006. **6**(12): p. 2748-2754.
62. Lu, Y., et al., *Effects of edge passivation by hydrogen on electronic structure of armchair graphene nanoribbon and band gap engineering.* Applied Physics Letters, 2009. **94**(12): p. 122111-122111-3.

63. Cai, J., et al., *Atomically precise bottom-up fabrication of graphene nanoribbons.* Nature, 2010. **466**(7305): p. 470-473.
64. Masubuchi, S., et al., *Fabrication of graphene nanoribbon by local anodic oxidation lithography using atomic force microscope.* Applied Physics Letters, 2009. **94**(8): p. 082107-082107-3.
65. Tapaszto, L., et al., *Tailoring the atomic structure of graphene nanoribbons by scanning tunnelling microscope lithography.* Nature nanotechnology, 2008. **3**(7): p. 397-401.
66. Wang, X. and H. Dai, *Etching and narrowing of graphene from the edges.* Nature Chemistry, 2010. **2**(8): p. 661-665.
67. Ci, L., et al., *Controlled nanocutting of graphene.* Nano Research, 2008. **1**(2): p. 116-122.
68. Li, X., et al., *Chemically derived, ultrasmooth graphene nanoribbon semiconductors.* Science, 2008. **319**(5867): p. 1229-1232.
69. Kosynkin, D.V., et al., *Longitudinal unzipping of carbon nanotubes to form graphene nanoribbons.* Nature, 2009. **458**(7240): p. 872-876.
70. Mohanty, N., et al., *Nanotomy-based production of transferable and dispersible graphene nanostructures of controlled shape and size.* Nature Communications, 2012. **3**: p. 844.
71. Son, Y.-W., M.L. Cohen, and S.G. Louie, *Energy gaps in graphene nanoribbons.* Physical Review Letters, 2006. **97**(21): p. 216803.
72. Raza, H. and E.C. Kan, *Armchair graphene nanoribbons: Electronic structure and electric-field modulation.* Physical Review B, 2008. **77**(24): p. 245434.
73. Dutta, S. and S.K. Pati, *Half-Metallicity in Undoped and Boron Doped Graphene Nanoribbons in the Presence of Semilocal Exchange-Correlation Interactions.* The Journal of Physical Chemistry B, 2008. **112**(5): p. 1333-1335.
74. Ershaad Ahamed, B., P. Prakash, and K.P. Swapan, *Electronic and magnetic properties of BNC nanoribbons: a detailed computational study.* New Journal of Physics, 2011. **13**(5): p. 053008.
75. Dutta, S., A.K. Manna, and S.K. Pati, *Intrinsic Half-Metallicity in Modified Graphene Nanoribbons.* Physical Review Letters, 2009. **102**(9): p. 096601.
76. Miyamoto, Y., K. Nakada, and M. Fujita, *First-principles study of edge states of H-terminated graphitic ribbons.* Physical Review B, 1999. **59**(15): p. 9858-9861.
77. Lieb, E.H., *Two theorems on the Hubbard model.* Physical Review Letters, 1989. **62**(10): p. 1201-1204.
78. Son, Y.-W., M.L. Cohen, and S.G. Louie, *Half-metallic graphene nanoribbons.* Nature, 2006. **444**(7117): p. 347-349.
79. Barnard, I.S.a.A., ed. *Graphene Nano-Flakes and Nano-Dots: Theory, Experiment and Applications*. Physics and Applications of Graphene - Theory, ed. S. Mikhailov. 2011, InTech.
80. Hod, O., V. Barone, and G.E. Scuseria, *Half-metallic graphene nanodots: A comprehensive first-principles theoretical study.* Physical Review B, 2008. **77**(3): p. 035411.
81. Potasz, P., et al., *Electronic and magnetic properties of triangular graphene quantum rings.* Physical Review B, 2011. **83**(17): p. 174441.
82. Dutta, M., et al., *ZnO/Graphene Quantum Dot Solid-State Solar Cell.* The Journal of Physical Chemistry C, 2012. **116**(38): p. 20127-20131.

83. Son, D.I., et al., *Emissive ZnO-graphene quantum dots for white-light-emitting diodes.* Nature nanotechnology, 2012. **7**(7): p. 465-471.
84. Chen, F. and N. Tao, *Electron transport in single molecules: from benzene to graphene.* Accounts of Chemical Research, 2009. **42**(3): p. 429-438.
85. Chen, F. and N.J. Tao, *Electron Transport in Single Molecules: From Benzene to Graphene.* Accounts of Chemical Research, 2009. **42**(3): p. 429-438.
86. Sheng, W., et al., *Magnetism and perfect spin filtering effect in graphene nanoflakes.* Nanotechnology, 2010. **21**(38): p. 385201.
87. Zhou, J., et al., *Intrinsic ferromagnetism in two-dimensional carbon structures: Triangular graphene nanoflakes linked by carbon chains.* Physical Review B, 2011. **84**(8): p. 081402.
88. Wang, W.L., S. Meng, and E. Kaxiras, *Graphene NanoFlakes with Large Spin.* Nano Letters, 2007. **8**(1): p. 241-245.
89. Zhi, L. and K. Müllen, *A bottom-up approach from molecular nanographenes to unconventional carbon materials.* J. Mater. Chem., 2008. **18**(13): p. 1472-1484.
90. Loh, K.P., et al., *The chemistry of graphene.* Journal of Materials Chemistry, 2010. **20**(12): p. 2277-2289.
91. Ci, L., et al., *Graphene shape control by multistage cutting and transfer.* Advanced Materials, 2009. **21**(44): p. 4487-4491.
92. Neubeck, S., et al., *From One Electron to One Hole: Quasiparticle Counting in Graphene Quantum Dots Determined by Electrochemical and Plasma Etching.* Small, 2010. **6**(14): p. 1469-1473.
93. Datta, S.S., et al., *Crystallographic etching of few-layer graphene.* Nano Letters, 2008. **8**(7): p. 1912-1915.
94. Yan, X., et al., *Independent Tuning of the Band Gap and Redox Potential of Graphene Quantum Dots.* The Journal of Physical Chemistry Letters, 2011. **2**(10): p. 1119-1124.
95. Ma, W.-L. and S.-S. Li, *Electrically controllable energy gaps in graphene quantum dots.* Applied Physics Letters, 2012. **100**(16): p. 163109-163109-4.
96. Tang, Q., Z. Zhou, and Z. Chen, *Molecular Charge Transfer: A Simple and Effective Route To Engineer the Band Structures of BN Nanosheets and Nanoribbons.* The Journal of Physical Chemistry C, 2011. **115**(38): p. 18531-18537.
97. Smalley, R., H. Kroto, and J. Heath, *C60: Buckminsterfullerene.* Nature, 1985. **318**: p. 162-163.
98. Tenne, R., et al., *Polyhedral and cylindrical structures of tungsten disulphide.* Nature, 1992. **360**(6403): p. 444-446.
99. Rosentsveig, R., et al., *Synthesis of fullerene-like MoS2 nanoparticles and their tribological behavior.* Journal of Materials Chemistry, 2009. **19**(25): p. 4368-4374.
100. Golberg, D., et al., *Octahedral boron nitride fullerenes formed by electron beam irradiation.* Applied Physics Letters, 1998. **73**(17): p. 2441-2443.
101. Iijima, S., *Helical microtubules of graphitic carbon.* Nature, 1991. **354**(6348): p. 56-58.
102. Chopra, N.G., et al., *Boron Nitride Nanotubes.* Science, 1995. **269**(5226): p. 966-967.
103. Rothschild, A., J. Sloan, and R. Tenne, *Growth of WS2 nanotubes phases.* Journal of the American Chemical Society, 2000. **122**(21): p. 5169-5179.

104. Ci, L., et al., *Atomic layers of hybridized boron nitride and graphene domains.* Nature materials, 2010. **9**(5): p. 430-435.
105. Shinde, P.P. and V. Kumar, *Direct band gap opening in graphene by BN doping: Ab initio calculations.* Physical Review B, 2011. **84**(12): p. 125401.
106. Han, M.Y., et al., *Energy band-gap engineering of graphene nanoribbons.* Physical Review Letters, 2007. **98**(20): p. 206805.
107. Ritter, K.A. and J.W. Lyding, *The influence of edge structure on the electronic properties of graphene quantum dots and nanoribbons.* Nature materials, 2009. **8**(3): p. 235-242.
108. Manna, A.K. and S.K. Pati, *Tuning the electronic structure of graphene by molecular charge transfer: a computational study.* Chemistry–An Asian Journal, 2009. **4**(6): p. 855-860.
109. Dong, X., et al., *Doping Single-Layer Graphene with Aromatic Molecules.* Small, 2009. **5**(12): p. 1422-1426.
110. Sun, J., et al., *Linear tuning of charge carriers in graphene by organic molecules and charge-transfer complexes.* Physical Review B, 2010. **81**(15): p. 155403.
111. Das, B., et al., *Changes in the electronic structure and properties of graphene induced by molecular charge-transfer.* Chemical Communications, 2008(41): p. 5155-5157.
112. Şahin, H. and S. Ciraci, *Structural, mechanical, and electronic properties of defect-patterned graphene nanomeshes from first principles.* Physical Review B, 2011. **84**(3): p. 035452.
113. Banhart, F., J. Kotakoski, and A.V. Krasheninnikov, *Structural defects in graphene.* 2010.
114. Neto, A.H.C., et al., *The electronic properties of graphene.* Reviews of modern physics, 2009. **81**(1): p. 109.
115. Helveg, S., et al., *Atomic-scale structure of single-layer MoS2 nanoclusters.* Physical review letters, 2000. **84**(5): p. 951-954.
116. Lebègue, S. and O. Eriksson, *Electronic structure of two-dimensional crystals from ab initio theory.* Physical Review B, 2009. **79**(11): p. 115409.
117. Han, W.Q., et al., *Structure of chemically derived mono-and few-atomic-layer boron nitride sheets.* Applied Physics Letters, 2008. **93**(22): p. 223103-223103-3.
118. Novoselov, K., et al., *Two-dimensional atomic crystals.* Proceedings of the National Academy of Sciences of the United States of America, 2005. **102**(30): p. 10451-10453.
119. Mak, K.F., et al., *Atomically Thin MoS_ {2}: A New Direct-Gap Semiconductor.* Physical Review Letters, 2010. **105**(13): p. 136805.
120. Xu, M., et al., *Graphene-Like Two-Dimensional Materials.* Chemical Reviews, 2013.
121. Ci, L., et al., *Atomic layers of hybridized boron nitride and graphene domains.* Nat Mater, 2010. **9**(5): p. 430-435.
122. Song, L., et al., *Large Scale Growth and Characterization of Atomic Hexagonal Boron Nitride Layers.* Nano Letters, 2010. **10**(8): p. 3209-3215.
123. Han, W.-Q., et al., *Structure of chemically derived mono- and few-atomic-layer boron nitride sheets.* Applied Physics Letters, 2008. **93**(22): p. 223103-3.
124. Zhi, C., et al., *Large-Scale Fabrication of Boron Nitride Nanosheets and Their Utilization in Polymeric Composites with Improved Thermal and Mechanical Properties.* Advanced Materials, 2009. **21**(28): p. 2889-2893.

125. Meyer, J.C., et al., *Selective Sputtering and Atomic Resolution Imaging of Atomically Thin Boron Nitride Membranes.* Nano Letters, 2009. **9**(7): p. 2683-2689.
126. Rao, C.N.R. and A. Nag, *Inorganic Analogues of Graphene.* European Journal of Inorganic Chemistry, 2010. **2010**(27): p. 4244-4250.
127. Zhou, J., et al., *Electronic and magnetic properties of a BN sheet decorated with hydrogen and fluorine.* Physical Review B, 2010. **81**(8): p. 085442.
128. Rao, C. and A. Nag, *Inorganic analogues of graphene.* European Journal of Inorganic Chemistry, 2010. **2010**(27): p. 4244-4250.
129. Zheng, F., et al., *Half metallicity along the edge of zigzag boron nitride nanoribbons.* Physical Review B, 2008. **78**(20): p. 205415.
130. Ramakrishna Matte, H., et al., *MoS2 and WS2 analogues of Graphene.* Angewandte Chemie, 2010. **122**(24): p. 4153-4156.
131. Zhou, K.G., et al., *A Mixed-Solvent Strategy for Efficient Exfoliation of Inorganic Graphene Analogues.* Angewandte Chemie International Edition, 2011. **50**(46): p. 10839-10842.
132. Liu, K.K., et al., *Growth of large-area and highly crystalline MoS2 thin layers on insulating substrates.* Nano letters, 2012. **12**(3): p. 1538-1544.
133. Yang, D. and R. Frindt, *Li-intercalation and exfoliation of WS< sub> 2</sub>.* Journal of Physics and Chemistry of Solids, 1996. **57**(6): p. 1113-1116.
134. Cheon, J., J.E. Gozum, and G.S. Girolami, *Chemical Vapor Deposition of MoS2 and TiS2 Films From the Metal-Organic Precursors Mo (S-t-Bu) 4 and Ti (S-t-Bu) 4.* Chemistry of Materials, 1997. **9**(8): p. 1847-1853.
135. Imanishi, N., K. Kanamura, and Z.i. Takehara, *Synthesis of MoS2 thin film by chemical vapor deposition method and discharge characteristics as a cathode of the lithium secondary battery.* Journal of The Electrochemical Society, 1992. **139**(8): p. 2082-2087.
136. Radisavljevic, B., et al., *Single-layer MoS2 transistors.* Nature nanotechnology, 2011. **6**(3): p. 147-150.
137. Wang, H., et al., *Integrated Circuits Based on Bilayer MoS2 Transistors.* Nano letters, 2012.
138. Ataca, C. and S. Ciraci, *Functionalization of Single-Layer MoS2 Honeycomb Structures.* The Journal of Physical Chemistry C, 2011. **115**(27): p. 13303-13311.
139. Ivanovskaya, V.V., et al., *Ab initio study of bilateral doping within the MoS_ {2}-NbS_ {2} system.* Physical Review B, 2008. **78**(13): p. 134104.
140. Ma, Y., et al., *Electronic and magnetic properties of perfect, vacancy-doped, and nonmetal adsorbed MoSe2, MoTe2 and WS2 monolayers.* Physical Chemistry Chemical Physics, 2011. **13**(34): p. 15546-15553.
141. Komsa, H.P., et al., *Two-dimensional transition metal dichalcogenides under electron irradiation: defect production and doping.* Physical review letters, 2012. **109**(3): p. 35503.
142. Sorescu, D.C., D.S. Sholl, and A.V. Cugini, *Density Functional Theory Studies of the Interaction of H, S, Ni-H, and Ni-S Complexes with the MoS2 Basal Plane.* The Journal of Physical Chemistry B, 2004. **108**(1): p. 239-249.
143. Hohenberg, P. and W. Kohn, *Inhomogeneous Electron Gas.* Physical Review, 1964. **136**(3B): p. B864-B871.
144. Kohn, W. and L.J. Sham, *Self-Consistent Equations Including Exchange and Correlation Effects.* Physical Review, 1965. **140**(4A): p. A1133-A1138.

145. Ceperley, D.M. and B.J. Alder, *Ground State of the Electron Gas by a Stochastic Method.* Physical Review Letters, 1980. **45**(7): p. 566-569.
146. Perdew, J.P., K. Burke, and M. Ernzerhof, *Generalized gradient approximation made simple.* Physical Review Letters, 1996. **77**(18): p. 3865-3868.
147. Perdew, J.P. and Y. Wang, *Accurate and simple analytic representation of the electron-gas correlation energy.* Physical Review B, 1992. **45**(23): p. 13244-13249.
148. Becke, A.D., *Density-functional exchange-energy approximation with correct asymptotic behavior.* Physical Review A, 1988. **38**(6): p. 3098-3100.
149. Lee, C., W. Yang, and R.G. Parr, *Development of the Colle-Salvetti correlation-energy formula into a functional of the electron density.* Physical Review B, 1988. **37**(2): p. 785-789.
150. Hamprecht, F.A., et al., *Development and assessment of new exchange-correlation functionals.* The Journal of Chemical Physics, 1998. **109**(15): p. 6264-6271.
151. Bachelet, G.B., D.R. Hamann, and M. Schlüter, *Pseudopotentials that work: From H to Pu.* Physical Review B, 1982. **26**(8): p. 4199-4228.
152. Vanderbilt, D., *Soft self-consistent pseudopotentials in a generalized eigenvalue formalism.* Physical Review B, 1990. **41**(11): p. 7892-7895.
153. Frisch M. J., G.W.T., H. B. Schlegel, G. E. Scuseria, M. A. Robb, J. R. Cheeseman, G. Scalmani, V. Barone, B. Mennucci, G. A. Petersson, H. Nakatsuji, M. Caricato, X. Li, H. P. Hratchian, A. F. Izmaylov, J. Bloino, G. Zheng, J. L. Sonnenberg, M. Hada, M. Ehara, K. Toyota, R. Fukuda, J. Hasegawa, M. Ishida, T. Nakajima, Y. Honda, O. Kitao, H. Nakai, T. Vreven, J. A. Montgomery, Jr., J. E. Peralta, F. Ogliaro, M. Bearpark, J. J. Heyd, E. Brothers, K. N. Kudin, V. N. Staroverov, R. Kobayashi, J. Normand, K. Raghavachari, A. Rendell, J. C. Burant, S. S. Iyengar, J. Tomasi, M. Cossi, N. Rega, J. M. Millam, M. Klene, J. E. Knox, J. B. Cross, V. Bakken, C. Adamo, J. Jaramillo, R. Gomperts, R. E. Stratmann, O. Yazyev, A. J. Austin, R. Cammi, C. Pomelli, J. W. Ochterski, R. L. Martin, K. Morokuma, V. G. Zakrzewski, G. A. Voth, P. Salvador, J. J. Dannenberg, S. Dapprich, A. D. Daniels, Ö. Farkas, J. B. Foresman, J. V. Ortiz, J. Cioslowski, and D. J. Fox, *Gaussian 09.* 2009.
154. Schmidt, M.W., et al., *General atomic and molecular electronic structure system.* Journal of Computational Chemistry, 1993. **14**(11): p. 1347-1363.
155. te Velde, G., et al., *Chemistry with ADF.* Journal of Computational Chemistry, 2001. **22**(9): p. 931-967.
156. Soler, J.M., et al., *The SIESTA method for ab initio order-N materials simulation.* Journal of Physics-Condensed Matter, 2002. **14**(11): p. 2745-2779.
157. Kresse, G. and J. Furthmuller, *Efficient iterative schemes for ab initio total-energy calculations using a plane-wave basis set.* Physical Review B, 1996. **54**(16): p. 11169-11186.
158. Kresse, G. and J. Furthmuller, *Efficiency of ab-initio total energy calculations for metals and semiconductors using a plane-wave basis set.* Computational Materials Science, 1996. **6**(1): p. 15-50.
159. Kresse, G. and D. Joubert, *From ultrasoft pseudopotentials to the projector augmented-wave method.* Physical Review B, 1999. **59**(3): p. 1758-1775.

160. Manna, A.K. and S.K. Pati, *Tuning the electronic structure of graphene by molecular charge transfer: a computational study.* Chemistry - An Asian Journal, 2009. **4**(6): p. 855-860.
161. Ramakrishna Matte, H., et al., *MoS2 and WS2 analogues of Graphene.* Angewandte Chemie International Edition, 2010. **122**(24): p. 4153-4156.
162. Chang, K. and W. Chen, *l-Cysteine-Assisted Synthesis of Layered MoS2/Graphene Composites with Excellent Electrochemical Performances for Lithium Ion Batteries.* ACS nano, 2011. **5**(6): p. 4720-4728.
163. Feng, C., et al., *Synthesis of molybdenum disulfide (MoS< sub> 2</sub>) for lithium ion battery applications.* Materials Research Bulletin, 2009. **44**(9): p. 1811-1815.
164. Yang, S., et al., *First-Principles Study of Zigzag MoS2 Nanoribbon As a Promising Cathode Material for Rechargeable Mg Batteries.* The Journal of Physical Chemistry C, 2011. **116**(1): p. 1307-1312.
165. Shi, H., A. Barnard, and I.K. Snook, *High throughput theory and simulation of nanomaterials: exploring the stability and electronic properties of nanographene.* Journal of Materials Chemistry, 2012.
166. Moses, P.G., et al., *Density functional study of the adsorption and van der Waals binding of aromatic and conjugated compounds on the basal plane of MoS[sub 2].* The Journal of Chemical Physics, 2009. **130**(10): p. 104709.
167. Raybaud, P., et al., *Adsorption of Thiophene on the Catalytically Active Surface of MoS_ {2}: An Ab Initio Local-Density-Functional Study.* Physical Review Letters, 1998. **80**(7): p. 1481-1484.
168. Soler, J.M., et al., *The SIESTA method for ab initio order-N materials simulation.* Journal of Physics-Condensed Matter, 2002. **14**(11): p. 2745.
169. Burke, K., J.P. Perdew, and M. Ernzerhof, *Why the generalized gradient approximation works and how to go beyond it.* International Journal of Quantum Chemistry, 1997. **61**(2): p. 287-293.
170. Troullier, N. and J.L. Martins, *Efficient pseudopotentials for plane-wave calculations.* Physical Review B, 1991. **43**(3): p. 1993.
171. Kleinman, L. and D. Bylander, *Efficacious form for model pseudopotentials.* Physical review letters, 1982. **48**(20): p. 1425-1428.
172. Geim, A.K. and K.S. Novoselov, *The rise of graphene.* Nat Mater, 2007. **6**(3): p. 183-191.
173. Rao, C.N.R., et al., *Graphene: The New Two-Dimensional Nanomaterial.* Angewandte Chemie International Edition, 2009. **48**(42): p. 7752-7777.
174. Bao, W.S., et al., *Nonlinear dc transport in graphene.* Journal of Physics: Condensed Matter, 2009. **21**(30): p. 305302.
175. Shishir, R.S. and D.K. Ferry, *Intrinsic mobility in graphene.* Journal of Physics: Condensed Matter, 2009. **21**(23): p. 232204.
176. Wang, Y., et al., *Room-Temperature Ferromagnetism of Graphene.* Nano letters, 2008. **9**(1): p. 220-224.
177. Castro Neto, A.H., et al., *The electronic properties of graphene.* Reviews of Modern Physics, 2009. **81**(1): p. 109-162.
178. Franklin, A.D., et al., *Sub-10 nm Carbon Nanotube Transistor.* Nano Letters, 2012. **12**(2): p. 758-762.
179. Dutta, S. and S.K. Pati, *Novel properties of graphene nanoribbons: a review.* Journal of Materials Chemistry, 2010. **20**(38): p. 8207-8223.

180. Sharma, Y.S.R.K.C., A. Bandyopadhyay, and K.P. Swapan, *Structural Stability, Electronic, Magnetic and Optical Properties of Rectangular Graphene and BN Quantum Dots: Effects of Size, Substitution and Electric Field.* Unpublished, 2013.
181. Manna, A.K. and S.K. Pati, *Doping single-walled carbon nanotubes through molecular charge-transfer: a theoretical study.* Nanoscale, 2010. **2**(7): p. 1190-1195.
182. Barone, V. and J.E. Peralta, *Magnetic Boron Nitride Nanoribbons with Tunable Electronic Properties.* Nano Letters, 2008. **8**(8): p. 2210-2214.
183. Lide, D.R., *CRC handbook of chemistry and physics*. 2012: CRC press.
184. Periyasamy, G., et al., *DFT Studies of Solvation Effects on the Nanosize Bare, Thiolated, and Redox Active Ligated Au55 Cluster†.* The Journal of Physical Chemistry C, 2010. **114**(38): p. 15941-15950.
185. Novoselov, K.S., et al., *Electric Field Effect in Atomically Thin Carbon Films.* Science, 2004. **306**(5696): p. 666-669.
186. Zhang, Z.Z., K. Chang, and F.M. Peeters, *Tuning of energy levels and optical properties of graphene quantum dots.* Physical Review B, 2008. **77**(23): p. 235411.
187. Pan, D., et al., *Hydrothermal Route for Cutting Graphene Sheets into Blue-Luminescent Graphene Quantum Dots.* Advanced Materials, 2010. **22**(6): p. 734-738.
188. Zhu, S., et al., *Strongly green-photoluminescent graphene quantum dots for bioimaging applications.* Chemical Communications, 2011. **47**(24): p. 6858-6860.
189. Frisch, M.J.T., G. W.; Schlegel, H. B.; Scuseria, G. E.; Robb, M. A.; Cheeseman, J. R.; Scalmani, G.; Barone, V.; Mennucci, B.; Petersson, G. A.; Nakatsuji, H.; Caricato, M.; Li, X.; Hratchian, H. P.; Izmaylov, A. F.; Bloino, J.; Zheng, G.; Sonnenberg, J. L.; Hada, M.; Ehara, M.; Toyota, K.; Fukuda, R.; Hasegawa, J.; Ishida, M.; Nakajima, T.; Honda, Y.; Kitao, O.; Nakai, H.; Vreven, T.; Montgomery, J. A., Jr.; Peralta, J. E.; Ogliaro, F.; Bearpark, M.; Heyd, J. J.; Brothers, E.; Kudin, K. N.; Staroverov, V. N.; Kobayashi, R.; Normand, J.; Raghavachari, K.; Rendell, A.; Burant, J. C.; Iyengar, S. S.; Tomasi, J.; Cossi, M.; Rega, N.; Millam, J. M.; Klene, M.; Knox, J. E.; Cross, J. B.; Bakken, V.; Adamo, C.; Jaramillo, J.; Gomperts, R.; Stratmann, R. E.; Yazyev, O.; Austin, A. J.; Cammi, R.; Pomelli, C.; Ochterski, J. W.; Martin, R. L.; Morokuma, K.; Zakrzewski, V. G.; Voth, G. A.; Salvador, P.; Dannenberg, J. J.; Dapprich, S.; Daniels, A. D.; Farkas, Ö; Foresman, J. B.; Ortiz, J. V.; Cioslowski, J.;; Fox, D. J., *Gaussian 09, Revision A. 02*, R.A. Gaussian 09, Editor. 2009: Wallingford CT.
190. Parr, R.G. and Y. Weitao, *Density-functional theory of atoms and molecules*. Vol. 16. 1989: Oxford University Press, USA.
191. Becke, A.D., *Density-functional thermochemistry. III. The role of exact exchange.* The Journal of Chemical Physics, 1993. **98**: p. 5648.
192. Levine, I.N., *Quantum chemistry*. Vol. 5. 2000: Prentice Hall Upper Saddle River, NJ.
193. Huang, B., et al., *Edge stability of boron nitride nanoribbons and its application in designing hybrid BNC structures.* Nano Research, 2012. **5**(1): p. 62-72.
194. Chen, R., C. Chang, and M. Lin, *Electric-field-tunable electronic properties of graphene quantum dots.* Physica E: Low-dimensional Systems and Nanostructures, 2010. **42**(10): p. 2812-2815.

195. Huang, B., et al., *Making a field effect transistor on a single graphene nanoribbon by selective doping.* Applied Physics Letters, 2007. **91**(25): p. 253122-253122-3.
196. Jena, D., et al., *Zener tunneling in semiconducting nanotube and graphene nanoribbon< equation> pn</equation> junctions.* Applied Physics Letters, 2008. **93**(11): p. 112106-112106-3.
197. Martins, T.B., et al., *σ-and π-Defects at Graphene Nanoribbon Edges: Building Spin Filters.* Nano Letters, 2008. **8**(8): p. 2293-2298.
198. Wang, X., et al., *Room-temperature all-semiconducting sub-10-nm graphene nanoribbon field-effect transistors.* Physical Review Letters, 2008. **100**(20): p. 206803.
199. Chen, Y.P., Y.E. Xie, and X.H. Yan, *Electron transport of L-shaped graphene nanoribbons.* Journal of Applied Physics, 2008. **103**(6): p. 063711-4.
200. OuYang, F., et al., *Transport properties of T-shaped and crossed junctions based on graphene nanoribbons.* Nanotechnology, 2009. **20**(5): p. 055202.
201. Wang, B., J. Wang, and H. Guo, *Ab initio calculation of transverse spin current in graphene nanostructures.* Physical Review B, 2009. **79**(16): p. 165417.
202. Zhou, B., et al., *Electronic transport for a crossed graphene nanoribbon junction with and without doping.* The European Physical Journal B-Condensed Matter and Complex Systems, 2010. **76**(3): p. 421-425.
203. González, J.W., et al., *Transport properties of graphene quantum dots.* Physical Review B, 2011. **83**(15): p. 155450.
204. Wang, Z., et al., *Z-shaped graphene nanoribbon quantum dot device.* Applied Physics Letters, 2007. **91**(5): p. 053109-053109-3.
205. Manna, A.K. and S.K. Pati, *Tunable Electronic and Magnetic Properties in BxNyCz Nanohybrids: Effect of Domain Segregation.* The Journal of Physical Chemistry C, 2011. **115**(21): p. 10842-10850.
206. Bandyopadhyay, A., S.R.K.C.S. Yamijala, and S.K. Pati, *Structural Stability, Electronic, Magnetic and Optical Properties of Rectangular Graphene and BN Quantum Dots: Effects of Size, Substitution and Electric Field.* Submitted, 2013.